

**IN VIVO OPTOGENETIC ACTIVATION
OF LOCUS COERULEUS AND CONSEQUENT
EFFECTS ON PERFORANT PATH EVOKED
POTENTIALS IN DENTATE GYRUS**

by

© Meghan Anne Laura Quinlan

A thesis submitted to the

School of Graduate Studies

in partial fulfillment of the requirements for the degree of

Masters of Science

Department of Psychology

Memorial University of Newfoundland

May 2017

ABSTRACT

Locus coeruleus (LC) is a nucleus composed of noradrenergic neurons, with extensive forebrain connections. Within hippocampus, the dentate gyrus (DG) receives its input predominantly from entorhinal cortex through glutamatergic fibers of the perforant pathway (PP). LC activation prompts norepinephrine (NE) release onto DG granule cells, which consequently potentiates the cellular response to glutamate. Previous research using electrical and/or chemical LC activation revealed NE-induced long-term potentiation (NE-LTP) in the DG, when paired with PP electrical stimulation. The current study investigates whether previous models of in vivo NE-LTP can be replicated with optogenetic manipulation of LC neurons in anesthetized rats. Transgenically modified rats (TH-CRE) were first infused with a virus (AAV8), containing photosensitive channels (ChR2h134r) and recovered for a minimum of 4-weeks. Recording and stimulating (.1Hz, 0.2ms pulse) electrodes were then situated in the DG and PP respectively, to monitor the evoked potentials. The evoked response was monitored for a 30-min period prior to optogenetic activation, using 10Hz trains of 150mA (60-70mW), 30ms pulses of blue light from a laser diode directed at LC to initiate NE release. A recording electrode was assembled with the laser diode to simultaneously monitor cellular responses to light. Successful infusions of AAV8 showed colocalization of LC neurons and virus uptake. The introduction of the light into LC increased neuronal firing, and when paired with PP electrical stimulation, induced enduring changes in the DG-PP evoked response, as measured by population spike amplitude. These results occurred despite the limited duration of LC firing, revealed by our concurrent recording, and are

consistent with the effects of chemical and electrical LC activation. They argue convincingly that PP-evoked potential spike potentiation is selectively related to a relatively brief period of LC-NE release. Developments in optogenetic technologies are promising steps toward a highly selective, reversible technique for nerve excitation and silencing. Light stimulation offers the potential for relating selective activation patterns of specific neurons to functional outcomes and for understanding the consequences of specific temporal interactions among neuronal networks.

ACKNOWLEDGEMENTS

The process of completing my master's degree has been one of my most challenging and rewarding experiences, and I was very fortunate to have tremendous support on my path to this accomplishment.

First and foremost, I would like to thank Dr. Susan Walling for her unwavering support and dedication to helping me achieve this goal. She took on the role of my mentor despite a challenging workload, and yet was still always available for questions and meetings, for check-ins when my baseline had just begun and it was already past dark, and even for confused phone calls when I was overthinking a concept. She has been my supervisor since I was a third year, undergraduate, honors student, and her faith and belief in my abilities has never failed to comfort (and amaze) me. I always feel reassured that if she thinks I can do something, I must be able to do it. I have, and will always feel truly privileged to have been her graduate student.

I would like to thank my co-supervisors Dr. Gerard Martin and Dr. Darlene Skinner, as well as Dr. Carolyn Harley, who also committed so much of her time and knowledge to this research. Throughout my master's work, I was often introduced as “the people's master's student,” in order to summarize who I was working with. This was ultimately my honor, as I not only had three additional sources of knowledge and first-hand experience, but also of support. I am indescribably grateful for the endless encouragement, the words of wisdom, ideas, suggestions, reminders, reassurance and the countless number of ways in which they all contributed to this research. A great debt of

gratitude is also owed to Stephen Milway, who offered so much of his time to facilitating my research. I hope I showed my appreciation for every door knock, every check in, every reassurance, every corrected setting and every resolved technical issue, but just in case, I would like to thank him once more.

This research would also not have been possible without our legendary research assistant, Vanessa Strong. Her commitment to establishing optogenetics at Memorial University set the foundation for not only my research, but several others hoping to use the technique. She made the lab an inviting and fun atmosphere, and I was incredibly fortunate to have been working alongside someone who quickly became a great friend. Her instruction, trouble-shooting and endless supply of encouragement (and coffee) helped me in times of great stress. She was never phased by my endless questions or my panicked moments, and taught me to believe in my own capabilities as researcher and as a person in general (W.W.V.D.) I am forever grateful for her.

I would also like to thank my fellow graduate student, Katelyn Fallon. Between us, we shared the stresses of our course work and research responsibilities, and were able to lean on each other for support. She often kept me company during the early (and sometimes very late) hours of my electrophysiology days. Her presence made any difficult task seem less daunting, and sometimes with the right music, even quite fun.

I would also like to offer my thanks to several of our students, specifically Jocelyn Barnes, Iain MacIntyre, Claire Wallace, Hilary Rowe and Isaac Hughes. During their time in the lab, they often saved me hours of work, and their contributions to this research were of great help. I would like to especially thank Jocelyn and Iain however,

for continuing to visit after their placement had ended; for their continued support, for keeping me company and of course, for bringing me coffee on long days.

Finally, I would like to thank my family and close friends for their love and support. This experience would have been immensely harder without their constant encouragement and their role in my success does not go unnoticed or unappreciated.

TABLE OF CONTENTS

ABSTRACT.....	iii
ACKNOWLEDGEMENTS.....	v
LIST OF FIGURES.....	xii
LIST OF ABBREVIATIONS.....	xiv
CHAPTER 1 – INTRODUCTION.....	1
1.1 Overview.....	1
1.2 Hippocampus: Anatomy and Connectivity.....	2
1.3 Norepinephrine (NE).....	5
1.3.1 NE Receptors.....	6
1.3.2 Mechanisms of NE Potentiation.....	7
1.4 Locus Coeruleus (LC): Anatomy and Connectivity.....	8
1.4.1 LC Projections to Hippocampus.....	13
1.4.2 LC Activity Patterns: A System of Arousal.....	14
1.4.3 Identifying Cells of the LC.....	16
1.5 Long-Term Potentiation (LTP).....	17
1.5.1 NE-Induced LTP (NE-LTP) in Hippocampus and the Role of LC.....	18
1.6 Electrophysiology in the DG.....	21
1.6.1 Evoked Potential Analysis.....	21
1.6.2 PP-LC Interstimulus Interval (ISI) Testing.....	22
1.6.3 Paired Pulses: Evoked Potential Analysis.....	23
1.6.4 Input-Output (I-O) Curves: Evoked Potential Analysis.....	25

1.7	Optogenetic Control of the LC.....	26
1.8	Past Optogenetic Research.....	29
1.9	Objectives.....	33
CHAPTER 2 – MATERIALS & METHODS.....		34
2.1	Subjects.....	34
2.2	Virus.....	35
2.3	Optogenetic Experimentation.....	36
2.3.1	Virus Infusion Surgeries.....	36
2.3.2	Virus Uptake.....	38
2.3.3	Electrophysiology.....	38
2.4	Experiment 1.....	39
2.4.1	LC Optogenetic Manipulation and Recording.....	39
2.4.2	Optogenetic Activation of LC.....	40
2.4.3	Data Analysis.....	41
2.4.3.1	Optogenetic Activation of LC: Analyzing Cell Responses.....	41
2.4.3.2	Identification of Putative LC Cells.....	41
2.4.4	Histology and Immunohistochemistry.....	42
2.4.5	Image Analysis.....	44
2.4.6	Verification of Placements.....	44
2.4.7	Virus Expression and Colocalization.....	45
2.4.8	Statistical Analysis.....	46
2.5	Experiment 2.....	46
2.5.1	Optogenetic Activation of LC.....	46

2.5.2	Electrical Stimulation of PP and Recording in DG.....	46
2.5.3	Optogenetically Induced NE-LTP.....	47
2.5.4	PP-LC Interstimulus Interval (ISI) Testing.....	48
2.5.5	Paired Pulse and I-O Curves.....	49
2.5.6	Data Analysis.....	49
2.5.6.1	Optogenetic Activation of LC: Cell Recorded Responses.....	49
2.5.6.2	NE-LTP of the Evoked Potential.....	50
2.5.6.3	PP-LC Interstimulus Interval (ISI) Testing.....	50
2.5.6.4	Paired Pulses: Evoked Potential Analysis.....	51
2.5.6.5	I-O Curves: Evoked Potential Analysis.....	51
2.5.7	Verification of Placements.....	52
2.5.8	Statistical Analysis.....	53
2.5.8.1	Optogenetic Activation of LC: Cell Recorded Responses.....	53
2.5.8.2	NE-LTP of the Evoked Potential.....	53
2.5.8.3	PP-LC Interstimulus Interval (ISI) Testing.....	54
2.5.8.4	Paired Pulses: Evoked Potential Analysis.....	54
2.5.8.5	I-O Curves: Evoked Potential Analysis.....	55
CHAPTER 3 – RESULTS.....		56
3.1	Subjects: LC-ChR2(h134r) Channel-Activated and Light Control.....	56
3.2	Virus Expression and Colocalization.....	57
3.3	Verification of Placements.....	59
3.4	LC Cellular Parameters.....	60
3.4.1	LC-ChR2(h134r) Channel-Activated (Experimental) Condition.....	60

3.4.2	Light Control (Control) Condition.....	60
3.5	Experiment 1.....	61
3.5.1	Optogenetic Activation of LC: Cell Recorded Responses.....	61
3.6	Experiment 2.....	64
3.6.1	Optogenetic Activation of LC: Cell Recorded Responses.....	64
3.6.1.1	Ten Hz Stimulation: 10s Light Protocol (100 Pulses).....	65
3.6.1.2	Ten Hz Stimulation: 10-Minute Light Protocol (6000 Pulses).....	66
3.6.2	Optogenetically Induced NE-LTP.....	70
3.6.2.1	Baseline Evoked Potential Parameters.....	70
3.6.2.2	NE-LTP: Evoked Potential Analysis.....	71
3.6.3	PP-LC Interstimulus Interval (ISI) Testing.....	73
3.6.4	Paired Pulses: Evoked Potential Analysis.....	76
3.6.5	I-O Curve: Evoked Potential Analysis.....	81
CHAPTER 4 – DISCUSSION.....		83
4.1	Summary of Major Findings.....	83
4.2	Virus Expression and Colocalization.....	85
4.3	Optimal Light Parameters for LC Activation.....	88
4.4	Identification of Putative LC Cells.....	91
4.5	Effect of Optogenetic Activation of LC.....	92
4.6	Use of Optogenetic Activation of LC to Induce NE-LTP.....	97
4.7	Effect of Optogenetic Activation of LC on Evoked Potential.....	100
4.8	Optogenetic Manipulation of PP-LC ISIs.....	105
4.9	Effect of Optogenetic Activation on Paired Pulses.....	107

4.10	Effect of Optogenetic Activation on I-O Curves.....	108
4.11	Verification of Placements.....	109
4.12	Consequences of Placements.....	110
4.13	Future Directions.....	112
CHAPTER 5 – CONCLUSIONS.....		114

LIST OF FIGURES

Figure 1. Hippocampal substructures and pathways.....	4
Figure 2. Distribution of noradrenergic projections in the rat brain.....	9
Figure 3. Manual assembly of optical fiber and recording electrode.....	40
Figure 4. Virus expression and colocalization per experimental condition.....	58
Figure 5. Placement of optrode assembly per subject during optogenetic manipulation.....	59
Figure 6. Optogenetic activation of LC with 5s and 10s light sequences.....	63
Figure 7. Optogenetic activation of LC with 10s light sequence in NE-LTP subgroup...	66
Figure 8. Optogenetic activation of LC in the first 10s of the 10-minute light protocol..	67
Figure 9. Optogenetic activation of LC with 10-minute light sequence.....	69
Figure 10. Effect of optogenetically induced NE-LTP on population spike.....	72
Figure 11. Effect of optogenetically induced NE-LTP on EPSP slope.....	73
Figure 12. Optogenetic manipulation of PP-LC ISIs.....	75
Figure 13. Population spike PPRs.....	78
Figure 14. EPSP slope PPRs.....	80
Figure 15. Pre- and post-light I-O curves with increasing PP current stimulation.....	82

LIST OF ABBREVIATIONS

5s	five seconds
10s	ten seconds
AAV	adeno-associated viruses
ANOVA	analysis of variance
<i>C. elegans</i>	<i>Caenorhabditis elegans</i>
CA	Cornu Ammonis
Ca ²⁺	calcium
cAMP	cyclicAMP
ChR2	channelrhodopsin-2
ChR2(h134r)	modified ChR2 light-sensitive channel that produces larger peak current than the normal ChR2 channel
CNS	central nervous system
DBH	dopamine β -hydroxylase
DBH ⁺	positively labelled for DBH
DG	dentate gyrus
DIO	double-floxed inverse open reading frame
EC	entorhinal cortex
EPSP	excitatory postsynaptic potential
E-S	EPSP slope to population spike
EYFP	enhanced yellow fluorescent protein gene
GABA	γ -aminobutyric acid
GFP	green fluorescent protein
GFP ⁺	positively labelled for GFP
G _s -protein	stimulatory G-protein
I-O	input-output
IPSP	inhibitory postsynaptic potential
ISI	interstimulus interval
K ⁺	potassium
LC	locus coeruleus
LC-ChR2(h134r)	locus coeruleus modified by viral construct
LC-NE	locus coeruleus produced norepinephrine
LED	laser emitting diode
LSD	least significant difference
LTP	long-term potentiation
NE	norepinephrine
NE-LLP	norepinephrine long-lasting potentiation
NE-LTP	norepinephrine induced long-term potentiation
NET	norepinephrine transporter
NMDA	N-methyl-D-aspartate receptors
PKA	cAMP-dependent kinase

PP	perforant path
PP1	first paired pulse stimulation
PP2	second paired pulse stimulation
PPR	paired pulse ratio
PVP	polyvinylpyrrolidone
SD	standard deviation
TH	tyrosine hydroxylase
TH-CRE	tyrosine hydroxylase-Cre recombinase
TH ⁺	positively labelled for TH
TH ⁻	negatively labelled for TH
vg	vector genome

CHAPTER 1 – INTRODUCTION

1.1 Overview

The first publication on long-term potentiation (LTP) occurred in 1973 by Bliss and Lomo following their experiments in the rabbit dentate gyrus (DG). Results of this research suggested two mechanisms to be responsible for long-lasting potentiation: an increase in the efficiency of synaptic transmission at the perforant path (PP) synapses, and an increase in overall granule cell excitability. Research has since repeatedly shown that an increase in the concentration of norepinephrine (NE) within the DG has a facilitating effect on the electrical responses generated (Lacaille & Harley, 1985; Neuman & Harley, 1983). The first report of NE-potentiation in the DG was induced by the *in vivo* iontophoresis of NE (Neuman & Harley, 1983), and was termed NE long-lasting potentiation (NE-LLP). Since this study, this phenomenon has been replicated in a variety of ways, including electrical and chemical manipulations of the NE input to the DG, *in vitro* and *in vivo*, and in both anesthetized and awake, behaving animals.

This thesis aimed to determine the cellular responses of the locus coeruleus (LC), which provides the NE input to the DG, to optogenetic manipulation, and the consequent effects produced on various aspects of the PP evoked potential of the DG. First I investigated the specificity and selective uptake of our viral gene construct, designed to insert a modified blue light-sensitive channel (CHR2(h134r)), similar to Channelrhodopsin-2 (ChR2), into LC neurons. The levels of fluorophore colocalization between the virus and labeled LC neurons were compared based upon experimental

condition and infusion placement; explanations are offered as to what may create the optimal conditions and the highest possible levels of colocalization. Second, I tested the ability of a laser diode fiber light source and optrode assembly to stimulate these ChR2-LC neurons to fire. The LC neuronal responses to both a 5 second (5s) and 10 second (10s) light protocol were first tested, to confirm the ability of light to successfully activate LC neurons in anesthetized rats. Next, a 10-minute light sequence was utilized to induce NE-LTP; this was indexed by two parameters of the PP evoked potential in DG, which were monitored for a three-hour period post-light. I additionally investigated the effect on potentiation of varying the interval length between a single light pulse to LC and an electrical stimulation delivered to the PP; the effects of optogenetic stimulation on traditionally reported evoked potential measurements: paired pulse manipulations and input-output (I-O) curves, are also analyzed. I provide a review of previous electrical and chemical models of both LC activation and NE-LTP, and discusses consistencies between our results and previous research, as well as the advantages and challenges to using an optogenetic manipulation. I also describe the characteristics of LC activation, NE release and NE-LTP, which appear to be unique to optogenetic stimulation, and outline in detail what next steps could be taken to improve and expand upon this research.

1.2 Hippocampus: Anatomy and Connectivity

The hippocampus is a structure located in the medial temporal lobe (Morris, Garrud, Rawlins, & O'Keefe, 1982), which is, in conjunction with the DG, subiculum, presubiculum, parasubiculum and entorhinal cortex, collectively termed the hippocampal

formation. Although there are dramatic variations in the volume of hippocampus across species, its structure remains relatively uniform (Lavenex, Banta Lavenex, & Amaral, 2007), thus allowing for translational research to be completed with rodents. The structure of the hippocampus consists of two enfolded sheets of cells, which differ in both their organization and principal cell type. The first is referred to as Ammon's horn or Cornu Ammonis (CA), a laminar cortex, containing mostly pyramidal cells. This type of cell has both short basal dendrites and a longer primary dendrite, which extends through multiple cell layers. The other cell sheet, DG, is also a laminar structure, comprised of three layers (Brown, 2003). The top layer, closest to the hippocampal fissure is referred to as the molecular layer, and is relatively cell free. The principal cell, or granule cell, layer, then lies beneath the molecular layer, and is primarily composed of densely packed, columnar stacks of granule cells (Witter & Amaral, 1991). Granule cells, in contrast to pyramidal cells, occur in a densely packed layer, but with dendrites that project uniformly into the molecular layer (Brown, 2003). The third DG layer is more appropriately described as a cellular region; known as the polymorphic cell layer, it is often used synonymously with the term hilus (Witter & Amaral, 1991). The structure of Ammon's horn has three major subdivisions known as CA1, CA2 and CA3 (Amaral, Scharfman, & Lavenex, 2007) each with three distinct layers: stratum oriens, stratum pyramidale and stratum radiatum (Choi & Koh, 2008).

The hippocampus also contains a pathway of synapses that connects its substructures and facilitates communication (see Figure 1). The entorhinal cortex (EC) is considered the major input to the hippocampus and is composed of six layers, which

project to different parts of the hippocampus and surrounding areas (Ramon, 1968).

Axons of cells within the EC project onto DG through the PP; this pathway is composed of axons of the pyramidal cells of the upper cell layers of the EC. Specifically, cell layer three of the EC projects to CA1, while cell layer two extends to the DG, where it synapses with granule cells, as well as with dendrites in CA1, CA2 and CA3 (Ramon, 1968). Granule cells within DG then project their axons onto pyramidal cells of CA3, forming a pathway known as the mossy fibers. These cells of CA3 synapse onto pyramidal cells in CA1 by way of Schaffer collateral axons. This pathway of synapses is commonly referred to as the “trisynaptic pathway” because its emphasis is placed upon the first three links of the complex hippocampal circuitry (Amaral et al., 2007).

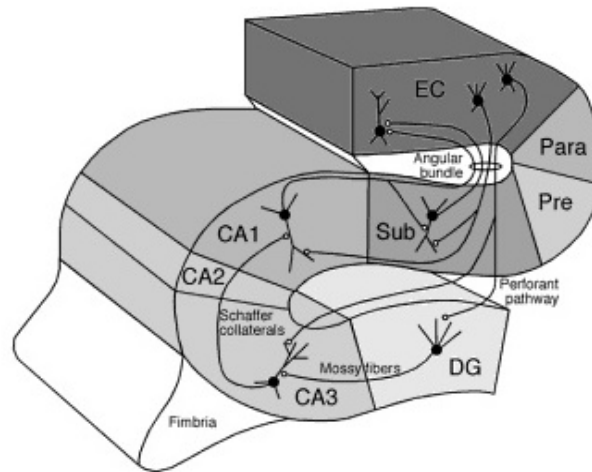


Figure 1. Hippocampal substructures and pathways. Image obtained from Hippocampal Neuroanatomy (Amaral & Lavenex, 2007). Displays entorhinal cortex projecting to dentate gyrus via perforant pathway, neurons projecting from dentate gyrus to CA3 via mossy fibers and projections from CA3 to CA1 via Schaffer collaterals.

The pyramidal cells of the EC fire in response to stimulation from the excitatory neurotransmitter glutamate, they consequently release additional glutamate onto the dendrites of both excitatory granule cells and inhibitory interneurons of the DG (Amaral et al., 2007). Activation of the PP results in the occurrence of excitatory postsynaptic potentials (EPSPs) in both granule cells and interneurons. These stimulated interneurons can then produce either feedforward inhibition, if excited by pyramidal cells in the EC, or feedback inhibition if excited by the DG granule cells themselves (Remondes & Schuman, 2003). Thus, it is possible for stimulation of the PP to result in either outcome.

1.3 Norepinephrine (NE)

As a neuromodulator, NE does not elicit effects solely on its own, but rather it alters the effects of other neurochemicals by facilitating or antagonizing them (Waterhouse & Woodward, 1980). NE-containing axons are distributed widely through the central nervous system (CNS), thus suggesting NE plays a prominent role in CNS function (Berridge & Waterhouse, 2003). It can produce different effects on its target neurons dependent upon the receptor with which it binds and which it subsequently activates (Foote, Bloom, & Aston-Jones, 1983). NE is one of several important neuromodulators found throughout the brain and is synthesized in the neuronal body through a series of sequential steps (Fornai, Ruffoli, Giorgi, & Paparelli, 2011). To begin, the amino acid tyrosine is first converted to DOPA, with the assistance of the enzyme tyrosine hydroxylase (TH). This is then converted to the neurotransmitter, dopamine, by

the aromatic enzyme, L-amino acid decarboxylase; and finally, dopamine is converted to NE by the enzyme, dopamine-beta-hydroxylase (DBH) (Menniti & Diliberto, 1989).

1.3.1 NE Receptors

Similar to other neurotransmitters, NE is capable of binding to multiple receptors in target tissues. Traditionally, there are two categories of noradrenergic G-protein coupled receptors with which NE may bind: these are known as alpha (α) and beta (β) receptors (Rogawski & Aghajanian, 1982). Located on neurons both pre- and post-synaptically, α -receptors can have activating or inhibiting effects depending on the subtype (α_1 or α_2) (Aston-Jones & Cohen, 2005). Presynaptic α_2 -receptors are located on the terminals of axons, they may be auto- or hetero-receptors, and can also occur on dendrites. Within the LC, the α_2 -receptor is the more common subtype, and is typically inhibitory in nature; this means it has an inhibitory effect on NE release from the LC, in addition to an inhibitory effect on LC activation. These LC receptors are also referred to as autoreceptors, and are responsible for monitoring and preventing substantial NE release from LC neurons (Aston-Jones & Cohen, 2005). The other subtype of α -receptors, α_1 -receptors, is excitatory in nature (Rogawski & Aghajanian, 1982).

The other category of G-protein coupled receptors, known as β -noradrenergic receptors, are primarily located post-synaptically on the cells of the hippocampus (Aston-Jones & Cohen, 2005). Like α -receptors, the β -receptors are also divided into subtypes: β_1 , β_2 , and β_3 ; although, of these subtypes, only the first two are found within the CNS (Cooper, Kamel, Sandler, Davey, & Bloomfield, 1996). The hippocampus and limbic

system contain a large quantity of β -receptors (Alexander, Davis, & Lefkowitz, 1975), with granule cells specifically containing a high density of postsynaptic β -receptors on their dendrites (Milner, Shah, & Pierce, 2000).

1.3.2 Mechanisms of NE Potentiation

β -receptors are coupled to adenylate cyclase and their activation increases the level of cyclic adenosine monophosphate (cAMP) (Stanton & Sarvey, 1985a); this increase of cAMP in the DG subsequently promotes plasticity at PP-DG synapses (Stanton & Sarvey, 1985a). The β -receptors facilitate the EPSP response in the DG, which is generated by glutamate release from the PP; they also facilitate the population spike. Studies have also shown a mild depolarizing effects of NE, accomplished through β -receptors and mediated by the closing of resting potassium channels. This consequently brings the membrane potential closer to threshold, and thereby closer to firing (Lacaille & Schwartzkroin, 1988). In an additional role, NE prevents cell hyperpolarization after firing; this is accomplished by blocking the calcium (Ca^{2+}) channels which permit potassium (K^+) channels to remain open long enough for the cells to hyperpolarize (Schofield, 1990). This decrease in the likelihood of cell firing is a process referred to as slow after hyperpolarization, and is attributed to a cAMP-mediated block of Ca^{2+} -activated K^+ currents (Haas & Rose, 1987; Lancaster, Hu, Ramakers, & Storm, 2001)

It has been repeatedly shown through pharmacological studies that it is the β -noradrenergic receptor which plays the dominant role in NE-dependent plasticity of evoked potentials (Neuman & Harley, 1983; Stanton & Sarvey, 1985b). As mentioned,

the β -receptor is a G-protein coupled receptor; more specifically it is a stimulatory G-protein (G_s -protein) receptor coupled to adenylyl cyclase. Stimulation of these receptors results in an increase of cAMP in the hippocampus, this can consequently activate cAMP-dependent kinase (PKA) (Li et al., 2000). PKA has several intracellular effects, including increasing the conductance of L-type voltage-gated Ca^{2+} channels through phosphorylation (Davare, Horne, & Hell, 2000) and regulating the conductance of N-methyl-D-aspartate (NMDA) receptors (Leonard & Hell, 1997). NMDA receptors have a unique property in that they contain a Ca^{2+} channel that is directly gated by glutamate. In the resting state, this Ca^{2+} channel is blocked by a magnesium ion, which prevents the influx of Ca^{2+} ions even when the receptor is bound to glutamate (Nowak, Bregestovski, Ascher, Herbet, & Prochiantz, 1984). During postsynaptic depolarization, this magnesium ion is expelled from the channel, subsequently permitting an influx of Ca^{2+} (Leonard & Hell, 1997). PKA has also been shown to indirectly affect cell excitability by repressing protein phosphatase I, which through dephosphorylation of receptors and ion channels, returns them to basal states. By opposing the action of this phosphatase, PKA enhances the flow of Ca^{2+} and thereby cell excitability (Wang & Kelly, 1996). Experiments by Stanton et al. (1989) revealed that blockage of NMDA receptors blocks the occurrence of NE-induced long-lasting potentiation. Thus, it is likely that NE long-lasting potentiation is reliant upon the influx of Ca^{2+} as well as the elevation of cAMP.

1.4 Locus Coeruleus (LC): Anatomy and Connectivity

The LC is a nucleus composed of noradrenergic neurons, located in the pons of

the brainstem. In rodents, despite its small size of only about 1,500 neurons bilaterally, it has more norepinephrine-containing neurons than any other brain structure (Samuels & Szabadi, 2008). The LC provides the sole source of NE to many areas of the brain, including the hippocampus (Aston-Jones & Cohen, 2005) and neocortex, regions that are critical to higher cognitive processes (Berridge & Waterhouse, 2003). The LC has extensive connections throughout the brain; in fact, the LC-NE system is one of several brainstem neuromodulatory nuclei with widely distributed projections that ascend to the neocortex (Grzanna & Molliver, 1980). Cells of the LC innervate the majority of forebrain structures, including the hippocampus and the LC-NE system in general, boasts a widespread influence on neuronal circuits (Berridge & Waterhouse, 2003), with extensive connections that promote the LC's role in a wide variety of cognitive tasks, including the facilitation of synaptic plasticity (Cooke & Bliss, 2006) (see Figure 2).

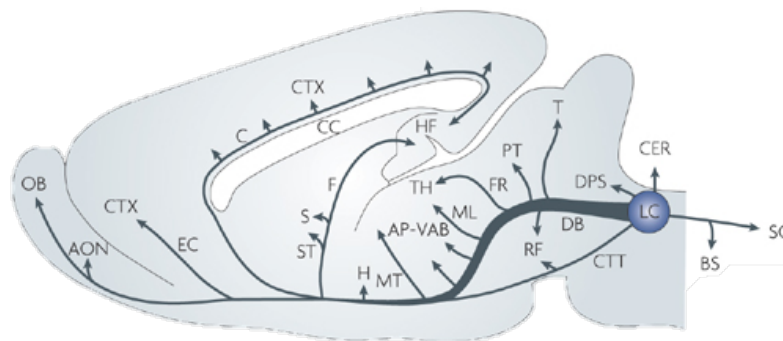


Figure 2. Distribution of noradrenergic projections in the rat brain. Image adapted from Sara, S.J. (2009). Efferents from the LC project to a vast number of diverse brain regions, including the frontal cortex (FC), thalamus (TH), amygdala (A), hippocampus (HF), brainstem (BS) and cerebellum (CER).

The LC proper is a compact, well-delineated nucleus of NE-containing neurons, easily identifiable in Nissl-stained sections as a tightly packed cluster of darkly stained cells. This small nucleus extends 1.2mm along the ventrolateral edge of the fourth ventricle in the pontine brainstem, contiguous with the medial side of the mesencephalic nucleus of the trigeminal nerve (Grzanna & Molliver, 1980). Various studies have examined the different types of neurons existing within this small but significant nucleus. In studies of the rodent LC, Swanson (1976) reported both medium-sized fusiform cells, as well as larger multipolar neurons. Meanwhile, an additional class of rounded and ovoid cells was also established (Shimizu & Imamoto, 1970). A study by Loughlin et al. (1986) analyzed retrogradely filled LC neurons following horse radish peroxidase injections, and distinguished six unique subpopulations of LC neurons, all of which have different efferent targets. These different cells have been additionally categorized on the basis of their dendritic orientation, which extend preferentially to four zones (Foote et al., 1983). Fusiform cells exist in position with the long axis extending in the anterior-posterior plane, while tilted in either dorsolateral and ventromedial orientations; this consequently suggests their dendrites to be extended in the sagittal and horizontal planes. Meanwhile, dendrites of the multipolar cells seem to extend primarily in the frontal plane (Sievers, Lolova, Jenner, Klemm, & Sievers, 1981).

LC has additionally been divided into subnuclei based upon the size of cells and orientation of dendrites. A large region of dorsal LC is composed of small, tightly packed cells; meanwhile a smaller region of ventral LC consists of larger, less densely packed cells, approximately 200 per nucleus. Another small subdivision of LC cells is formed by

a group of multipolar neurons, scattered in the ventral portion of the periaqueductal grey. These cells have prominent dendrites that extend in all directions; they exist rostrally to the compact regions of LC and are distinguishable from neighboring cells only by their NE content (Sievers et al., 1981). The ventral portion of the nucleus, also known as the subcoeruleus or subcoeruleus, is described as the ventral extension of the LC; it is a more sparsely packed region, known to contain large multipolar cells (Bjorklund & Lindvall, 1979), although to date, delineation of this area has been inconsistent (Aston-Jones, 2004). The NE-containing cells of ventral LC have been described as part of a system of NE cells, which extends to include several other NE positive nuclei – designated A4 through A7; LC is termed A6 (Dahlstrom & Fuxe, 1964). Axons of A5, in combination with fibers from A7 and the anterior portion of LC, travel ventrally to the forebrain (Maeda & Shimizu, 1972). However, despite the NE cell bodies that connect the ventral part of the LC and the A5 and A7 nuclei, these nuclei are considered to be separate from the subcoeruleus (Olson & Fuxe, 1972). In terms of proximity, A4 is the closest nucleus to LC, existing adjacently and extending dorsolaterally from the periaqueductal grey. A4 is sometimes regarded as part of the LC in fact, as dendrites from this nucleus extend both medially and ventrally (Aston-Jones & Bloom, 1981a). Despite this heterogeneity in morphology, all neurons in the rat LC contain NE making the widespread presence of this neurotransmitter and its biosynthetic enzymes, such as DBH (Mazzanti et al., 1987), the defining property of the rodent LC. Notable however, is the limited population of small, round neurons, which have also been identified within LC, that express γ -aminobutyric acid (GABA). Located in the rostral pole of the LC, this

area is described as more neurochemically heterogeneous, containing many non-NE neurons intermingled with typical NE LC neurons, and potentially resulting in properties not seen in the caudal LC regions. Together the compact nucleus of the rat LC, as well as the subcoeruleus, are responsible for noradrenergic innervations to the forebrain, cerebellum, brainstem and both dorsal and ventral horns of the spinal cord (Clark & Proudfit, 1991; Schuerger & Balaban, 1993).

Neurons originating in the LC project to a vast number of diverse brain regions and cover more area than any other noradrenergic structure. In fact, Foote et al. (1983) described the LC as the “most ubiquitous of all neural projection systems in the CNS,” with innervations on all levels of the neuraxis. Dendritic processes of LC neurons have been shown to extend for hundreds of micrometers outside of the compact nucleus, with axonal projections extending throughout the neuraxis, from the spinal cord to the neocortex (Foote et al., 1983). The dendritic processes congregate in two specific pericoerulear areas – rostroventro-medial to the LC and extending from the caudal juxtapeduncular boundary, near the fourth ventricle (Gallyas, Gorcs, & Merchenthaler, 1982). To identify the nature of these processes, Shipley et al. (1996) analyzed the tissue following DBH and TH-labelling. Over 500 processes were labelled between the two abovementioned areas, with all but 3 reported as dendrites. Thus, it appears that while LC proper is a small nucleus, LC neurons have a considerable postsynaptic surface, which extends hundreds of micrometers beyond the confines of the nucleus itself and is preferentially distributed in these two discrete pericoerulear zones (Cintra, Diaz-Cintra, Kemper, & Morgane, 1982; Grzanna & Molliver, 1980; Swanson, 1976).

A more regimented organization of LC has been established based upon the targeting of its efferents (Loughlin, Foote, & Bloom, 1986). For instance, ventral regions of LC give rise to the descending projections that target the spinal cord and cerebellum; meanwhile more dorsal regions of LC send projections rostrally toward the forebrain. The anterior portions of LC tend to innervate both the hypothalamus and thalamus, while dorsal (Loughlin, Foote, & Bloom, 1986) and posterior regions of LC project to hippocampus and other areas of cortex and forebrain. Interestingly, through retrograde tracing studies, it has been shown that individual LC cells have the ability to project to multiple areas (Mason & Fibiger, 1979; Room, Postema & Korf, 1981). More recent evidence has suggested that individual LC neurons have the capacity to innervate functionally related, yet discrete elements within ascending sensory pathways (Simpson et al., 1997); thus they display a propensity to send axon collaterals to multiple targets (Berridge & Waterhouse, 2003). This phenomenon has been supported by electrophysiological methods, in which a single LC cell was antidromically activated from multiple sites (Nakamura & Iwama, 1975; Takigawa & Mogenson, 1977).

1.4.1 LC Projections to Hippocampus

LC is the sole provider of NE to the hippocampus, with its projections accounting for all NE input to the hippocampal formation. The LC neurons which project to the hippocampus are primarily located in dorsal regions of the LC (Mason & Fibiger, 1979) and are debated to originate from either the fusiform cell population (Haring & Davis, 1983) or the larger, multipolar LC neurons (Loughlin, Foote, & Grzanna, 1986). NE

projections from LC collectively travel to the hippocampal formation through the dorsal tegmental and medial forebrain bundles (Brown, 2003). From this point on, there are three distinct routes through which the fibers are said to reach the hippocampal formation. A portion of the fibers enter through the ventral amygdaloid pathway and temporal pole, meanwhile the dorsal collection of fibers continues rostrally; the remaining fibers enter through the fornix and cingular pathway. NE fibers from all of these projection pathways innervate DG (Cintra et al., 1982; Shimizu & Imamoto, 1970).

1.4.2 LC Activity Patterns: A System of Arousal

The LC-NE system is activated in parallel with the autonomic system in response to biological needs; this response can be spontaneous or in relation to unexpected, threatening or noxious stimuli. These responses can also be classically conditioned to relevant stimuli (Sara & Segal, 1991). LC neurons can fire in two distinct activity modes, referred to as tonic and phasic. Tonic activity is characterized by lower frequency, sustained and regular firing patterns; it is often state-dependent, with the highest firing rates occurring during waking, and the lowest during slow-wave and REM sleep (Hobson, McCarley, & Wyzinski, 1975). Under conditions of high arousal or stimulation, tonic firing rates as high as 15Hz have been reported for limited durations (Foote, Aston-Jones, & Bloom, 1980), however the extent to which these rates of high tonic activity can be sustained remain unclear (Berridge & Waterhouse, 2003). While in an awake state, and dependent upon the subject's situational context, LC can present either firing mode. While the subject is engaged in everyday behaviors such as eating and grooming, LC

cells will fire in a slow, rhythmic pattern around 0.5-4Hz (Aston-Jones & Bloom, 1981a). LC neurons can also display phasic alterations in firing rates, typically in response to salient sensory stimuli (Aston-Jones & Bloom, 1981a); phasic responses typically have a short latency and are composed of a brief burst of firing, following by a more prolonged period of suppression. These bursts of cell firing are typically produced when stimuli interrupt stereotypical behaviors, with the presentation of a novel stimulus or in response to noxious stimuli, such as toe or tail pinches (Foote et al., 1980); however this phasic burst-pause firing can also be habituated with repeated stimulus presentation (Aston-Jones, Rajkowski, Kubiak, & Alexinsky, 1994).

In addition to having a role in memory consolidation, NE released in forebrain structures aids in sensory processing, cognitive flexibility and executive functioning (Sara & Bouret, 2012). Jouvett (1969) first reported variation in LC activity occurring in accordance with the state of vigilance. In rodents, it has since been shown that the rate of LC firing varies according to the level of arousal and attentiveness (Bouret & Sara, 2004). The burst firing mode of LC has also been shown to occur in response to cognitively complex stimuli. For instance, in rodents, LC bursting has been shown to occur in response to salient stimuli presented during classical conditioning, and to subsequently cease when the conditioning of the stimuli becomes well-established. Interestingly, the burst firing pattern will return should there be an interruption in conditioning and thus a change in the meaning of the stimulus, such as extinction or reversal (Sara & Segal, 1991); these instances have also been shown to release NE at post-synaptic LC targets (Dalley et al., 2001). A study by Aston-Jones et al. (1994)

showed that in monkeys, the presence of LC bursts was predictive of their successful performance on auditory and visual tasks; additionally, it has been reported that any pharmacological manipulations resulting in a decrease in this firing pattern, would decrease performance levels (Aston-Jones, Rajkowski, & Kubiak, 1997). This area of research suggests a role for LC in attention, a role that has been supported by studies in rodents. For instance, a study by Sara, Dyon-Laurent and Herve (1995) showed that performance of rodents on novelty seeking tasks was dependent upon the integrity of the LC; either blocking β -receptors or activating the inhibitory α_2 -receptors resulted in a cessation of investigative behaviors, and consequently a decrease in performance on the afore-mentioned behavioral tasks.

1.4.3 Identifying Cells of the LC

LC cells are targeted as lying slightly lateral to and just beneath the fourth ventricle (Eschenko & Sara, 2008), at a depth of roughly 5.2 to 6.5mm below the surface, dependent upon the angle of entry (Bouret, Duvel, Onat, & Sara, 2003). In anesthetized animals, LC neurons exhibit a slow, spontaneous firing frequency between 0 to 5Hz, as well as broad action potentials (600 μ s - 2000 μ s) and burst discharges that are followed by a period of decreased firing, often referred to as the “burst-pause” response (Berridge & Waterhouse, 2003; Korf, Bunney & Aghajanian, 1974; Vankov, Hervé-Minvielle & Sara, 1995). Typically, LC neurons will exhibit these phasic bursts of activity in response to strong nociceptive stimuli, such as a paw or tail pinch (Aston-Jones & Bloom, 1981b). However, in the present study, a lack of response to this criterion was not considered

exclusionary, as numerous extraneous variables could influence this parameter, including a potential habituation of the phasic LC response to the toe pinch stimulus.

Due to the nature of the multiple unit recordings from a low impedance tungsten electrode, cluster cutting techniques are often employed to perform waveform separation from the multi-unit recordings. In the present study, this was accomplished exclusively by cluster cutting, in which waveform parameters, such as peak time and amplitude are measured, allowing unique waveforms to be assigned to their own cluster. The technique of cluster cutting allows not only for cellular waveforms to be separated from noise, but also assists in the separation of waveforms representing different cellular subpopulations of LC. This consequently allows for a better representation of the effect of light activation on specific LC cell subpopulations, which may be present in the recording.

1.5 Long-Term Potentiation (LTP)

Bliss and Lomo (1973) published the first record of LTP following their experiments in the rabbit dentate gyrus. Their results indicated two mechanisms to be responsible for long-lasting potentiation: an increase in the efficiency of synaptic transmission at the perforant path synapses, and an increase in overall granule cell excitability. Interestingly, a year prior to this publication, Seymour Kety (1970) had predicted a role for NE in LTP, proposing the activation of LC to be capable of initiating memory storage due to the capacity of NE to elevate cAMP levels through β -receptors. He theorized that “the state of arousal by means of adrenergic input to each (cerebral, hippocampal and cerebellar cortices) may serve to concurrently reinforce and consolidate

the significant sensory patterns, the affective adaptations and the motor programs necessary in the learning of a new adaptive response” (p. 331). As mentioned previously, LC has since been consistently shown to respond to both novel, significant and noxious stimuli. (Aston-Jones & Bloom, 1981b; Aston-Jones et al., 1994; Cedarbaum & Aghajanian, 1978; Chen & Sara, 2007; Sara, Vankov, & Herve, 1994).

1.5.1 NE-Induced LTP (NE-LTP) in Hippocampus and the Role of LC

NE is known to play a role in inducing both short- and long-term potentiation in the hippocampus (Neuman & Harley, 1983). As a neuromodulator acting on adrenergic receptors, NE can have effects both pre- and post-synaptically. Pre-synaptically, NE can enhance the release of glutamate from the PP axons, while post-synaptically, it can enhance strength of the signal, by strengthening the synapses on the dendrites of the granule cells; both of these occurrences would increase the probability of the firing of the granule cells of the DG (Segal & Bloom, 1976). Both the LC and its production of NE are essential components of the natural occurrence of NE-induced potentiation in the hippocampus. When naturally activated, numerous noradrenergic LC neurons release NE among the granule cells of the DG (Aston-Jones & Cohen, 2005).

Research has repeatedly shown that an increase in the concentration of NE within the DG will have a facilitating effect on the electrical responses generated in the DG (Lacaille & Harley, 1985; Neuman & Harley, 1983; Stanton & Sarvey, 1985b). The first report of NE- potentiation in the DG was noted following *in vivo* iontophoresis of NE (Neuman & Harley, 1983). Following a single NE application, the effect lasted between

thirty minutes to eleven hours, and was subsequently referred to as NE-LLP. Since this study, this phenomenon has been replicated in a variety of ways. It has been reliably reproduced with both in vivo preparations with anaesthetized subjects (Harley & Milway, 1986) as well as in vitro (Lacaille & Harley, 1985). This has additionally been demonstrated in awake, behaving animals, however the effect of the LC-NE system upon potentiation in awake animals was less clear. Klukowski and Harley (1994) resolved the discrepancies by investigating the effect of similar glutamate activation on the PP-evoked potential in an awake rat. They reported that glutamate activation of LC in their awake subjects induced both short- and long-term population spike potentiation, which did not appear to differ from that seen in the anesthetized rats.

NE typically enhances the effect of PP glutamate release on the granule cells; that is, it increases granule cell excitability, a parameter indexed by a larger amplitude of the population spike of the PP-evoked potential. However, this NE-LTP typically occurs with variable effects on the EPSP, or without increasing the synaptic strength, a parameter indexed by EPSP slope (Walling & Harley, 2004). In vivo studies performed on anesthetized rats have repeatedly shown that activation of the LC via electrical (Dahl & Winson, 1985) and glutamate manipulations induces potentiation of the population spike. LC-electrically induced short-term potentiation was demonstrated by Harley, Milway and Lacaille (1989), as well as by Babstock and Harley (1992); meanwhile, in chemical manipulations, LC has been activated by both glutamate (Harley & Milway, 1986; Harley et al., 1989) and orexin (Walling, Nutt, Lalies, & Harley, 2004). In vitro studies have demonstrated NE-LTP of the PP synaptic strength in the DG as well as the increase in

population spike to be dependent upon β -receptors and coupled to the elevation of cAMP levels (Dahl & Sarvey, 1989). Research by Lacaille and Harley (1985) also used brain slices with a direct application of NE, and found potentiation effects to be specifically dependent upon β -noradrenergic receptors in the DG. In this research, it was first shown that while potentiation could be mimicked with use of a β -receptor agonist, known as isoproterenol, it was inhibited with the use of a β_1 -receptor antagonist, known as timolol. Importantly, it was also noted that the application of an α_1 -receptor agonist had no effect, thereby indicating potentiation in the DG to be dependent upon only the β -noradrenergic receptors (Lacaille & Harley, 1985). These results have since been consistently replicated. Stanton and Sarvey (1985a) tested this effect with another β -receptor antagonist, metoprolol, in the brain slice and found that it too inhibited LTP. Meanwhile, propranolol, a nonspecific β -receptor antagonist, prevented LC activation from initiating potentiation in the DG (Harley & Milway, 1986; Harley et al., 1989; Swanson-Park et al., 1999; Walling et al., 2004). Since the potentiation seen in these research models can be blocked by the local application of a β -receptor antagonists to the DG (Harley & Evans, 1988) it follows that local NE is directly responsible for the effect (Klukowski & Harley, 1994).

While the actions of NE through β -receptors have long been implicated in mammalian memory, a subset of data has suggested short- and long-term memory may be dependent upon distinct biological mechanisms (Izquierdo, Ibanez, Gonzalez-Badillo & Gorostiaga, 2002; Sullivan & Sagar, 1991). Walling and Harley (2004) investigated the duration of NE-LTP over extended periods of time; their research investigated the effects

of glutamatergic activation of the LC on granule cell excitability and synaptic plasticity over what was classified as short term (3 hours) and long-term (24 hours) periods. Results displayed an increase in population spike amplitude at both short-term and long-term intervals; however, they also indicated that while an increase in synaptic strength, as indicated by EPSP slope, occurred at 24 hours, it did not occur during the three hours immediately following LC activation. This was in accordance with similar results in *Aplysia*, in which the occurrence of cAMP-dependent long-lasting synaptic facilitation was not preceded by short-term facilitation (Emptage & Carew, 1993). These findings were in agreement with the theory of distinct biological mechanisms, with synaptic potentiation initiated by the LC-NE system selectively supporting longer-term memory.

1.6 Electrophysiology in the DG

Electrophysiological field potential studies allow experimenters to monitor and explore the firing patterns of cells within many areas of the brain. For the purposes of the present experiment, the electrophysiological index is an evoked field potential generated by a brief stimulation to the axons of the PP, and generating a characteristic alteration of the electrophysiological signal in the DG.

1.6.1 Evoked Potential Analysis

An electrical pulse delivered to the axons of the PP induces their release of glutamate at their synapses with the dendrites of DG granule cells (Stanton et al., 1989)

and produces a characteristic evoked potential waveform. When examining the PP-evoked potential waveform, three parameters are primarily identified: an EPSP slope and a population spike amplitude, occurring at a specific latency. The EPSP is measured in the initial slope of the waveform response, which follows the PP stimulus artifact. The amplitude of the population spike, measured by the size of the spike from its peak to its trough, is indicative of the number of cells firing in response to the EPSP, with a larger spike representing more cells firing (Andersen, Blackstad, & Lomo, 1966).

1.6.2 PP-LC Interstimulus Interval (ISI) Testing

There has been debate as to the optimal LC stimulation latencies and the parameters which evoke NE release in the hippocampus; especially so, for the optogenetic parameters that may elicit said response. Early research by Bliss and Lomo (1973) reported that the efficacy of synchronous firing of granule cells in the DG which is produced by stimulating the PP, could be enhanced by previous locus coeruleus stimulation. Following this, Assaf et al. (1979) reported that stimulation of the ascending noradrenergic pathway could also increase the efficacy of this input; to accomplish this, they electrically stimulated LC with 5 pulses at a frequency of 300Hz and voltage of 15V

In an attempt to replicate results found by Assaf et al. (1979), Harley, Milway and Lacaille (1989) performed electrical stimulations of LC, while varying the intervals between the LC train and the PP stimulus. To accomplish this, they delivered a 15ms train of 0.2ms pulses at 333Hz to the LC, while systematically varying the ISI from 40 to 20 and 50 to 80ms in 10ms steps. Assaf et al. (1979) had reported the optimal interval

between PP-LC stimulations to be 40ms. This was consistent with the maximum population spike amplitude induced by LC stimulation (Harley et al., 1989) which also occurred at a 40ms ISI. However, they both also noted a clear increase in population spike occurring with a 20ms interval, thereby suggesting the existence of additional, faster fibers to mediate that potentiation. Meanwhile, in terms of EPSP slopes, they reported a trending increase at longer intervals, with the peak increase occurring at 70ms. Their peak potentiation seen at 40ms ISI is consistent with reports that LC neurons are activated antidromically from the hippocampus, cerebellum and cerebral cortices with a latency between 30-70ms (Berridge & Waterhouse, 2003; Nakamura & Iwama, 1975). However, it was speculated that there must be additional, faster fibers, which mediate the weaker potentiation that was reported at 20ms ISI. The authors also examined the effects of propranolol on LC glutamate and LC electrically-induced PP-population spike potentiation. While the effects of NE applied exogenously to the DG cell layer, and the effects of glutamate-induced and electrical stimulation of LC on DG input appeared comparable, when testing the effects with propranolol, the results suggested separate systems. The electrically stimulated potentiation was not altered by propranolol suggesting another system or other neuromodulators such as peptides, mediated both the electrically stimulated long-term potentiation effect and the short-term effect at 40ms ISI.

1.6.3 Paired Pulses: Evoked Potential Analysis

The paired pulse technique is designed to assess the dynamics of neuronal circuits within the dentate gyrus (Brown, 2003) and has been studied previously with

manipulations of LC activation. The effects of paired-pulse stimulation on population spike are a function of its effect on synaptic transmission, and can provide a good indicator of inhibitory function (DiScenna & Teyler, 1994). This technique involves the delivery of a second “pulse” or stimulation to the PP occurring shortly after the first. This second pulse allows experimenters to assess the impact of the first pulse on the neural network; in other words, how it alters the evoked potential waveform produced by the second pulse.

The length of intervals (ms) between the first and second pulses are varied during testing to examine various local circuitry properties. This paired-pulse testing delivered to the PP can thus be analyzed to reveal the phases of short-term change in dentate granule cell excitability by varying the time interval between pulses (Austin, Bronzino, & Morgane, 1989). The degree of facilitation or depression of a synapse can be quantified by computing the paired pulse ratio (PPR); this is defined as the amplitude of the second over the first postsynaptic response and, for the EPSP, is dependent upon the release probability of glutamate (Branco & Staras, 2009). Following a shorter interval (10-40ms), there is typically inhibition of the test pulse. This has been referred to as early inhibition, which lasts for approximately 15 to 40ms after a conditioning pulse; it is characterized by a marked depression of DG cell firing (Austin et al., 1989) and thus decreases of the population spike amplitude or EPSP slope, as indexed by the changed response to a second pulse delivered within this 15-40ms period. This short-latency inhibition reflects the fast GABAergic feedback effects, and the consequent GABA_A-mediated inhibitory postsynaptic potential (IPSP) (DiScenna & Teyler, 1994). The secondary, or facilitatory

phase, occurs following intermediate intervals. There has been some debate however, as to what is considered an intermediate interval, with some research suggesting as little as 30ms (Austin et al., 1989), while others indicate intervals closer to 50-80ms (DiScenna & Teyler, 1994). This secondary phase is generally said to occur between 30 to 200ms after an initial stimulus, and is characterized by an increase in granule cell firing, which thus enhances components of the response as they can recruit NMDA-related excitability changes (Brown, 2003). The late inhibitory phase occurs with longer intervals (>200ms) and is said to be mediated by the late GABA_B IPSP; characterized by a notable depression of granule cell excitability, this phase is known to mediate longer latency inhibitory effects and thus induce longer-lasting, but less potent inhibition (DiScenna & Teyler, 1994).

1.6.4 Input-Output (I-O) Curves: Evoked Potential Analysis

With evoked potential analysis, there are typically input-output current intensity relationships (I-O curves) established at both the start and conclusion of recording. I-O curves illustrate the relationship between the excitatory input to a neuron and the probability it will generate an action potential (Campanac & Debanne, 2008; Daoudal & Debanne, 2003). A neuron's I-O curve is generally represented by a sigmoidal function and is characterized by two components, often referred to as the threshold and the gain. The magnitude of the excitatory stimulus can be varied by adjusting the strength of the electrical pulse delivered to PP; typically, the aim for baselines is an evoked potential with a population spike amplitude that is 50% of the maximal response seen.

Previous research has established that LTP can alter the threshold of the I-O function (Andersen, Sundberg, Sveen, Swann, & Wigstrom, 1980) though the exact mechanisms responsible for the LTP-induced elevations in the I-O curve remain unclear (Campanac & Debanne, 2008; Frick, Magee, & Johnston, 2004). It is postulated that the balance of excitation and inhibition is a contributing factor. For instance, following NE-LTP, it is anticipated that a lower current will be required to elicit the same size of EPSP or population spike as before. This is thought to be due to an increase in the ratio between excitation and inhibition (Carvalho & Buonomano, 2009); one mechanism that may contribute to spike potentiation is that smaller effective stimulation intensities will recruit fewer inhibitory neurons with longer latencies and should thereby facilitate the generation of action potentials (Marder & Buonomano, 2004).

1.7 Optogenetic Control of the LC

The optogenetic approach has enormous potential for basic research; it is a technique which offers the ability to excite and silence, depolarize or hyperpolarize a select group of neurons, with a high degree of precision and in a reversible manner (Pupe & Wallen-Mackenzie, 2015). This is accomplished through activation of light-sensitive proteins, otherwise known as opsins; the responses of which can vary dependent upon the specific light-sensitive channel being synthesized. Opsins can be selectively expressed in targeted cells through the Cre-Lox recombinase system, which drives targeted expression of opsin-encoding DNA. The Cre-Lox system was discovered in bacteriophages and has

been adapted for use in the genetic editing which produces transgenic animals. This system involves the interaction of a Cre recombinase with “Lox” sites, which can be introduced into DNA sequences (Nagy, 2000); then, dependent upon the sites’ orientation, the flanked DNA sequence will either be excised or inverted in the presence of Cre recombinase (Pupe & Wallen-Mackenzie, 2015).

Similar to the present study, the majority of optogenetic research has utilized transgenic mouse and rat Cre-driver strains, in which Cre expression is driven by promoters associated only with a specific neurotransmitter (Pupe & Wallen-Mackenzie, 2015), in the present study, dopamine and NE. The most commonly used strategy for introducing photosensitive channels into neural tissue has been through viral transfection. Viral vectors which drive channel expression can be delivered directly into specific brain regions efficiently and with limited tissue damage (Cardin et al., 2010); specifically, adeno-associated viral coats (AAVs) achieve extensive spread and high expression levels shown to last for years (Zhang et al., 2010). ChR2 is an excitatory opsin channel that mediates cation entry into the cell and is activated by blue light (~475 nm) (Carter et al., 2010; Hickey et al., 2014). Thus, activation of this channel in LC cells would cause an increase in depolarizations, which theoretically would activate LC cell firing and induce the release of NE in the postsynaptic targets of LC, including the hippocampus. Using a different wavelength of light however, can offer the opportunity to activate a different set of photosensitive channels. Halorhodopsins for instance, conduct chloride ions into the cytoplasm in response to yellow light (~570nm); thus in contrast to ChR2 channels,

halorhodopsin permits a negative ion influx into the cell and consequently results in inhibition (Fenno, Yizhar, & Deisseroth, 2011; Hickey et al., 2014).

This exciting new area of neuroscience has several advantages over past methods that used both chemical and electrical manipulation. The infusion of a virus containing the gene for light sensitive channel proteins, subsequently allows for the specific targeting of cells expressing this gene. In the present research, the genes could only be transcribed in TH⁺ cells due to the afore-mentioned Cre-Lox system. This consequently means that only cells which can invert the gene to permit its transcription when the promoter is active will be manipulated, while all other cells remain unaffected; a result which has been demonstrated in various recent studies (Carter et al., 2010; Hickey et al., 2014; Rossi et al., 2015). As most neurons in the brain are not naturally light-sensitive, the selective expression of opsins in targeted areas allow for specific control over the activity of these populations (Zhang et al., 2010). This key advantage provides the experimenter with a degree of spatial control and selectivity that was not possible in the past with other well-utilized techniques. With optogenetics, any alterations to the physiological parameters of interest due to the presence of light, can only come from cells belonging to the targeted brain area. This is of specific relevance to the study of LC, as both spatial control and the degree of selectivity have been significant limitations in the past; this is due to the small size of the LC and the many nearby structures which can respond to chemical or electrical manipulation.

With its enormous potential and with significant developments occurring in the field of optogenetics in recent years, this technique is rapidly becoming the most sophisticated

new method for manipulating the brain. This highly precise technique allows for selective manipulation of specific neuronal activity and allows for examination of intact neuronal circuitry. Additionally, in a clinical setting, having precise control over distinct populations of cells will plausibly lead to the development of new treatments (Aravanis et al., 2007). The present study aims to utilize an optogenetic approach to establish activation of the LC in vivo. Then, in a sequential experiment, it aims to activate LC optogenetically, while also recording LC changes, and monitoring the PP-evoked potential in the DG. The overall goal is to replicate previous successful manipulations of LC with electrical and chemical techniques. The present study will attempt this through infusions of an AAV coat, containing genes for a modified blue light-sensitive channel, targeting LC bilaterally in both male and female TH-Cre Sprague-Dawley rats. With use of a 450nm blue laser, this study aims to selectively activate the LC cells expressing the photosensitive channels, and to consequently produce NE-induced long-term potentiation in the DG.

1.8 Past Optogenetic Research

In recent years, optogenetics research has occurred in a diverse group of animal models, ranging from *Caenorhabditis elegans* (*C. elegans*) to primates (Fenno, Yizhar, & Deisseroth, 2011). In *C. elegans*, the capacity of optogenetic techniques to control both the muscle wall motor neuron and mechanosensory neuron activity were highlighted (Nagel et al., 2005). Additional optogenetic animal models have included flies, zebrafish, mice, rats and primates, with mice being the most widely researched optogenetic model

organism (Fenno et al., 2011). Optogenetic work in rats was initially limited by a lack of viral promoters capable of driving specific expression, however with the development of transgenic rat lines expressing Cre recombinase, the potential for using rat models has increased dramatically (Fenno et al., 2011).

The majority of optogenetic research is completed *in vitro*, analyzing neuronal circuitry in a more controlled environment. These techniques have led to discoveries about complex neuronal circuitry, for instance the co-release of glutamate by dopamine neurons in the nucleus accumbens (Tecuapetla et al., 2010). However, the physiological significance of observed neuronal and synaptic circuitry with *in vitro* preparations is at a disadvantage, since the entire neuronal circuits are rarely preserved, and natural or physiological stimulations are not possible (Sugiyama et al., 2012). *In vivo* preparations offer the chance to overcome these issues. Optogenetic research performed on awake, behaving, transgenic mice has identified causal relationships between specific dopamine neuron activity and reward behavior, revealing the superiority of phasic dopamine release in driving reward behavior (Tsai et al., 2009). In optogenetics research, to study the behavior of awake animals, the conventional method is to connect the external light source to chronically implanted cannulas via optical fibers (Aravanis et al., 2007; Zhang et al., 2010). However, this physical connection has several disadvantages in that it can constrain natural movements and behaviors and/or restrict mobility. To avoid these issues, Rossi et al. (2015) developed a wireless optogenetic system containing compact light emitting diodes (LEDs), which were utilized in mice to study the behavioral effects of stimulating striatonigral neurons. This work found optogenetic activation of neurons in

the striatum to produce robust twitching and circling behaviors, and allowed for the observation of a quantitative relationship between stimulation frequency and twitching rate to be established.

In anesthetized animals, *in vivo* optogenetic modulation has been employed with optrodes: devices composed of fiberoptic cables and tungsten electrodes (Fenno et al., 2011). Several studies, including one by Carter et al. (2010), have experimented with optogenetic manipulation of the LC in transgenic tyrosine hydroxylase-Cre recombinase (TH-Cre) mice. Similar to the present experiment, these mice received infusions of ChR2 photosensitive channels via an AAV2/5. Their objective was to identify a causal role of the LC-NE system in the promotion and maintenance of wakefulness. To test this, they recorded activity in the prefrontal cortex while employing bidirectional optogenetics in LC; that is, they inhibited LC neurons with halorhodopsin and stimulated them with ChR2. From this they concluded the LC initiated wake episodes, with stimulation causing immediate sleep-to-wake transitions and reducing the amount of time subjects spent sleeping. In an additional *in vitro* preparation, they found stimulations of 10ms blue light pulses directed at the LC reliably produced single spike action potentials. Although the role of LC in arousal is well known, the opportunities afforded by research due to optogenetic techniques suggest LC is finely tuned to influence wakefulness, with subtle variations in stimulation frequency or duration producing behavioral effects.

Another recent publication by Hickey and colleagues (2014) in rats using lentivirus also reported success with optogenetic control of the LC, specifically investigating the known role of LC in the descending pain control circuit (Jones, 1991;

Millan, 2002). They aimed to replicate electrical and chemical manipulations of the LC, which have reported reductions in the response to temperature related pain in rats (Jones, 1991; Jones & Gebhart, 1986). Again similar to the present study, the rats in this experiment were infused with a virus expressing ChR2 photosensitive channels. Not only did they report LC cells to be driven strongly by 30mW of continuous blue light stimulation and accordingly the pain response to be altered by light activation, but they reported the nature of the response to be dependent upon the specific area of LC neurons that were stimulated. As previously mentioned, while LC cells are typically considered homogenous with respect to their neurochemistry, they can be divided into several subgroups based upon cell morphology and efferent targets (Aston-Jones, 2004; Berridge & Waterhouse, 2003). In this case, the specific projections linked to pain control are predominantly located in the ventral areas of LC and in the subcoeruleus. Their experiment showed dorsal LC neuronal activation to be anti-nociceptive, but ventral LC neuronal activation was pro-nociceptive. This surprising result was only possible through the use of the optogenetic approach, which improved the selectivity of activation targeting.

The recent successes of optogenetic techniques are very promising. However, it is these specific successes in the optogenetic activation of LC that further support the foundation upon which the present experiment is based. These experiments have demonstrated that neurons of the LC can be activated by light pulses, as well as driven by continuous light stimulation; they have also shown successful downstream effects of LC activation by way of immediate sleep-to-wake transitions, increases in wakefulness and

variations in the observed pain response. Thus, based upon the successes of the aforementioned research, the optogenetic activation of LC cells in the present experiment should not only result in increased firing of LC neurons themselves, but in NE modulation of PP glutamate effects in the DG, including the increased excitability of DG granule cells, as indexed by population spike amplitude, and as reliably produced via electrical and chemical manipulations (Assaf, 1979; Dahl & Winson, 1985; Harley & Evans, 1988; Harley & Milway, 1986; Harley & Sara, 1992; Walling & Harley, 2004; Washburn & Moises, 1989).

1.9 Objectives

The purpose of these experiments was to gain insight and experience with the optogenetic manipulation of LC, and the consequent effects that could be produced on various aspects of the PP evoked potential of the DG. We also aimed to gain insight into the modulatory responses of the well-studied pathway from LC to DG, with optogenetic activation; specifically by varying the interval between a single light pulse and an electrical stimulation delivered to the PP. We hypothesized that if sufficient uptake of our viral construct into LC cells could be achieved via infusion, this would result in successful optogenetic activation of LC neurons, and the consequent induction of NE-LTP during electrophysiological recording. Specifically, this research sought to investigate whether previous models of LC activation and in vivo NE-LTP could be replicated through optogenetic manipulation of LC neurons in anesthetized rats.

CHAPTER 2 – MATERIALS & METHODS

2.1 Subjects

The subjects were 4 male and 17 female TH-Cre Sprague Dawley rats weighing 315-610 grams, aged 4 to 13 months at time of electrophysiology recording. The rats were bred from homozygous TH-Cre males, obtained from Sage Laboratories (Boyertown, Pennsylvania, USA) and wildtype females, obtained from Charles River (Saint-Constant, Quebec, Canada). These rats were genetically modified to ensure only TH⁺ cells were capable of uptake and expression of a photoactivatable channel gene, which was delivered by viral infusion. The rats were housed in individual cages on a reverse light-dark cycle, and received food and water *ad libitum*. All procedures were approved by the Institutional Animal Care Committee, and followed the guidelines of the Canadian Council on Animal Care.

Subjects in this experiment were categorized into two groups: the LC-ChR2(h134r) channel activated group (experimental group) or light controls (control group). Subjects in the experimental group had a successful viral infusion and successful placement of the light probe within the boundaries of LC. Meanwhile, those classified as the light controls also received the viral infusion but had unsuccessful gene expression and/or unsuccessful light probe placement, that is, outside the boundaries of LC.

2.2 Virus

The photoactivatable channel gene was delivered by infusion near the LC as part of a gene construct, packaged in an adeno-associated viral coat (AAV2/8). The infusion solution contained the following viral coat and enclosed gene construct: AAV8-Efla-DIO-eChR2(h134r)-EYFP-WPRE; with a titer of 1.20^{14} and a working solution of $\sim 5^{12}$ vector genome (vg)/ml. Within the viral coat was a gene construct under the control of an elongation factor 1 alpha promoter, and gene expression was restricted to TH-Cre positive cells by the double-floxed inverse open reading frame (DIO) insertion element. The genes expressed were comprised of a modified blue light-sensitive channel (ChR2(h134r)) that produces larger peak current. Compared to the normal ChR2 channel, our variant, ChR2(h134r), has a modest reduction in desensitization, a slightly increased light sensitivity and a slower channel closing (Nagel et al., 2005; Lin, Lin, Steinbach & Tsien, 2009; Lin, 2011); this increases photocurrents and allows the channel to be more temporally precise than ChR2 (Lin et al., 2009). The genes also expressed an enhanced yellow fluorescent protein gene (EYFP) coupled to the channel gene. The latter permits visualization of the location and level of channel expression. The woodchuck hepatitis post-transcriptional regulatory element was a standard inclusion to enhance overall gene expression. The AAV infusion material with its associated genes were provided by Dr. Karl Deisseroth's lab at Stanford University.

2.3 Optogenetic Experimentation

2.3.1 Virus Infusion Surgeries

All instruments were sterilized prior to each use with the Germinator 500 glass bead sterilizer (CellPoint Scientific, Gaithersburg, MD, USA). The rats were anesthetized with isoflurane (15%), and left until they were unresponsive to both toe and tail pinch. They were also given subcutaneous injections (0.1mg/kg body weight) of Meloxicam (Metacam, Boehringer Ingelheim Canada Ltd., Burlington, ON, Canada) analgesia (diluted to 0.25mg/ml in sodium chloride). The surgical area on the rat's head was then shaved, lidocaine anesthetic was applied to both ears to prevent irritation, and tear gel was applied to keep their eyes from drying out during surgery. Next, the rats were placed in a stereotaxic apparatus in the skull flat position, atop a heating pad to maintain their internal temperature at approximately 37°C. The surgical area was cleaned with a Betadine microbicide soap, followed by 70% isopropyl rubbing alcohol and a Betadine microbicide solution. A surgical incision was then made along the skull from the anterior bregma suture lines to the posterior lambda sutures, and the area was subsequently cleaned. Stereotaxic coordinates were taken for bregma, from which locations of LC were determined (12.0mm posterior and both 1.2mm and 1.3mm lateral) bilaterally in both hemispheres. The coordinate locations were then marked, holes were drilled with a mounted surgical drill to expose brain tissue, and the holes were cleared of debris.

At an angle of 20° anterior to the vertical, an internal cannula was then lowered to

a depth of 5.5mm below surface and a 0.5 μ l aliquot of the appropriate virus was infused at both LC coordinates, bilaterally, for a total of 1.0 μ L per hemisphere. In addition to the virus, for 11 rats, 0.07 μ l of fluorescent beads (1-5 μ m; 407-445nm excitation-emission spectrum; Cospheric, Santa Barbara, CA, USA) were infused at each coordinate to mark the specific infusion's location. All infusions were completed using a Hamilton 1.0 μ l syringe over the span of 5 minutes (0.1 μ l/min), using a NE-4000 programmable 2 channel syringe pump (New Era Pump Systems Inc., Trumbull, CT, USA). Of the 21 rats who received viral infusions, nineteen were bilaterally infused with 1 μ l of AAV8 Ef1a-DIO eChR2 (H134R)-EYFP virus (Deisseroth, K., Stanford University, Stanford, CA, USA) diluted 24x in sterile water, while two rats were infused with 1 μ l of the same virus diluted 6x in sterile water. An additional 5-10 minutes was given to ensure the entire volume of virus was infused before the internal cannula was removed. To cover the exposed brain post-surgery, small pieces of Surgifoam absorbable sponge (SAS, West Columbia, SC, USA) were placed in the holes, and the incision was closed with five to six sutures (wax coated, braided silk Sofsilk sutures SS-684; Covidien, Saint-Laurent, Quebec, Canada). Rats were then put in a clean cage, placed on a heating pad and monitored until they awoke. Finally, each rat was given subcutaneous injections of Meloxicam analgesia (0.1mg/kg body weight) for two consecutive days following surgery.

2.3.2 Virus Uptake

Following their infusion surgeries, the rats were once again housed in single cages, given food and water *ad libitum* and kept on a reverse dark-light schedule. All rats had an incubation period of at least four-weeks post-surgery, to permit adequate levels of channel expression in LC cells.

2.3.3 Electrophysiology

Optogenetic experimentation on the rats was performed 4 to 37 weeks following infusion of the virus. The rats were anesthetized with 15% urethane (approximately 1ml/100g), and monitored in their cage until no longer responsive to toe or tail pinches. The rat was then placed in a stereotaxic, skull flat position, and its body temperature was maintained at 37°C. A similar incision was made along the length of the skull from anterior to posterior; all stereotaxic coordinates were obtained for bregma, from which locations of the relevant targets were calculated and marked: DG (3.5mm posterior and 2.0mm lateral), PP (7.2mm posterior and 4.1mm lateral) and LC (12.0-12.8mm posterior and 1.3mm lateral). For all subjects except two, optogenetic activation was carried out in the left hemisphere. The remaining Surgifoam absorbable sponge was removed from the previously drilled LC holes; additional holes were drilled with a hand-held surgical drill, and all holes were then cleared of debris to expose clean, unobstructed brain tissue. Finally, a skull screw was placed in the contralateral hemisphere, anterior to the bregma suture line, and both the skull screw and stereotaxic apparatus were grounded.

2.4 Experiment 1

2.4.1 LC Optogenetic Manipulation and Recording

In accordance with the electrophysiology set up outlined above, for this experiment, holes were drilled to target LC only. The optrode assembly was hand constructed prior to each use; a 400 μ m glass optic fiber (Thorlabs Inc., Newton, NJ, USA) was securely aligned contiguous and posterior to a tungsten electrode (2-3 μ m, 4Meg; FHC, Bowdoin, ME, USA) (see Figure 3A) with the electrode protruding approximately 50-100 μ m ventral to the optic fiber (see Figure 3B). The assembly was then aligned with designated LC coordinates (12.0-12.8mm posterior and 1.3mm lateral of bregma) and lowered at a 20° angle, to 6.1-6.9mm below brain surface until putative LC cells could be identified. The putative LC cells were examined utilizing both the audio-monitor and oscilloscope and were identified by several criteria, including a slow spontaneous firing frequency, broad action potentials and a response to pinch. The optic fiber was connected to a 450nm laser diode fiber light source (Doric Lenses, Quebec City, Quebec, Canada) via a patch cord, which in turn was connected to a computer running the Doric Lenses software to control light parameters.

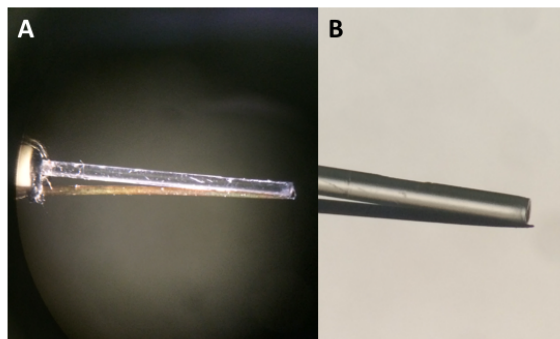


Figure 3. Manual assembly of the optical fiber and recording electrode.

Cells firing within the vicinity of the tungsten electrode tip were recorded by DataWave, allowing for later analysis of each cell's unique waveform parameters, as well as its firing frequency before, during and after the light stimulation. The responses from the recording electrode were collected using SciWorks (DataWave, Loveland, CO, USA) and the input was digitized at 20kHz. Input was band pass filtered from 600Hz-3kHz, and was collected with 10s sweeps, with an average program processing time of 26ms in between.

2.4.2 Optogenetic Activation of LC

To test light activation of the LC and cellular responses to light within each subject, the stimulating light (450nm) was programmed to produce short trains. These light sequences employed 10Hz, 30ms wide pulses of 150mA light, with 60-70mW of light delivered at the end of the optrode. These trains of light activation lasted for either 5s or 10s. Each light trial was separated by at least two minutes; this allowed for a pre-

light period of resting cellular activity, as well as a post-light period to allow the cells to return to baseline levels of firing.

2.4.3 Data Analysis

2.4.3.1 Optogenetic Activation of the LC: Analyzing Cell Responses

Analysis thresholds were set to only count cells at least 1.5x larger in amplitude than background; relevant features of cell waveforms were then extracted by DataWave's autosort protocol, based on six dimensions: peak time, peak amplitude, valley 1 amplitude, valley 2 amplitude and two principal components. Unique cellular waveforms were then separated and assigned to their own cluster. Next, frequency histograms were completed within DataWave for each light trial and each unique waveform respectively; these histograms provide a count of cells firing per second, with one minute baselines collected both before and after the light protocol. Frequency histograms were then completed in GraphPad Prism (GraphPad Software Inc., La Jolla, CA, USA) to compare the firing rate of LC cells before, during and after each light protocol and determine if there was any change in activity.

2.4.3.2 Identification of Putative LC Cells.

All cellular waveforms recorded from each subject were analyzed for several key parameters, including amplitude (μV), peak latency (μs), half width (μs) and asymmetry.

These values were then averaged according to the respective experimental conditions, and the waveform most consistent with these average values was then chosen as representative of its condition. Amplitude was defined as the voltage difference between the waveform's valley (minimum point) and the second maximum, while peak latency reflects the time between those two points. Half-width was defined by the width of the spike half way between the maximum and minimum points. Asymmetry was calculated as the ratio of amplitude of the second maximum point to the amplitude of the first maximum (Weir, Blanquie, Kilb, Luhmann, & Sinning, 2014). Of the waveforms identified within each subject, the specific waveforms which were selected for inclusion in our analysis, best reflected the known characteristics of an LC cell: broad action potentials and a slow firing rate of <6Hz.

2.4.4 Histology and Immunohistochemistry

Following experimentation, subjects were sacrificed via transcardial perfusion with 0.9% saline and 4% paraformaldehyde, and then received cervical dislocation. The brains were stored in refrigerated 4% paraformaldehyde for at least 24 hours, and then refrigerated in 20% sucrose (made in 0.1M phosphate buffer) for at least three days. Finally, the brains were flash frozen in methyl butane, and stored in a -80°C freezer until processed. The brains were sectioned coronally for all relevant, targeted areas, at 30µm using a Leica CM3050 S cryostat; sections were then stored in polyvinylpyrrolidone (PVP) storage solution until immunohistochemical analysis was performed. Alternating sections were stained using a Nissl procedure for perfused tissue, in order to verify

placement of electrodes within targeted structures. This procedure entailed first dehydrating and rehydrating the tissue with ethanol (100%, 95% and 70%) and xylene, followed by a quick wash in distilled water and then five minutes in 1% cresyl violet. This was subsequently followed by washes in distilled water, 1% acetic acid and distilled water again, before a final series of dehydration steps and cover-slipping with Permount (FisherChemicals, Fair Lawn, NJ, USA).

Utilizing the alternating Nissl sections to verify, six sections of LC, as well as two sections with the deepest probe placement if they did not coincide, were then selected for immunohistochemical analysis. Cells of the LC were visualized using a monoclonal antibody raised in mouse against DBH (Millipore, Etobicoke, Ontario, Canada). Free-floating sections were washed with Tris buffer (0.1M, pH 7.6) three times, at five minute intervals to remove any remaining fixative. They were then transferred by brush to new wells and washed with 1% hydrogen peroxide in Tris buffer for 30 minutes. Several washes followed, beginning with Tris for 5 minutes, Tris A (0.1% Triton X in Tris buffer) for 10 minutes and Tris B (0.1% Triton X + 0.005% BSA in Tris) for 10 minutes. The sections were next incubated for one hour in 10% normal donkey serum (Jackson ImmunoResearch; West Grove, PA, USA) diluted in Tris B, to bind non-specific antigens. Following the incubation period, sections were once again washed in Tris A for 10 minutes and Tris B for 10 minutes, and were then incubated in primary antibody at a 1:10 000 dilution in Tris B (2-7 days, ~4°C). Next, sections were washed in Tris A for 10 minutes and Tris B for 10 minutes. Sections were then incubated in a 1:400 dilution of Alexa-555 donkey α -mouse (Invitrogen, Carlsband, CA, USA) in Tris B for one hour;

and finally, washed twice in Tris buffer for 10 minutes consecutively. Sections were then wet mounted onto dipped slides with Tris buffer and cover slipped using Vetashield antifading mounting medium with DAPI (Vector Labs, Burlington, Ontario, Canada).

2.4.5 Image Analysis

All sections that underwent immunohistochemistry were subsequently imaged with an Olympus BX-2 brightfield microscope with a DP-72 digital camera, using the appropriate filters when needed. Images were procured at 4x-20x magnification.

Fluorescent images revealing DBH and green fluorescent protein (GFP) were then overlaid to examine colocalization of GFP expression and DBH-labelled LC cells (see section 2.4.7).

2.4.6 Verification of Placements

The sections of brain tissue stained with 1% cresyl violet were viewed under a microscope to identify optrode and electrode tracts. Once identified, these sections were matched to an anterior/posterior coordinate according to the anatomy of a Paxinos and Watson rat brain atlas (1998). Subjects whose tracts were located within range of the LC ($\pm 300 \mu\text{m}$) were considered successfully targeted, while subjects whose tracts were located outside of the LC served as the light control group. Measurements and calculations were completed to determine the distance in all planes (anterior/posterior, medial/lateral, dorsal/ventral) from the edge of LC. Average placements were then

calculated for the specific subjects in each grouping undergoing statistical analysis.

To be included in the experimental group it was also necessary to have good LC channel expression (see section 2.4.7). In addition to the LC sections, if the sections with the deepest probe damage did not coincide, they were also analyzed for both DBH-labelled cells and GFP expression. The results from both experimental and control groups were compared to determine if light activation had an effect on the firing of LC cells.

2.4.7 Virus Expression and Colocalization

For each subject, three fluorescent images were chosen to represent the anterior, middle and posterior LC. Cell counts were completed on each section for the number of clearly labeled DBH cells and GFP cells (GIMP, Orinda, CA, USA). A semi-transparent marker was placed on each identifiable cell, first for the DBH⁺ cells and then separately for the GFP⁺ cells. These two altered images were then overlaid, and an additional marker was placed where any DBH/GFP markers overlapped by more than 25%. Through this, counts were obtained for the number of DBH⁺ LC cells, the number of GFP⁺ LC cells and the number of cells expressing both. The colocalization percentages were subsequently calculated by dividing the number of co-labelled cells by the total number of DBH⁺ and GFP⁺ cells respectively.

2.4.8 Statistical Analysis.

A repeated measures analysis of variance (ANOVA) was performed to analyze differences in neuronal firing patterns before, during and after the light protocols. Additional testing, by way of paired samples t-tests, were run to examine any specific differences between the neuronal firing patterns just before and during the light protocols; as well as in the time just following the light. Identical analysis was run independently for the experimental and control groups. Criterion was set to $p < .05$ for significance.

2.5 Experiment 2

2.5.1 Optogenetic Activation of LC

Identical to the procedures completed in Experiment 1, to test light activation of the LC specifically within the subjects also receiving the NE-LTP protocol, the stimulating light (450nm) was programmed to produce a short 10s train, involving 10Hz pulses of 150mA light, with a pulse width of 30ms.

2.5.2 Electrical Stimulation of PP and Recording in DG

Following the electrophysiology set up outlined above (see section 2.3.3), placements of the stimulating electrode in the PP and a recording electrode in the DG were aligned specifically according to their coordinates in relation to bregma. The stimulating electrode was an NE-100 concentric bipolar electrode (Kopf, Tujunga, CA,

USA); it was placed 7.2mm posterior and 4.1mm lateral from bregma, and ~3.0mm below surface in the left hemisphere. The recording electrode was a tungsten electrode (2-3 μ m, 4Meg; FHC, Bowdoin, ME, USA) placed 3.5mm posterior and 2.0mm lateral from bregma, and between 3.0-4.0mm below brain surface in the left hemisphere. The recording wire connected the recording electrode to the head stage (Grass Instrument Co., Quincy, MA, USA) and a wire connected to the skull screw was used as a ground.

The depth of the recording electrode was varied to give the largest possible PP-evoked potential population spike. For four of the eight NE-LTP animals, the stimulating current was adjusted to give a PP-evoked population spike of ~50% the maximum amplitude; while for the remaining four, a stimulating current that provided the maximum amplitude for the PP-evoked population spike was used. The PP was stimulated with a 0.2ms pulse every 10s to probe the PP-DG evoked response for the duration of the experiment. The responses from the recording electrode in DG were collected using SciWorks (DataWave, Loveland, CO, USA) and the input was digitized at 10kHz. Input was band pass filtered from 1Hz-3kHz, and was collected with 10s sweeps, with an average program processing time of 26ms in between.

2.5.3 Optogenetically Induced NE-LTP

A baseline recording of the PP-evoked potential waveform was taken for at least 30 minutes of stable recording before light manipulations began. Throughout the recording, three parameters of the waveform were monitored: population spike amplitude, EPSP slope and spike latency (trough). To induce NE-LTP, the stimulating

light was then programmed to produce 10Hz pulses, 30ms wide, of 150mA light for a span of 10 minutes. Following the light manipulations, all activity was recorded for three hours to monitor any effects of the light.

2.5.4 PP-LC Interstimulus Interval (ISI) Testing

To test the effect of varying the interstimulus interval between the electrical stimulation of PP and the optogenetic stimulation of LC cells, a series of subroutines were employed. This additional testing was completed immediately following the cessation of the NE-LTP post-light baseline. Each subroutine produced either a single 30ms or 50ms light pulse directed at the LC and occurring either 20, 30, 40 or 50ms after the .2ms electrical pulse was delivered to the PP. These parameters created a total of eight subroutine variations; each of which was tested 10 times, occurring every 10s, and thus each subroutine spanned a period of one minute and forty seconds. Each subroutine was separated by a period of at least two minutes, to allow the cells to return to baseline levels of firing, and the order was randomized to prevent any potential additive effects from accumulating. During this testing, the evoked potential waveform was once again monitored for any changes in the same three parameters, this time in response to the subroutines. Both the pre- and post-testing baselines for the ISI subroutine testing were 30- minute periods; thus the last 30-minutes of the previously described 3-hour post-light baseline, also served as a pre-testing baseline for this additional experiment.

2.5.5 Paired Pulses and I-O Curves

Each recording session for Experiment 2 began and concluded with the determination of an input-output current intensity relationship (I-O curve), and thus measurements of the evoked potential waveform's population spike amplitude and EPSP slope at differing PP stimulation intensities. At the same time, three sets of paired pulses stimulations at 30ms, 70ms and 200ms intervals, were delivered to PP for each current tested; the stimulation current was manually increased from 100-1000 μ A.

2.5.6 Data Analysis

2.5.6.1 Optogenetic Activation of the LC: Cell Recorded Responses

Analysis for the three shorter trains that proceeded the NE-LTP light protocol was completed identically to the methods outlined in section 2.4.3.2. Analysis thresholds were once again set to only count cells at least 1.5x larger in amplitude than background and relevant features of cell waveforms were extracted by DataWave's autosort protocol. Unique waveforms were then assigned to their own cluster and frequency histograms were once again created in GraphPad Prism (GraphPad Software Inc., La Jolla, CA, USA) to compare the firing rate of LC cells before, during and after each light protocol to determine if there was any change in activity.

2.5.6.2 NE-LTP of the Evoked Potential

The PP-evoked potentials recorded in the DG were digitally stored on a computer using SciWorks DataWave software. Through DataWave analysis programs, values for the spike latency (ms), slope (mV/ms) and population spike amplitude (mV) of the PP-evoked potential were determined for each individual pulse. Data on each of these parameters were recorded every 10s, prompted by the electrical stimulations delivered to the PP. Five-minute averages were then computed and graphed for each individual subject using GraphPad Prism (GraphPad Software Inc., La Jolla, CA, USA). In addition, each of the values were divided by their respective amplification settings and then converted into normalized values, representing a percentage of the 30-minute pre-light baseline. These normalized values were then graphed similarly. The values were compared to determine if there was a change in activity following the light protocol, and if so, whether this change later returned to the original baseline value.

2.5.6.3 PP-LC Interstimulus Interval (ISI) Testing

The data were collected and analyzed in a manner similar to the NE-LTP evoked potential analysis. Data were once again collected every 10s for the population spike and EPSP slope parameters; the specific 10 points corresponding to each subroutine were identified and these values were then converted into normalized values, representing a percentage of the subject's respective 30-minute pre-testing baseline. Identical bar graphs were then constructed for the 30ms pulse subroutines and the 50ms pulse subroutines using GraphPad Prism (GraphPad Software Inc., La Jolla, CA, USA).

2.5.6.4 Paired Pulses: Evoked Potential Analysis

Evoked potential waveform parameters, population spike and EPSP slope, were recorded for the 30, 70 and 200ms paired pulse intervals. The waveform before the interval is referred to as PP1, while the second waveform is referred to as PP2. Calculations were completed for PP2/PP1 ratios (PPRs) in order to determine if the length of interval induced facilitation or inhibition of the second waveform. The data were first analyzed to determine which level of current produced the maximum amplitude, and which level of current produced the half maximum amplitude. Using GraphPad Prism, bar graphs were then created to report the PPR for the level of current which gave the half maximum amplitude in the pre-light (baseline) values. Similarly, the PPR at that same level of current was graphed for the post-light values. Data were additionally analyzed to determine which level of current produced a similar amplitude (mV) post-light to the amplitude produced by the level of current which gave the half maximum amplitude at baseline (pre-light); the corresponding PPR for those levels were reported in what is referred to as the “matched” parameter. Data analysis for population spike and EPSP slope measurements were completed identically; data were also analyzed identically but independently for each respective paired pulse interval.

2.5.6.5 I-O Curves: Evoked Potential Analysis

For the I-O curves, the evoked potential waveform parameters collected for the 30, 70 and 200ms paired pulse intervals were first averaged, and then normalized to give

a percentage of the largest mean value produced by the pre- I–O curve. Both population spike and EPSP slope I-O curves were analyzed identically and graphed with GraphPad Prism. The line graphs exhibit changes between pre- and post- light measurements, with relation to the effect of light testing and the increasing current levels. The effect of NE-LTP on EPSP slope to population spike (E-S) coupling was also examined in a line graph, which analyzed the mean percentage EPSP slope versus population spike amplitude.

2.5.7 Verification of Placements

The sections of brain tissue stained with 1% cresyl violet were viewed under a microscope to identify optrode and electrode tracts, and were matched to an anterior/posterior coordinate according to the anatomy of a Paxinos and Watson rat brain atlas (1998). Measurements and calculations were then completed identically to those completed for Experiment 1 (see section 2.4.6). Average placements were then calculated for the specific subjects in each grouping undergoing statistical analysis.

For stimulating and recording electrodes in PP and DG respectively, tract damage was identified to verify placement within the appropriate, targeted structure. It should be noted however, that correct placement of these electrodes is predominantly indicated by obtaining the desired shape of the evoked potential waveform during electrophysiology.

2.5.8 Statistical Analysis

2.5.8.1 Optogenetic Activation of LC: Cell Recorded Responses

A repeated measures ANOVA was performed to analyze differences in neuronal firing patterns before, during and after the light protocols, identical to experiment 1. Additional testing, by way of paired samples t-tests, was run to examine any specific differences between the neuronal firing patterns just before and during the light protocols; as well as in the time just following the light. For the 10-minute light protocol, an additional paired samples t-test was run to compare the first 10s during the light protocol to the 10s just before the light. Identical analysis was run independently for the experimental and control groups. Criterion was set to $p < .05$ for significance.

2.5.8.2 NE-LTP of the Evoked Potential

Means and SD were calculated for pre-light baseline values for each variable, in each subject (one data point every 10s, resulting in thirty points for each five-minute interval, for thirty minutes). A repeated measures ANOVA was then performed to determine if the introduction of the NE-LTP light protocol produced significant deviation from these baseline values. Criterion was set to $p < .05$ for significance.

The I-O curve data were analyzed with a 2 (pre/post data) x 10 (current level) within ANOVA to determine if there was a significant deviation in evoked potential parameters from the beginning to the end of the NE-LTP experiment. Criterion was set to $p < .05$ for significance.

2.5.8.3 PP-LC Interstimulus Interval (ISI) Testing

The eight subroutine variations were analyzed identically but as two independent groups, the 30ms pulses and the 50ms pulses. All values were first normalized to the average pre-testing baseline value for their respective animal. Means and SDs were then calculated across all four subroutines, for both EPSP slope and population spike amplitude. A repeated measures ANOVA was performed to determine if varying the interstimulus interval between the electrical stimulation of PP and the optogenetic stimulation of LC cells would produce significant deviations. Criterion was set to $p < .05$ for significance.

2.5.8.4 Paired Pulse: Evoked Potential Analysis

Measurements for each paired pulse interval were analyzed identically but independently. All population spike and EPSP slope measurements were first converted into PPRs; means and SDs were then calculated for the LC-ChR2(h134r) channel-activated subjects, at the levels of current identified as having produced their half maximum amplitudes. A one-way ANOVA was then completed on the 3 components of this data previously identified: the PPRs at the level of current producing the half maximum amplitude pre-light, the post-light PPRs at this same level of current, and the PPRs for the levels of current which produced similar amplitudes (in mV) post-light to that given by the half maximum level of current pre-light.

2.5.8.5 I-O Curves: Evoked Potential Analysis

These measurements were analyzed for both population spike amplitude and EPSP slope parameters, across ten levels of increasing PP current stimulation (100-1000 μ A). Population spike amplitude and EPSP slope were once again analyzed in an identical manner, but as independent items. The normalized values produced for each current level, both pre- and post-light testing, were analyzed with a 2x10 within ANOVA to determine if there was any effect of light testing (a pre/post effect), or any interactions present.

CHAPTER 3 – RESULTS

3.1 Subjects: LC-ChR2(h134r) Channel-Activated and Light Control

The subjects were divided into two categories – LC-ChR2(h134r) channel-activated (n=10) and light controls (n=11), based upon the expression of virus by LC cells, and the successful placement of the light probe within the boundaries of LC. To be included in the experimental group, optrode placement was required to be within range of the LC ($\pm 300\mu\text{m}$); it was also necessary to have adequate LC channel expression. To be categorized as a light control, the animal either displayed very minimal expression of virus (GFP) and/or the light probe was not placed within range of LC. One of the 11 subjects initially classified as a light control was ultimately excluded from all analysis due to a disruption of LC cells by the fluorescent beads, thus there was a final count of 10 in the light control group and 20 subjects overall.

The results from both experimental and control groups were identically analyzed and compared to determine if light activation had an effect on the firing of LC cells. As these animals were genetically modified to ensure only TH-positive (TH^+) cells could express the photosensitive channels, light shone on nearby non-TH (TH^-) cells would not encounter light-activatable channels. This was confirmed by the failure to see cell firing changes in those subjects. Similarly, if the viral infusion placements were not within range of LC, and consequently no expression of the virus occurred, there would be no

photosensitive channels present within TH⁺ cells to respond to light. Thus, no effect of the light stimulus would be anticipated, as is the case in the light controls.

3.2 Virus Expression and Colocalization

Immunohistochemical analysis of the LC sections revealed substantial expression of GFP within the confines of LC (DBH⁺ cells), notable in DBH⁺ (LC) cells, as well as in some fibers. The GFP expression was closely tied to the LC in all subjects, with little expression seen in the tissue or in cells adjacent to LC. For some subjects, the sections of LC analyzed by immunohistochemistry did not coincide with the sections containing the deepest optrode placement. In these instances, these additional sections were analyzed identically through immunohistochemistry to ensure the presence of DBH and GFP expression surrounding the optrode placement.

Colocalization counts for each subject were completed to obtain a percentage of DBH⁺ cells expressing GFP, as well as a percentage of GFP⁺ cells expressing DBH. These percentages were then averaged across experimental conditions, to give us a level of colocalization representative of the LC-ChR2(h134r) channel-activated subjects and the light control subjects. The average percentage of DBH⁺ cells expressing GFP was 54.2% (SD = 10.3%) for the LC-ChR2(h134r) channel-activated subjects, and 42.9% (SD = 19.7%) for light controls. Meanwhile, the average percentage of GFP⁺ cells expressing DBH was 61.6% (SD = 5.5%) for LC-ChR2(h134r) channel-activated subjects, and 58.0% (SD = 12.2%) for light controls (see Figure 4).

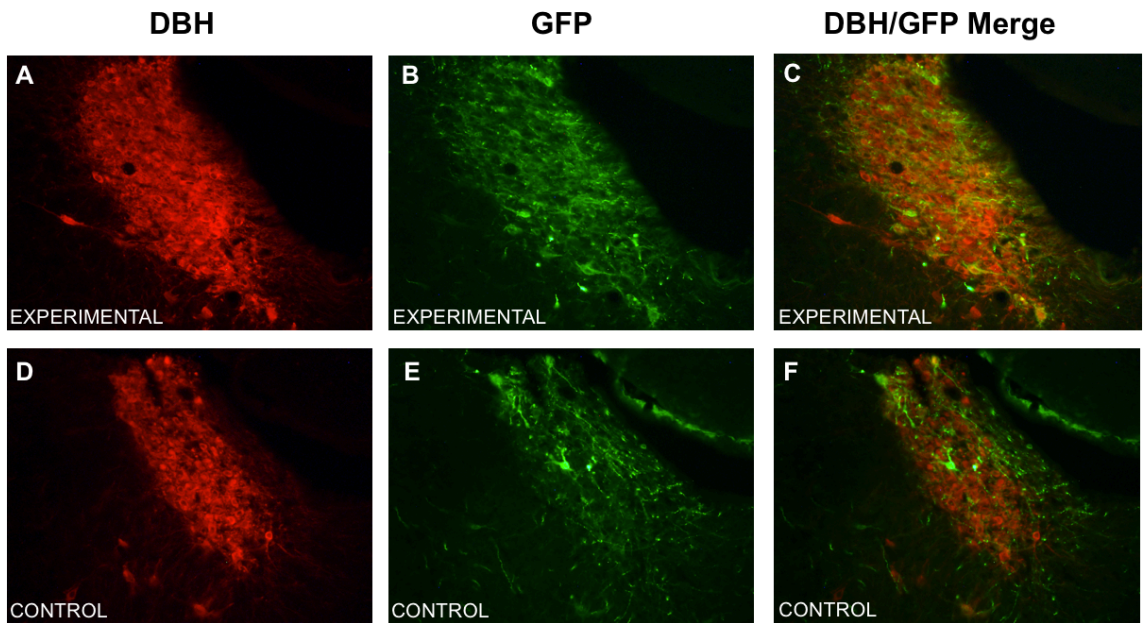


Figure 4. Virus expression and colocalization per experimental condition. Average expression of AAV8-Ef1a-DIO-eChR2(h134r)-EYFP-WPRE in LC-ChR2(h134r) channel-activated (n=10) and light control subjects (n=10) following bilateral LC injections. Tissue sections were chosen from subject with expression levels most representative of and closest to their group averages. At a minimum of four-weeks post-infusion, there is robust, selective expression in cell bodies and processes positive for tyrosine hydrolase, specifically for the LC-ChR2(h134r) channel-activated subjects (*A-C*). In comparison, there is only slightly less selectivity and colocalization in light controls. This is due to most of the control subjects being so labelled because of placement issues. (*D-F*). DBH immunoreactivity is shown in red (*A/D*), virus uptake and EYFP expression is shown in green (*B/E*), and overlaid images (*C/F*) display colocalization.

3.3 Verification of Placements

The average placement of the optrode for both the LC-ChR2(h134r) channel-activated subjects and the light control subjects were calculated in two ways. It was first calculated as an overall average for both groups and additionally, more precise averages were calculated according to the placement for the specific subjects included in each analysis grouping. These specific averages can be found within their appropriate results section, accompanying data from that test. The overall average placement for the light control subjects (n=10) was 4.0 μ m anterior to the edge of LC, 260 μ m lateral, and 470 μ m ventral. Meanwhile, for the LC-ChR2(h134r) channel-activated subjects (n=10), the light probe was consistently within the anterior-posterior confines of LC, placed an average of 20 μ m lateral and 100 μ m ventral (see Figure 5).

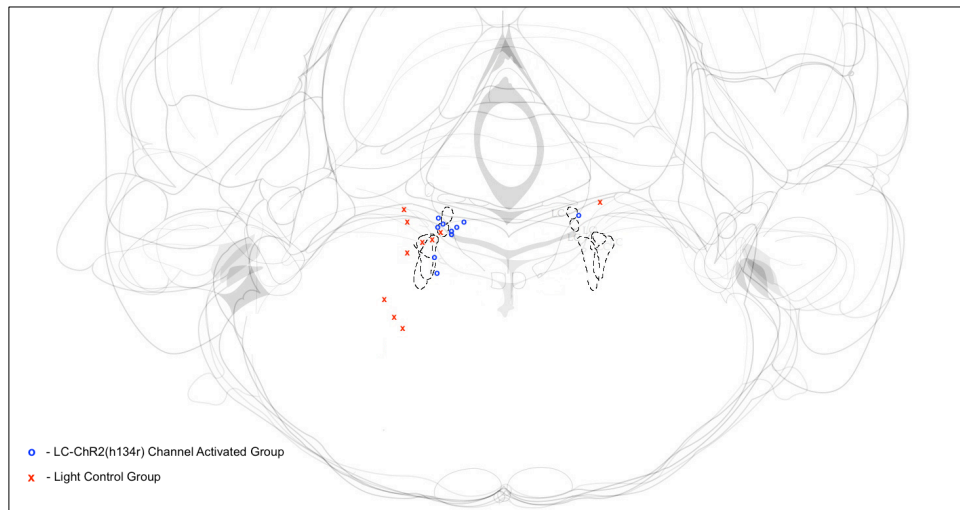


Figure 5. Placement of optrode assembly per subject during optogenetic manipulation. The experimental condition, LC-ChR2(h134r) Channel-Activated subjects (n=10) are represented by blue circles. The light controls (n=11) are represented by red x's. Image adapted from multiple

coronal slice images in Paxinos and Watson Rat Brain Atlas (1998), ranging from anterior posterior coordinates of -8.72mm to -10.30mm from bregma. Dashed lines indicate the confines of LC as seen on each coronal image. In this figure, the control condition includes an additional subject who was later excluded from all analysis.

3.4 LC Cellular Parameters

Descriptive parameters, including amplitude, peak latency, half width and asymmetry, were determined for each LC cellular waveform included in our analysis. These values were then averaged, and the individual waveform with values most consistent with these averages was chosen as the representative cellular waveform for their respective condition.

3.4.1 LC-ChR2(h134r) Channel-Activated (Experimental) Condition

The average experimental LC waveform in this group (n=10) had an amplitude of 64.25 μ V (SD =49.18 μ V), half width of 280 μ s (SD=54 μ s), peak latency of 185 μ s (SD=21 μ s) and asymmetry ratio of 2.07 (SD=6.99). The average pre-baseline frequency of the experimental condition was 3.17Hz (SD = 2.87Hz).

3.4.2 Light Control (Control) Condition

The average control waveform in this group (n=10) had an amplitude of 44.30 μ V (SD =14,13 μ V), half width of 300 μ s (SD=85 μ s), peak latency of 180 μ s (SD=37 μ s) and

asymmetry ratio of 0.245 (SD=0.849). The average pre-baseline frequency of the control condition was 3.61Hz (SD = 2.79Hz).

3.5 Experiment 1

3.5.1 Optogenetic Activation of LC: Cell Recorded Responses

All animals included in this experiment experienced a light protocol during testing; the light parameters utilized were 150mA, 10Hz and 30ms wide pulses. These parameters were run for periods of either 5s and/or 10s, or 10 minutes. Data analysis differs because of the variation in subjects receiving 5s and 10s of light testing and given the 10-minute protocol. The LC response values for each animal represent the neuronal firing frequency of the cellular waveform that best fit inclusion parameters. An average value was then obtained for each group, representing the average neuronal firing frequency of the pre-baseline period, during the light protocol and the post-light period.

A total of fifteen animals received both bilateral AAV infusions, and optogenetic testing with the 5s (50 pulse) light protocol. The average placement of the optrode for the light control subjects (n=8) was 40 μ m anterior to the edge of LC, 300 μ m lateral, and 588 μ m ventral. Meanwhile, for the LC-ChR2(h134r) channel-activated subjects (n=7), the light probe was within the anterior-posterior confines of LC, placed an average of 35 μ m lateral and 50 μ m ventral. The total number of animals having received both bilateral AAV infusions and optogenetic testing with the 10s (100 pulse) light protocol

was also fifteen. Average placement of the optrode for these light control subjects (n=6) was within the anterior/posterior confines of LC, but 225 μ m lateral and 483 μ m ventral. Meanwhile, for the LC-ChR2(h134r) channel-activated subjects (n=9), the light probe was well within the anterior-posterior confines of LC, placed an average of 22 μ m lateral and 72 μ m ventral.

A repeated measures ANOVA on the LC-ChR2(h134r) channel-activated group (n=7), confirmed the 5s (50 pulse) light protocol to result in a consistent and significant increase in LC cell firing during the light ($F_{(2,12)}=4.73$, $p < 0.05$). The average firing rate increased from 1.89Hz (SD = 1.84Hz) to 7.60Hz (SD = 6.93Hz) during the light, and returned close to baseline at 2.94Hz (SD = 2.25Hz) in the 5s following the light. The light controls (n=8) were analyzed independently but identically to the experimental condition. They showed no variation in LC cell firing during the light protocol ($F_{(2,14)} = .105$, $p = 0.901$), and maintained a firing frequency during the light of 1.53Hz (SD = 1.78Hz), which was consistent with both pre-light baseline, 1.68Hz (SD = 1.07Hz) and post-light baseline, 1.55Hz (SD = 1.05Hz) (see Figure 6A)

Meanwhile, a repeated measures ANOVA of the LC-ChR2(h134r) channel-activated group (n=9) also revealed the 10s (100 pulse) light protocol to produce consistent and significant increases in LC cell firing during the light ($F_{(2,16)} = 14.07$, $p < 0.001$). The average firing rate increased from 2.60Hz (SD = 2.47Hz) in the 10s preceding the light, to 10.62Hz (SD = 7.65Hz) during the light, and returned to baseline at 2.26Hz (SD = 1.87Hz) post-light. Further analysis through paired sample t-tests confirmed this significant activation of LC cells by analyzing differences of LC firing

during light, specifically to that of 10s interval preceding ($t_{(8)} = -3.72, p < 0.01$) and following ($t_{(8)} = -3.82, p < 0.01$) the light train. The light controls ($n=6$) were once again analyzed identically and independently, to show no significant variation in LC cell firing patterns during the light protocol ($F_{(2,10)} = .577, p = 0.579$). In the 10s preceding the light protocol, the average neuronal firing rate was 3.40Hz (SD = 0.992Hz), during the light it remained low at 4.37Hz (SD = 3.61Hz) and during the 10s following the light, it was 3.48Hz (SD = 1.72Hz) (see Figure 6B).

The firing frequencies specifically during the 5s and 10s of light were compared with an independent samples t-test. This revealed there to be no significant difference ($t_{(8)} = -0.816, p = .428$), despite a 2.31Hz larger increase above baseline resulting from the 10s light protocol.

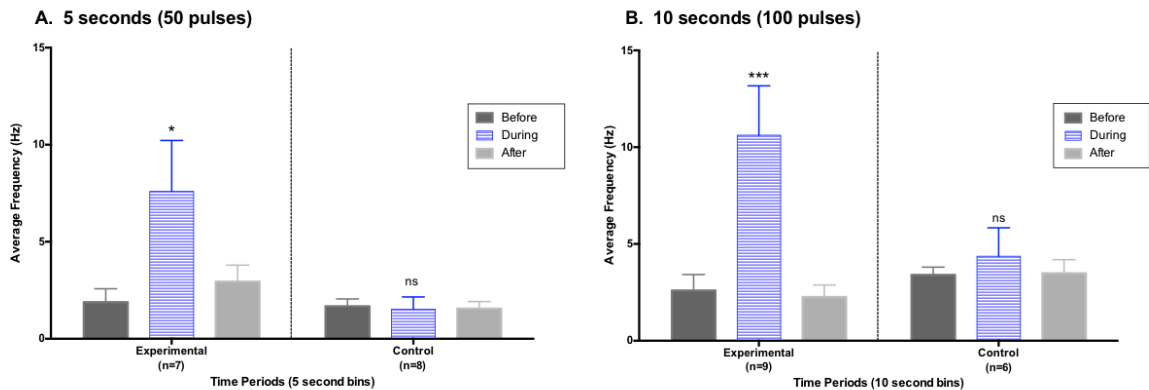


Figure 6. Optogenetic activation of LC with 5s and 10s light sequences. LC cell firing responses to the 5s light protocol (**A**) and the 10s light protocol (**B**). (**A**) During the 5s light protocol, the average LC firing rates of the experimental group ($n=7$) showed an approximate 4x increase, when compared to both the 5s immediately preceding and following the light. The average LC firing rates of the control group ($n=8$) showed no response to the light, retaining a

rate of neuronal firing consistent with both the 5s immediately preceding and following the light. **(B)** During the 10s light protocol, the average LC firing rates of the experimental group (n=9) showed an approximate 3x increase, when compared to both the 10s immediately preceding and following the light. The average LC firing rates of the control group (n=6) showed no response to the light, retaining a rate of neuronal firing consistent with both the 10s immediately preceding and following the light.

3.6 Experiment 2

3.6.1 Optogenetic Stimulation of LC: Cell Recorded Responses

The 10-minute light train was utilized as our NE-LTP light protocol; as such, it was only tested on a subset of animals. Eight animals received both bilateral AAV infusions, and optogenetic testing with the 10-minute light protocol. Six of these animals met the criteria for inclusion in the LC-ChR2(h134r) channel-activated condition. Of the remaining two animals, one was classified as a light control, while the other was the subject excluded from all analysis due to an apparent disruption of LC cells. These eight NE-LTP subjects had also received a 10s light train – and as such, were analyzed as a subset comparison to the larger group of fifteen animals having received the same 10s train.

3.6.1.1 Ten Hz Stimulation: 10s Light Protocol (100 Pulses)

When considering only these six subjects as a subset group, the average placement of the optrode for the LC-ChR2(h134r) channel-activated subjects (n=6), was well within the anterior-posterior confines of LC, placed an average of 58 μ m lateral and 108 μ m ventral. It is also worth noting that although there is only one light control in this group, its optrode placement was consistent with a “hit” to LC; the optrode placement was well within both the anterior/posterior and dorsal/ventral confines of LC, and placed approximately 100 μ m lateral. However, since there was a lack of sufficient channel expression due to the earlier placement of its viral infusion, it acts as a true control.

In the LC-ChR2(h134r) channel-activated group (n=6), the 10s protocol significantly increased the LC cell firing rate from 2.32Hz (SD = 1.72Hz) preceding the light, to 9.88Hz (SD = 8.00Hz) during the light, and returning to baseline at 2.18Hz (SD = 1.44Hz) post-light. A repeated measures ANOVA, analyzing the response of this subset of 6 experimental subjects revealed a significant increase in LC firing during the 10s light ($F_{(2,10)} = 7.24$, $p < 0.05$). Further analysis through paired sample t-tests, confirmed this activation of LC cells by specifically comparing LC firing during the light, to that of 10s interval preceding ($t_{(5)} = -2.73$, $p < 0.05$) and following ($t_{(5)} = -2.69$, $p < 0.05$) the light train. Within this subset of animals, there was only one classified as a light control; while the optrode for this animal was also located within the confines of LC, it was so categorized due to a lack of virus/channel expression. As a result, no statistical analysis could be completed regarding the control response to light stimulation. For this animal,

the pre-light firing rate increased slightly from 2.20Hz, to 5.90Hz during the light, but remained at 5.40Hz post-light (see Figure 7).

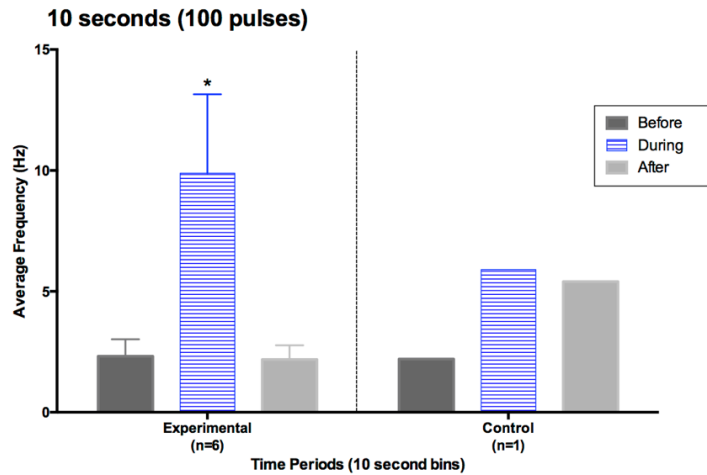


Figure 7. Optogenetic activation of LC with 10s light sequence in NE-LTP subgroup.

LC cell firing responses to the 10s light protocol in rats who also received the 10-minute light protocol. The average LC firing rates of the experimental group (n=6) showed an approximate 5x increase during the light, when compared to both the 10s immediately preceding and following the light. The LC firing rate of the control animal (n=1) showed no significant response to the light, retaining a neuronal firing rate that is relatively consistent with both the 10s immediately preceding and following the light.

3.6.1.2 Ten Hz Stimulation: 10-Minute Light Protocol (6000 Pulses)

Five of the six experimental subjects had a similar pattern of firing changes during the 10-minute light protocol and will be described as a group. One subject had a different pattern of activation and will be described separately. This subject was excluded from the NE-LTP evoked potential analysis as well. As such, average placement for this

amended subset of LC-ChR2(h134r) channel-activated subjects (n=5), was still well within the anterior-posterior confines of LC, but now an average of 90 μ m lateral and 130 μ m ventral.

Due to variation in LC firing patterns over the 10-minute NE-LTP light protocol, the response of LC cells to light was analyzed over the first 10s of the 10-minute block, to confirm consistently effective light activation (see Figure 8). A paired samples t-test compared the first 10s of the light protocol to a 10s interval before the light, and found the experimental condition to show immediate increases in neuronal firing ($t_{(4)} = -3.13$, $p < 0.05$). The LC firing patterns changed from a pre-light baseline of 5.78Hz (SD = 4.36Hz) to 14.72Hz (SD = 10.59Hz) during the light. The light control (n=1) did not show any apparent changes following the commencement of the light, with unaffected firing patterns of 1.30Hz before the light and 1.40Hz during it.

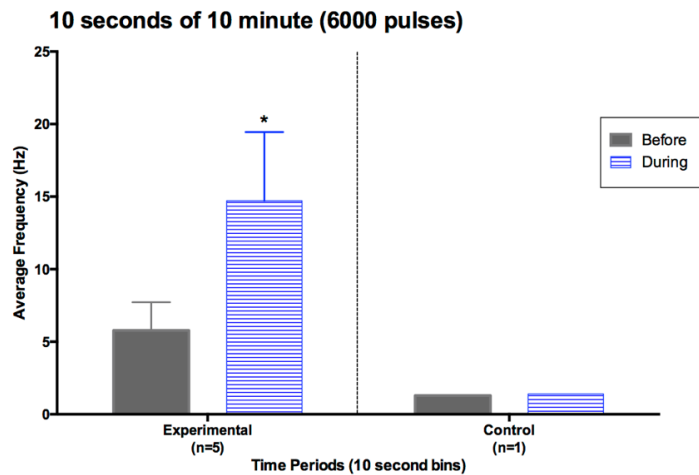


Figure 8. Optogenetic activation of LC in the first 10s of the 10-minute light protocol.

The average LC firing rates of the experimental group (n=5) showed an approximate 2.5x

increase during the first 10s of light, when compared to the 10s immediately preceding it. The LC firing rate of the control animal (n=1) showed no significant response to the light, retaining a neuronal firing rate that is nearly identical to the 10s immediately preceding the light.

Additionally, LC cell firing data for the 10-minute light protocol was organized into one minute averages for the following statistical analyses. In comparison with the two minute intervals preceding and following the 10-minute light protocol, a repeated measures ANOVA showed significant variation ($F_{(13,52)} = 3.81$, $p < 0.0001$) in LC cell firing for the LC-ChR2(h134r) channel-activated subjects (n=5), with a trend towards a linear effect ($F_{(1,4)} = 5.29$, $p = 0.083$). The average baseline for the two minutes preceding the light was 5.84Hz (SD = 6.90Hz), which increased to 9.83Hz (SD = 8.58Hz) during the first two minutes of the light protocol. Following this initial increase, there was a consistent decline in neuronal firing to an average of 1.34Hz (SD = 2.44Hz) for the remaining eight minutes of light activation. This diminished firing rate was also maintained in the two minutes immediately following the light, when the average frequency was 1.02Hz (SD = 2.28Hz) (see Figure 9A). The additional LC-ChR2(h134r) channel-activated subject, which was analyzed separately, showed a contrasting response pattern during the 10-minute light protocol, with a gradual increase in neuronal firing. The average baseline firing rate of the two-minutes prior to light activation was 1.12Hz (SD = 0.264Hz); this gradually increased over the first eight minutes of light, with an average neuronal firing rate of 3.35Hz (SD = 2.43Hz). In contrast to the initial two minute increases for typical LC-ChR2(h134r) channel-activated subjects, this subject exhibited maximal increases in the last two minutes of light, 8.18Hz (SD = 0.587Hz), which

diminished in the two minutes following the light protocol to 5.25Hz (SD = 0.707Hz). The firing rate of this subject also never decreased below baseline, again unlike the characteristic pattern of the NE-LTP experimental group (see Figure 9B). The light control (n=1) did not exhibit a similar variation, although no statistical analysis could be completed (see Figure 9A).

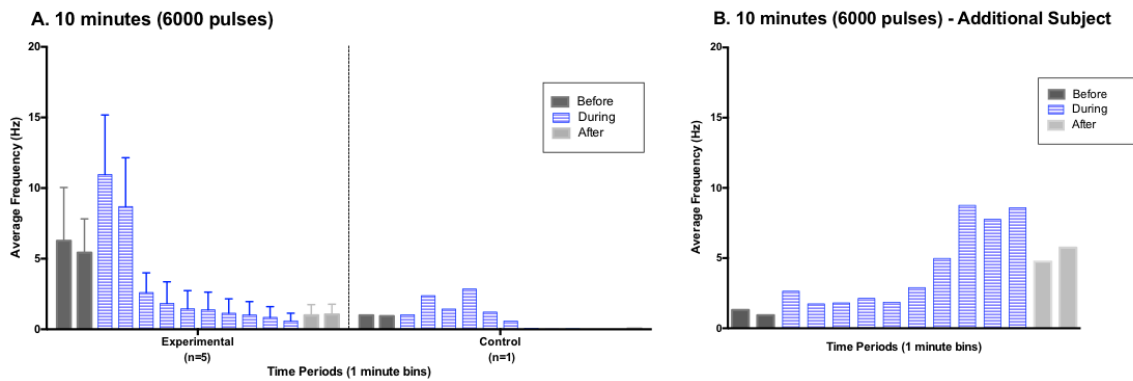


Figure 9. Optogenetic activation of LC with 10-minute light sequence. One minute averages of LC cell firing across the 10-minute light protocol. **A.** The average LC firing rates of the experimental group (n=5) showed an increase during the first two minutes of light, when compared to the 10s immediately preceding it. The LC firing rate of the control animal (n=1) showed no significant response to the light, retaining a neuronal firing rate consistent to that of the pre-baseline. **B.** The additional subject was analyzed separately due to its contrasting pattern of activation, which had a gradual increase in LC firing over the 10-minute light protocol and did not return to baseline firing rates following the light.

When solely analyzing the 10 minutes of light activation, without pre- or post-baseline consideration, a trend toward a quadratic effect was revealed ($F_{(1,4)} = 7.17$, $p =$

0.055) in LC-ChR2(h134r) channel-activated subjects, due to sharp increases in neuronal firing rates in the first two minutes ($F_{(9,36)} = 5.79$, $p < 0.001$), followed by a maintained decrease below baseline; a contrasting pattern was seen in the additional subject although statistical analysis could not be completed. The virus-injected controls display no effect ($F_{(9,9)} = .701$, $p = 0.698$), maintaining an average neuronal firing rate of 1.81Hz (SD = 1.65Hz) throughout the first 6 minutes, before ceasing entirely.

3.6.2 Optogenetically Induced NE-LTP

For NE-LTP evoked potential analysis, it was necessary to exclude an additional subject from the original LC-ChR2(h134r) channel-activated (experimental) group. One subject, as previously mentioned, was analyzed separately from the group due to a contrasting pattern of LC cell activation; meanwhile another subject displayed a distinctive change in evoked potential shape during the recording. As such, both subjects were excluded from the evoked potential parameter analysis, leaving four subjects to be included as the experimental group.

3.6.2.1 Baseline Evoked Potential Parameters

Average baseline descriptive parameters, including population spike amplitude (mV), EPSP slope (mV/ms) and latency (ms), were determined for each subject included in the evoked potential analysis. Values from both experimental and control groups were then averaged to allow for comparison between experimental conditions.

The LC-ChR2(h134r) channel-activated subjects (n=4) had an average baseline population spike amplitude of 3.69mV (SD = 2.32), an average EPSP slope of 5.78mV/ms (SD = 2.51mV/ms) and an average latency of 4.614ms (SD = 0.83). The light control subject (n=1) had an average baseline population spike amplitude of 10.22mV, an average EPSP slope of 8.88mV/ms and an average latency of 4.00ms. Meanwhile, the additional light-activated subject analyzed separately for this experiment, had an average baseline population spike amplitude of 0.15mV, an EPSP slope of 1.72mV/ms and a latency of 4.59ms.

3.6.2.2 NE-LTP: Evoked Potential Analysis

Optogenetic stimulation of the LC resulted in gradual but substantive increases in the DG cell response to PP input over the three-hour post-light baseline, as measured by increases in the population spike amplitude (125.67%, SD = 9.09%). A repeated measures ANOVA confirmed this increase to be significant ($F_{(41,123)} = 2.57$, $p < 0.0001$) (see Figure 10A). All rats in the LC-ChR2(h134r) channel-activated group (n=4) exhibited similar increases over their previous baseline levels. This group also exhibited a minimal but sustained increase in EPSP slope (109.19%, SD = 5.80%); the increase coincided with the beginning of light testing and followed a previously stable baseline of at least 30 minutes. However, a repeated measures ANOVA of the EPSP slope data determined it to be non-significant ($F_{(41,123)} = 0.989$, $p = 0.501$) (see Figure 11A). A lesser amount of GFP expression, as noted in the light control NE-LTP subject, resulted in no apparent effect of the NE-LTP light protocol on population spike amplitude (see

Figure 10B) and EPSP slope (see Figure 11B), although statistical analysis could not be completed. For this control animal, the average percentage increase in population spike amplitude (116.00%) and EPSP slope (101.05%) is very minimal. To reiterate, this lack of overall effect was seen due to a lack of channel expression from an infusion placement issue, and not a misplaced optrode during electrophysiology.

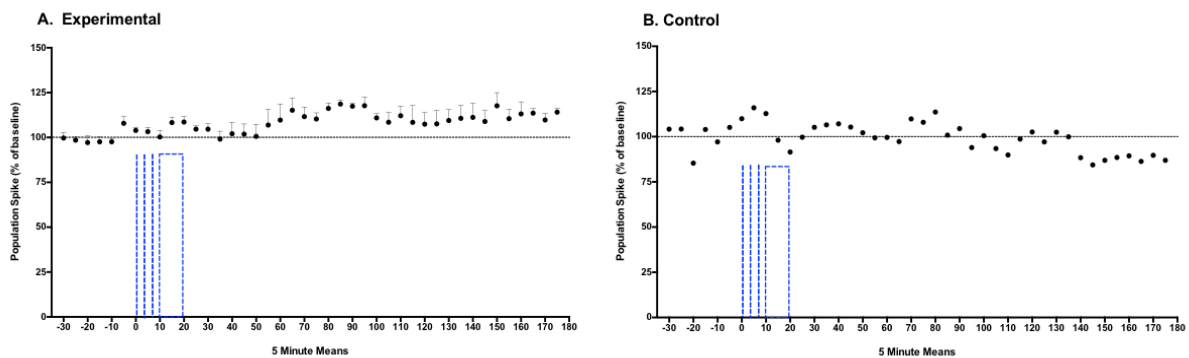


Figure 10. Effect of optogenetically induced NE-LTP on population spike. NE-induced long-term potentiation via electrical stimulation of perforant pathway and optoactivation of locus coeruleus neurons in the anesthetized rat. Five minute averages of evoked potential waveform parameters for 30 minutes prior to optoactivation and 3 hours post-testing. Normalized population spike amplitude graphed as a percentage of the average baseline value. Dotted lines represent short 5 and/or 10s light trains utilized for LC unit activation; dotted rectangle represents the 10-minute light protocol. **A.** In the LC-ChR2(h134r) channel-activated group (n=4), a significant and sustained increase in PP-evoked population spike amplitude developed slowly after LC light activation. **B.** The light-control subject (n=1) presented no distinct increases in population spike amplitude following the 10-minute light protocol.

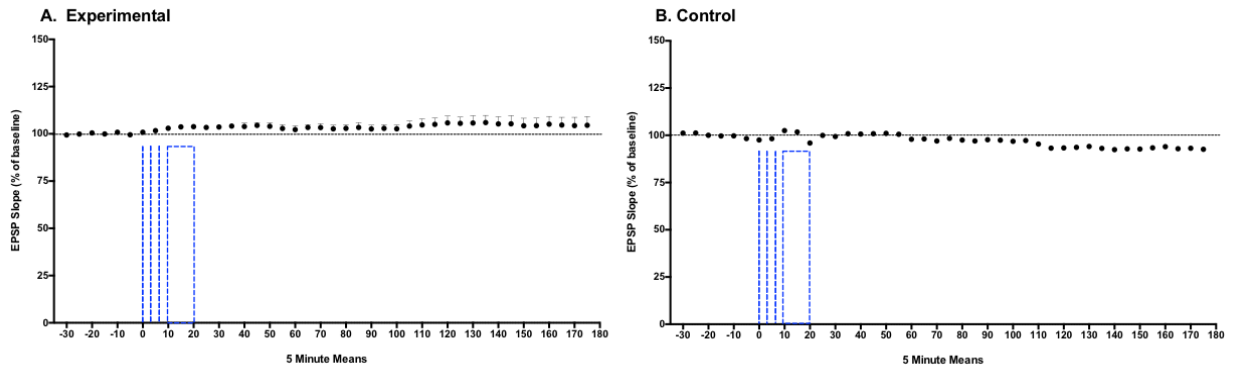


Figure 11. Effect of optogenetically induced NE-LTP on EPSP slope. NE-induced long-term potentiation via electrical stimulation of perforant pathway and optoactivation of locus coeruleus neurons in the anesthetized rat. Five minute averages of evoked potential waveform parameters for 30 minutes prior to optoactivation and 3 hours post-testing. Normalized EPSP slope measurements graphed as a percentage of the average baseline value. Dotted lines represent short 5s and/or 10s light trains utilized for LC unit activation; dotted rectangle represents the 10-minute light protocol. **A.** In the LC-ChR2(h134r) channel-activated group (n=4), there was a sustained, minimal but non-significant increase in EPSP slope following the commencement of light activation. **B.** The light-control subject (n=1) presented no similar increase in EPSP slope following the 10-minute light protocol.

3.6.3 PP-LC Interstimulus Interval (ISI) Testing

Each subroutine produced either a single 30ms or 50ms light pulse directed at the LC and occurring either 20, 30, 40 or 50ms after the .2ms electrical pulse was delivered to the PP. These eight subroutine variations were analyzed identically but as two independent groups, the 30ms pulses and the 50ms pulses. Although statistical analysis

could not be completed on the light control (n=1), there were no similar trends noted in comparison to those present with the LC-ChR2(h134r) channel-activated subjects (n=4). The relation of parameter increases to ISI length variations seems entirely variable, as would be expected with only one control subject (see Figure 12B and D).

For the 30ms pulses, with reference to population spike amplitude, the LC-ChR2(h134r) channel-activated subjects (n=4) presented an average of 102.47% (SD =11.78%) of baseline across all 4 subroutine variations, with a highest increase of 107.87% (SD =24.00%) reported by the 50ms ISI subroutine (see Figure 12A). Despite these minimal increases, there was no apparent pattern to be ascertained with relation to the variation in ISI length. A repeated measures ANOVA reported no significant effect ($F_{(3,9)} = 0.405$, $p = 0.753$). The EPSP slope values for the LC-ChR2(h134r) channel-activated subjects (n=4) presented an average of 99.25% (SD =3.63%) across all 4 subroutine variations, with a highest value of 100.51% (SD = 1.97%) reported by the 30ms ISI subroutine. There was no apparent effect upon slope by any subroutine variation ($F_{(3,9)} = 1.12$, $p = 0.390$) (see Figure 12C). For the 50ms pulses, the LC-ChR2(h134r) channel-activated subjects (n=4) presented an average population spike amplitude increase of 106.21% (SD = 10.09%) of baseline across all 4 subroutine variations. The population spike amplitude seems to increase along with the increasing ISI length, with a highest increase of 116.89% (SD = 13.16%) reported with the 50ms ISI subroutine (see Figure 12A). A repeated measures ANOVA confirmed this increase to be significant ($F_{(3,9)} = 3.982$, $p < 0.05$), with a significant quadratic trend ($F_{(1,3)} = 13.828$, $p < 0.05$). The EPSP slope values for the LC-ChR2(h134r) channel-activated subjects (n=4)

presented an average of 99.55% (SD = 3.16%) across all 4 subroutine variations, with a highest increase of 100.95%(SD = 2.01%) reported by the 50ms ISI subroutine, though this mild increase above baseline was not enough to reach significance ($F_{(3,9)} = 0.554$, $p = 0.665$) (see Figure 12C).

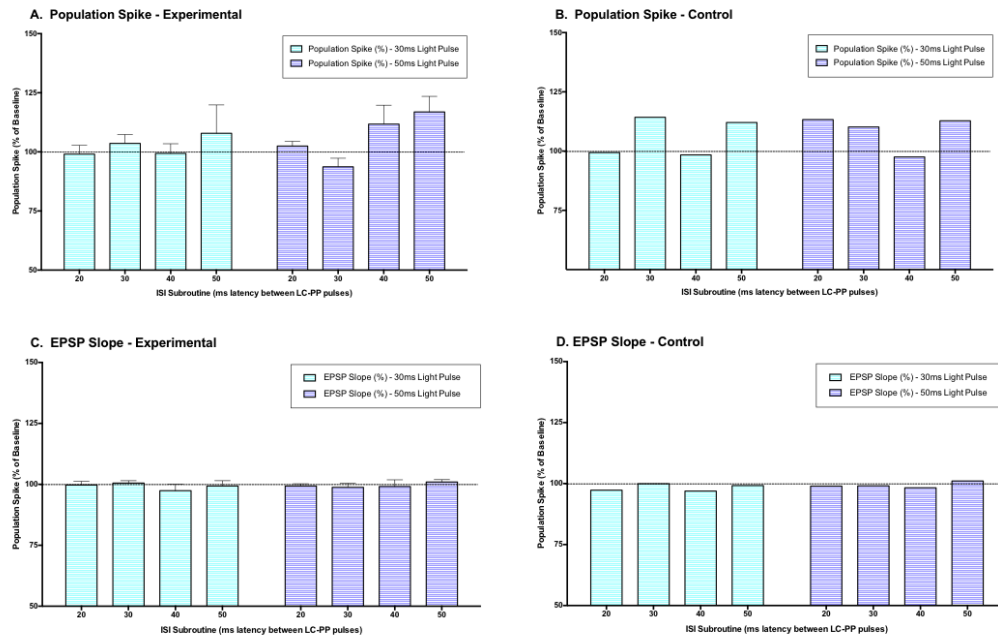


Figure 12. Optogenetic manipulation of PP-LC ISIs. Testing the effect of varying ISI length electrical stimulation of PP and optoactivation of LC neurons in the anesthetized rat. Normalized population spike amplitude and EPSP slope is graphed as a percentage of the average baseline value and average values per group are graphed for each subroutine variation. Light blue represents the 30ms pulses and dark blue represents the 50ms pulses. **A.** Population spike amplitude in the LC-ChR2(h134r) channel-activated group (n=4) significant increased above baseline for the 50ms pulses as the ISI length increased; there was no significant effect seen for the 30ms pulses. **B.** The light-control subject presented no similar trend of increase in population spike amplitude. **C.** EPSP slope in the LC-ChR2(h134r) channel-activated group (n=4), was

minimally and insignificantly increased above baseline for the 50ms pulses as the ISI length increased; there was again no significance seen for the 30ms pulses. **D.** The light-control subject presented no overall effect of increase in EPSP slope.

3.6.4 Paired-Pulses: Evoked Potential Analysis

Evoked potential waveform parameters, population spike and EPSP slope, were recorded for the 30, 70 and 200ms paired pulse ISIs. For the LC-ChR2(h134r) channel-activated subjects, the average level of current which produced the half maximum amplitude in pre-light testing was 425 μ A for the population spike, with an average half maximal population spike amplitude across all three intervals of 1.97mV. Analysis of post-light amplitudes revealed the levels of current required to produce a similar average population spike amplitude (2.35mV) were slightly decreased, with an average level of 375 μ A. Contrastingly, in the only light control subject, a higher level of current (600 μ A) was required post-light, to produce the pre-light testing half maximum population spike amplitude of 2.75mV, which had been produced at 500 μ A. It is worth noting that only the light control subject required a higher level of current post-light to reproduce a spike of similar amplitude to that given by the half maximum level of current pre-light. For three of four LC-ChR2(h134r) channel-activated subjects, the level of current producing the half maximum amplitude spike was similar following light testing, while the other decreased by 100 μ A.

Repeated measures ANOVAs were performed on each paired pulse interval data set; additionally, PPRs were averaged for each parameter and specific paired pulse

interval, to determine if the interval length resulted in inhibition ($PPR < 1$) or facilitation ($PPR > 1$). Only the 30ms ISI produced a significant effect ($F_{(2,6)} = 5.82, p < 0.05$), with an average PPR of 1.48 (SD = 0.864) at baseline and 1.07 (SD = 0.798) post-light at the same level of current. The average PPR given by matched levels of current was 1.11 (SD = 0.784) (see Figure 13A). Post-hoc analysis was then run on this specific interval data set, but the test of least significant difference (LSD) revealed no significant comparisons. Analysis of both the 70ms and 200ms ISIs revealed no significant differences in PPRs across the parameters ($F_{(2,6)} = .489, p = 0.635$; $F_{(2,6)} = .413, p = 0.679$). The 70ms ISI had an average PPR of 2.01 (SD = 0.894) at baseline and 1.77 (SD = 0.347) post-light at the same level of current. The average matched PPR was 1.78 (SD = 0.339) (see Figure 13B). The 200ms ISI had an average PPR of 0.870 (SD = 0.303) at baseline and 0.763 (SD = 0.503) post-light at the same level of current. The average matched PPR was 0.852 (SD = 0.519) (see Figure 13C). Though no statistical analysis was completed on the sole light-control subject, the PPRs for each interval were examined for any indication of potential trends. The 30ms ISI had a PPR of 0.408 at baseline, 1.45 post-light at the same level of current, and a matched PPR of 0.655 (see Figure 13D). The 70ms ISI had a PPR of 0.821 at baseline, 0.911 post-light at the same level of current, and a matched PPR of 1.00 (see Figure 13E). Meanwhile, the 200ms ISI had a PPR of 0.262 at baseline, 0.387 post-light, and a matched PPR of 0.553 (see Figure 13F).

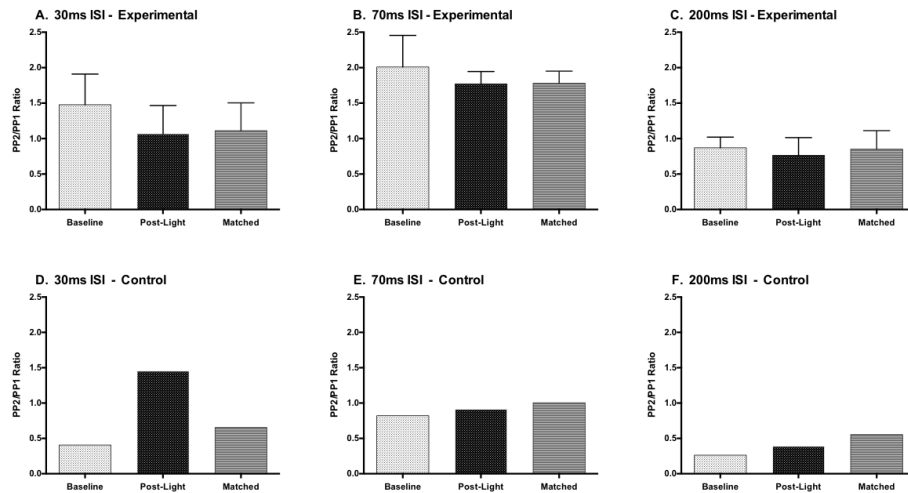


Figure 13. Population spike PPRs. *A.* Average PPRs for the 30ms ISI in the LC-ChR2(h134r) channel-activated group (n=4) showed significant variation, with average ratio values consistently greater than 1. *B.* No significant variation across parameters was found for the 70ms ISI; the average PPRs for this interval were the highest reported, all being greater than 1.5. *C.* No significant variation was found for the 200ms ISI, with average PPRs slightly below 1. *D.* The light-control subject (n=1) showed the most notable difference across parameters in the 30ms ISI, reporting a ratio greater than 1 only in the post-light parameter. *E.* PPRs for 70ms interval in the light-control subject were below 1 for all but the matched parameter, which was slightly increased to a value of 1.00 exactly. *F.* PPRs for 200ms interval in the light-control subject were all consistently below 1.

For the LC-ChR2(h134r) channel-activated subjects, the average level of current which produced the half maximum amplitude in pre-light testing was also 425 μ A for the EPSP slope, with an average slope amplitude across all three intervals of 4.57mV/ms. Analysis of post-light amplitudes revealed the levels of current required to produce a

similar average slope amplitude (4.64mV/ms) were slightly increased, with an average level of 475 μ A. The light control subject also required a higher level of current (600 μ A) post-light, to produce the pre-light testing half maximum EPSP slope amplitude of 6.10mV/ms, which had been produced at 500 μ A. For two of four LC-ChR2(h134r) channel-activated subjects, the level of current producing the half maximum EPSP slope amplitude was retained following the light, while one decreased by 300 μ A and the other increased by 500 μ A.

The statistical analysis for the EPSP slope parameters was identical to that of the population spike amplitude, with repeated measures ANOVAs performed on each paired pulse interval data set and averaged PPRs for each parameter and specific paired pulse interval. However, none of the three paired pulse intervals produced a significant effect in the LC-ChR2(h134r) channel-activated subjects (n=4). Despite being significant in the population spike parameter for the 30ms ISI, PPR differences across EPSP slope parameters were found to be insignificant, ($F_{(2,6)} = .581$, $p = 0.588$), with an average PPR of 0.862 (SD = 0.0664) at baseline and 0.881 (SD = 0.0300) post-light at the same level of current. The average PPR given by matched levels of current was 0.847 (SD = 0.0734) (see Figure 14A). Analysis of both the 70ms and 200ms ISIs similarly revealed no significant differences in PPRs ($F_{(2,6)} = .702$, $p = 0.532$; $F_{(2,6)} = .962$, $p = 0.434$). The 70ms ISI had an average PPR of 0.895 (SD = 0.0761) at baseline and 0.959 (SD = 0.0314) post-light at the same level of current. The average matched PPR was 0.916 (SD = 0.0843) (see Figure 14B). The 200ms ISI had an average PPR of 0.815 (SD = 0.709) at baseline, 0.795 (SD = 0.0153) post-light and an average matched PPR of 0.752 (SD =

0.0600) (see Figure 14C). PPRs for the EPSP slope of the light-control subject were also examined for any indication of potential trends. The 30ms ISI reported a PPR of 0.912 at baseline, 0.845 post-light at the same level of current, and a matched PPR of 0.879 (see Figure 14D). The 70ms ISI had a PPR of 0.883 at baseline, 0.828 post-light at the same level of current, and a matched PPR of 0.909 (see Figure 14E). Meanwhile, the 200ms ISI had a PPR of 0.821 at baseline, 0.756 post-light, and a matched PPR of 0.878 (see Figure 14F).

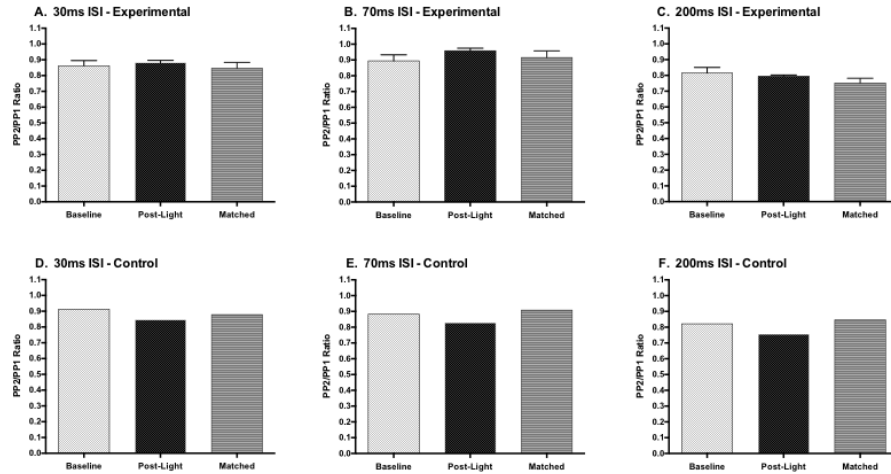


Figure 14. EPSP slope PPRs. *A.* Average PPRs for the 30ms ISI in the LC-ChR2(h134r) channel-activated group (n=4) were very consistent across variables, all less than 1. *B.* No significant variation was found for 70ms ISI average ratios, which were consistently just below 1. *C.* No significant variation was found for the 200ms ISI, with average PPRs slightly below 1. *D.* The light-control subject (n=1) also showed consistent PPRs in the 30ms ISI, reporting ratios all less than 1. *E.* PPRs for 70ms interval in the light-control subject were all less than 1. *F.* PPRs for 200ms interval in the light-control subject were all consistently below 1.

3.6.5 I-O Curves: Evoked Potential Analysis

The I-O curves revealed differences between measurements obtained preceding the light stimulation and again at the end of the three-hours post-light protocol. These measurements were analyzed for both population spike amplitude and EPSP slope parameters, across ten levels of increasing PP current stimulation (100-1000 μ A).

For the LC-ChR2(h134r) channel-activated group (n=4) the population spike amplitude was increased over pre-light (baseline) measures for all currents higher than 200 μ A. A 2x10 within ANOVA found no significant effect of the pre/post variable ($F_{1,3} = 2.951$, $p = 0.184$), but a significant interaction between pre/post and current levels ($F_{9,27} = 2.880$, $p < 0.05$). Additional paired samples t-tests were performed for every current level, however, did not reveal any significant pre/post comparisons (see Figure 15A). The EPSP slope parameter was increased at all but the lowest current, yet there was no significant effect of pre/post measurements ($F_{(1,3)} = 0.316$, $p = 0.614$), nor a pre/post variable and current interaction ($F_{(9,27)} = 0.638$, $p = 0.755$) (see Figure 15C). The light control subject had consistent population spike amplitudes at currents of 400 μ A and below, with decreased amplitudes between 500-1000 μ A (see Figure 15B). However, their EPSP slope showed consistent decreases at all current intensities (see Figure 15D).

The effect of NE-LTP on E-S coupling was examined by analyzing the mean percentage EPSP slope versus population spike amplitude in both LC-ChR2(h134r) channel-activated and light control subjects. The post-light values for LC-ChR2(h134r) channel-activated subjects showed a slight leftward shift, with all currents greater than 400 μ A occurring above the 100% pre- baseline. Meanwhile, for the light control, the

post-light values showed a dramatic rightward shift, with no increase in baseline occurring until the highest currents (see Figure 15E & F)

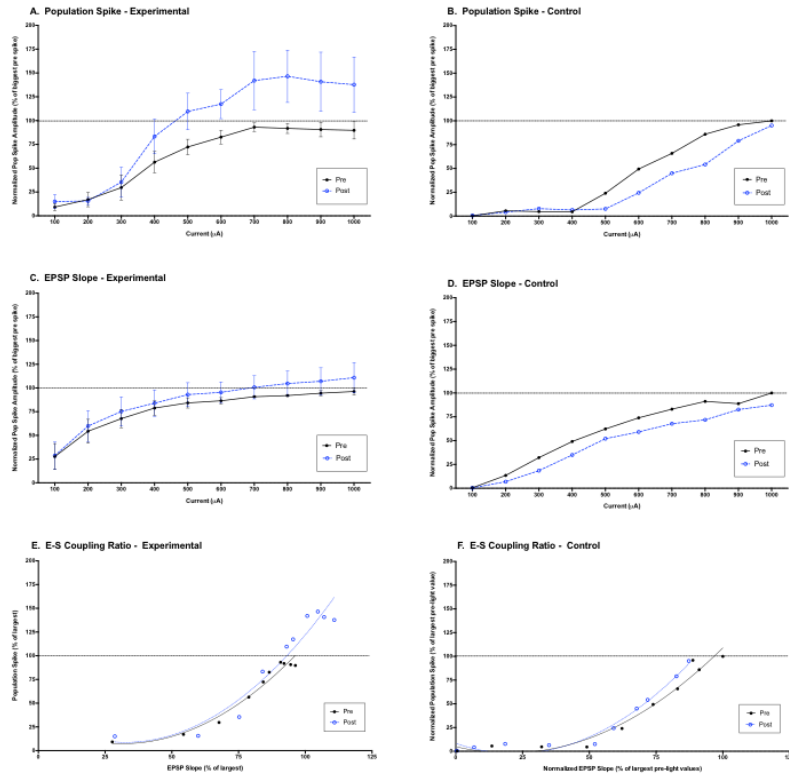


Figure 15. Pre- and post-light I-O curves with increasing PP current stimulation.

Normalized population spike amplitude and EPSP slope measurements graphed as a percentage of the largest value pre-light protocol. **A.** Population spike amplitude in LC-ChR2(h134r) channel-activated group showed significant increases above baseline. **B.** No increases in population spike amplitude seen in the light control. **C.** EPSP slope in LC-ChR2(h134r) channel-activated group was minimally increased above pre-light values. **D.** Light-control subject showed consistent decreases in EPSP slope at all levels. **E.** The post-light E-S coupled values for LC-ChR2(h134r) channel-activated subjects showed increases above the 100% pre- baseline for all currents greater than 400µA. **F.** E-S coupled values in the light control had no increase above the 100% pre-baseline.

CHAPTER 4 – DISCUSSION

4.1 Summary of Major Findings

The purpose of these experiments was to investigate whether previous models of LC activation and in vivo NE-LTP could be replicated through optogenetic manipulation of LC neurons in anesthetized rats. We first examined the uptake and expression of the photoactivatable channel gene, delivered by infusion near the LC and packaged in an AAV viral coat. We examined the viral expression of GFP in LC cells via immunohistochemical analysis, which allowed us to complete counts of the number of LC cells labelled with DBH (DBH⁺ cells), the number of LC cells expressing GFP (GFP⁺ cells) and the number of cells expressing both. We were subsequently able to calculate colocalization percentages, which were on average, between 54-61% for LC-ChR2(h134r) channel-activated subjects and 42-58% in light control subjects.

We next tested the ability of our laser diode fiber light source and optrode assembly to stimulate LC neurons to fire. For LC-ChR2(h134r) channel-activated subjects, in which there was adequate channel expression and the optrode assembly was placed within range of LC, the 450nm light consistently stimulated LC neurons to fire. Two light protocols were tested, which varied only in length (i.e., 5s (50 pulse) and 10s (100 pulse) trains). The 5s light protocol consistently increased the neuronal firing rate, with an average increase during the light of 4x the baseline frequencies, an increase which immediately returned to baseline levels following cessation of light. The 10s light

protocol was slightly more successful; it too produced effects that occurred directly in relation to the light activation and consistently increased the LC neuronal firing rates by an average of almost 6x baseline levels.

We next tested the hypothesis that the LC activation we accomplished, through optogenetic manipulations, could induce NE-LTP of the PP evoked potential waveform in DG. A 10-minute (6000 pulse) light protocol was utilized for this experiment, and resulted in gradual but significant increases in the DG cellular response to PP input, as measured by an average increase of 125.67% in population spike amplitude. A statistically insignificant, but sustained, average increase of 109.19% was also seen in EPSP slope, which coincided with the start of our light protocol. In addition to monitoring the evoked potential waveform, the neuronal firing rates of LC neurons were also analyzed during this experiment. In LC-ChR2(h134r) channel-activated subjects, the 10-minute light protocol dependably resulted in an initial, significant increase in firing rates during the first two minutes, followed by a strongly diminished firing suggestive of feedback inhibition by NE. In one additional subject, analyzed separately, there was a contrasting response pattern seen during the light protocol, with a gradual increase in neuronal firing (see Sections 4.6 and 4.12 for discussion). Following the 3-hours post-light, we tested several subroutines which varied the length between a single light pulse to LC and an electrical stimulation delivered to the PP. Through this, we hoped to gain insight into the responses to optogenetic activation of the well-studied pathway from LC to DG. The subroutines utilizing a slightly longer pulse width of 50ms were favorable,

and displayed a significant increase of up to 116.89% as measured by population spike amplitude and corresponding to increasing lengths of ISI.

4.2 Virus Expression and Colocalization

Colocalization counts completed on all subjects, regardless of experimental condition, proved the success of virus uptake and expression to be primarily dependent upon proximity of the infusions to LC. Of the eleven subjects who received viral infusions in conjunction with fluorescent beads, the average infusion placement was 300 μ m anterior to LC. The subjects categorized as LC-ChR2(h134r) channel-activated (n=6) did have slightly better infusion placement, sitting only 190 μ m anterior to LC on average. One LC-ChR2(h134r) channel-activated subject did not express fluorescent beads however, due to an issue which arose during the virus infusion surgery, but which did not affect the infusion of virus itself. The light control subjects (n=4) received infusions which were on average 420 μ m anterior. Despite the infusion placements typically being anterior to the LC, all but one subject showed colocalization levels of at least 20%. This suggests that an infusion which is proximal to, but not within LC, may be optimal, as it allows for the virus to be taken up by LC cells but avoids any potential physical damage to them, which could occur as a result of the tract and/or potentially the fluorescent beads. In one subject, which was ultimately excluded from all analyses, the infusion placement was exactly within the boundaries of LC. The histology of this subject revealed that the presence of the fluorescent beads seemed to disrupt the LC neurons, thus the results of this animal were deemed unreliable. All other subjects did not

experience this issue, and presented with anteriorly placed fluorescent beads and intact LC neurons, expressing GFP. It is important to note that while adequate virus expression was required for any subject to be categorized as LC-ChR2(h134r) channel-activated, 10 of the 11 light control subjects were so categorized due to misplacements of the optrode assembly during electrophysiology and light activation protocols.

Two average colocalization percentages were calculated per animal: the average percentage of DBH⁺ cells expressing GFP and the average percentage of GFP⁺ cells expressing DBH. On average, the LC-ChR2(h134r) channel-activated subjects boasted higher colocalization percentages of 54.2% and 61.6% respectively, meanwhile light control subjects also reported averages of 42.9% and 58.0%. This level of uptake and expression of the viral construct is quite impressive, especially considering its specificity to TH-positive cells and the anatomical proximity of LC to the fourth ventricle. Despite the variation of 4 to 37 weeks in viral incubation periods between subjects, there was no significant reduction or loss of expression. In fact, the shortest incubation period of 4 weeks and 6 days reported 48% of DBH⁺ cells expressing GFP, and 60% of GFP⁺ cells expressing DBH. Meanwhile, the longest incubation period of 37 weeks and 2 days, reported highly consistent percentages, with reported 44% of DBH⁺ cells expressing GFP, and 59% of GFP⁺ cells expressing DBH. This is consistent with previous literature showing high expression levels of AAVs to last for years (Zhang et al., 2010).

Since all LC cells contain NE however, and thus should be labelled by an antibody against DBH, we would anticipate the specific percentage of GFP⁺ cells expressing DBH to be closer to 100%. Since we did not see these 100% colocalization

percentages, it suggests there may be a form of occlusion or competitive labelling occurring between the DBH and GFP. Notably lower levels of DBH expression can be seen in the vector-transduced GFP⁺ cells, with often the brightest GFP⁺ cells having the lowest DBH signal. There are several potential explanations for this occurrence, which may include toxicity of the vector, or fluorophore competition. As previously mentioned, DBH is an enzyme responsible for converting dopamine to NE (Menniti & Diliberto, 1989). The antibody responsible for labeling DBH for immunohistochemical analysis is referred to as anti-DBH; it is localized and expressed intracellularly, commonly in cytoplasmic vesicles and secretory vesicles (Abcam, 2016a). The areas of cellular localization of DBH are very similar to those of GFP, the fluorescent tag on our viral construct, which allows for estimation of cellular uptake and expression in our LC neurons. As GFP is also expressed intracellularly, competitive labeling or occlusion may occur with DBH, thereby causing the expression of both, to be more challenging and less prevalent. Specifically, the photoreceptors of our viral construct may bind the phox2 transcription factor which regulates DBH expression; thus, with each copy of the vector genome, there are 8 binding sites added. With multiple copies of the vector genome, this could potentially induce a sequestration of this phox2 transcription factor away from the nucleus, which would consequently lead to a reduction in the DBH expression (A. Pickering, personal communication, September 28, 2015). This did not appear to impact the cell's ability to synthesize and release NE however, as is made clear by the success in our reported electrophysiological data; though it would explain the percentages of colocalization seen in our subjects.

In order to address this issue of potential occlusion, we attempted immunohistochemical analysis with a NE transporter (NET) antibody, instead of DBH, to label LC cells. The rationale behind this choice of antibody was simple, we wanted to utilize an antibody which would be less likely to interfere with the intracellular expression of the fluorescent tag of our viral construct; NET, unlike both DBH and TH, does not depend on the phox2 transcription factor for expression. Antibodies for NET are generated against the unique N-terminal peptides of the transporter itself (Abcam, 2016b). NET is an amine transporter, located in the plasma membrane of noradrenergic neurons; it functions as the primary mechanism for the reuptake of synaptically released NE and thus the inactivation of norepinephrine signaling (Zhou, 2004). Since the cellular localization of this NET antibody would thereby be in the membrane, we hypothesized that it would allow for more potent expression of GFP intracellularly, and thus result in improved colocalization percentages. Unfortunately, there was an issue with the manufacturing of this antibody and as a result, the immunohistochemistry was unsuccessful. Due to constraints of time and tissue availability, it was not feasible to attempt a second round of immunohistochemical analysis with a new NET antibody; however, this avenue should be pursued with future research.

4.3 Optimal Light Parameters for LC Activation

Initial research in this lab by an undergraduate student (Wallace, 2015) had similar objectives to the current experiment, but utilized a dual channel programmable LED driver (LEDRVP_2ch_1000) (Doric Lenses, Quebec City QC), which controlled the

light via a patch cord. The output of this LED driver was 2A, which was delivered to the LC in 10Hz sequences via a similar electrophysiological set up. Though it is important to note that the viral constructs were slightly different than those used in the current research, the LED light was shown to have no effect on either LC firing rates or evoked potential parameters. The findings of this study were used as the foundation upon which we built our experimental protocol, aiming to improve upon previous limitations which may have prevented the desired outcomes. In accordance with the future directions stated by Wallace (2015), we upgraded our light output by implementing the 450nm laser diode fiber light source (Doric Lenses, Quebec City QC).

In the very initial stages of this research, we attempted several manipulations to the light protocol in order to determine the optimal parameters for stimulating LC neurons with the laser diode fiber light source. Each light protocol has four parameters: pulse width (ms), frequency (Hz), current (mA) and number of pulses per sequence (i.e., length of sequence). Through experimentation on confirmed LC neurons in an electrophysiological set-up consistent with that of these experiments, we found that pulse widths less than 30ms appeared to be too short to produce activation of LC neurons. The 30ms pulse widths were consistently effective, as were 50ms pulse widths, although they were less reliable when used in sequences or trains of light than 30ms pulses. Due to the success of 50ms pulses seen in this initial testing, this pulse width was later included in the PP-LC ISI testing experiment. Pulse widths of 100ms were also tested, however, were less effective than both the 50ms and 30ms pulses, especially when used in sequence. In terms of frequency, multiple sequences were tested, which varied only in frequencies of

3, 5 and 10Hz. While the 10Hz could reliably elicit a response from LC neurons during the light protocol, the lower frequencies of 3Hz and 5Hz did not elicit consistent responses. This was in accordance with research by Carter et al. (2010), who reported success with frequencies higher than 5Hz. The maximum current output for our laser diode fiber light source was 150mA, which was determined to produce the most reliable and robust activation of LC neurons. The intensity of light delivered by the end of the optrode was additionally measured at our chosen current level, and determined to be reliably between 60-70mW of power. This was more powerful than the light utilized by previous optogenetic work by Carter et al. (2010) and Hickey et al. (2014), which was reported as 20mW and 1-30mW respectively. Various lengths of light protocol were additionally attempted and analyzed; sequences of up to 30 seconds produced reliable and sustained increases of LC neuronal firing rates during the light. The amount of increase in firing rate did not appear to be affected by the length of sequence; in other words, a 5s or 10s light train produced a proportion of firing rate increase comparable to that produced by 30 seconds of light. Sequences lasting 1-minute were less reliable at producing an effect sustained through the light protocol. Since our methodology would require us to run multiple light protocols on the same subject, shorter light sequences were deemed more desirable in an attempt to prevent any potential exhausting of LC neurons. Thus, our optimal light parameters for optogenetic stimulation of LC were determined to be 30ms pulse widths, 10Hz, 150mA and sequence lengths of 5s to 10s.

4.4 Identification of Putative LC Cells

During data analysis, we utilized customized programs within SciWorks DataWave to perform exact cell counts, and subsequently to extract parameters from the cellular waveforms included for analysis. In order to be counted for analysis, cells had to be at least 1.5x larger in amplitude than background; this was calculated manually by tape measurement, and was always completed by the same person to improve reliability. Once thresholds were set to the appropriate levels, the file was played through and cellular parameters were collected as described in the methods, by the autosort protocol. The program presented a suggestion for the organization of waveforms by distinct features, at which point it was at the discretion of the researcher to ensure these categorizations were as accurate as possible. Due to the subjectivity of this step of the analysis, precautions were taken to ensure the cellular waveforms were categorized effectively. The analysis of each file, termed “cluster cutting,” typically took 3-5 hours, and resulted in the discrimination of 1-3 unique cellular waveforms in each subject. Each file was analyzed at least twice, ensuring the results from both analyses were consistent; should there have been discrepancy between the numbers of cellular waveforms identified, the file was analyzed an additional time. The firing frequencies for all waveforms were then translated into frequency histograms, which detailed the specific response for each waveform to any light protocol employed. Additionally, the cellular parameters for each waveform in each respective subject were recorded and analyzed, as described in the methods section. Of the waveforms identified within each subject, only one waveform was included in the data; this analysis was completed without details of

each waveform's response to the light protocols. Comparisons between the waveforms were made based on the amplitude, half-width, peak latency and asymmetry measurements, and the waveform which most accurately illustrated the typical characteristics of an LC cell was chosen for inclusion in the analysis.

In several of the LC-ChR2(h134r) channel-activated subjects, there was an additional cellular waveform which appeared to also be affected by the light protocol. Though this waveform was not included for analysis, it was both an interesting and unexpected result. There are a couple of potential explanations as to how more than one waveform could respond to optogenetic stimulation, when only LC cells had the capacity to express the ChR2(h134r) channels. Since the LC is known to support six unique subpopulations of neurons, it is plausible that both waveforms are LC neurons, with subtle variations in their cellular waveforms occurring as a result of their differing subpopulation. Additionally, as previously discussed, the LC has a multitude of efferents and extensive connections throughout the forebrain; thus the apparent response of an additional waveform may be the result of the subsequent release of NE following optogenetic stimulation of LC, as opposed to a response to the light protocol itself.

4.5 Effect of Optogenetic Activation of LC

An objective of this research was to determine whether optogenetic methods would be capable of activating LC neurons in vivo. This was successfully and reliably accomplished by utilizing short light sequences of 30ms pulse width, at a frequency of 10Hz and current of 150mA. Both 5s and 10s sequences were shown to be effective at

increasing neuronal LC firing rates, with average increases of 5 to 8Hz above baseline levels of firing. These increases were immediate and specific only to the period of light use, producing an increase in cellular activity that could be both heard through the audio-monitor as well as seen on the oscilloscope. The burst of LC unit activity was followed by an immediate return to baseline firing levels in the seconds following the cessation of light; there was no silence or diminution of cellular activity noted across subjects.

For the 5s (50 pulse) light protocol, the LC-ChR2(h134r) channel-activated subjects (n=7) showed consistent and promising increases in response to the light, despite the subtle variations in neuronal firing frequencies between subjects. These natural variations were often due to the specific placement of the electrode tip; for example, if, and the extent to which, it was situated in cell bodies versus dendrites. For subjects with LC cells firing consistently at their typical low frequency of 1 to 5Hz, the light protocol dramatically increased firing rates and often tripled the frequencies, up to between 10 to 20Hz, during the 5s the light was in use. In one subject, the light protocol resulted in an increase of up to 30Hz in the fourth second of the protocol, and 50Hz in the last second; since tonic activation of LC has only been shown up to 15 to 20Hz, these transient increases are likely due to the recruitment of nearby LC cells with similar waveforms. In a few subjects, the baseline firing patterns were more sporadic - likely due to cells being in close proximity to, but not exactly on the tip of the electrode. In these instances, the firing rates were less consistent during both the pre- and post- baseline periods, with firing frequencies of roughly 2Hz every 1 to 3 seconds. This was reliably improved during the light, with cells becoming consistent and firing during each of the 5s of light

protocol. In each instance, the increases and improvements seen to the neuronal firing patterns were tied specifically to the short period of seconds when light was in use. Post-light baseline typically returned to the same firing patterns that had existed prior to the light protocol, with a couple exceptions being that the previously sporadic cells were slightly more consistent following the light.

For the 10s (100 pulse) light protocol, the LC-ChR2(h134r) channel-activated subjects (n=9) showed consistent increases in response to the light. Interestingly, while the 10s light protocol seemed to result in a larger overall increase in firing frequencies above baseline, the patterns of response between subjects that received both a 5s and 10s light protocol was very consistent. For subjects with LC cells firing consistently, the light protocol dramatically increased firing rates, with frequencies increasing from 1 to 5Hz to upwards of 15Hz during the light. In the same subject which boasted the 50x increase in firing frequency during the 5s protocol, this was replicated with the 10s protocol, and once again reached a frequency of 50Hz during the ninth second of light use. One additional subject also reached a firing frequency of 40Hz during the light protocol, with the lowest firing rate being 20Hz. There was no decline in response seen in the later seconds of this protocol, in fact cells often reached their highest frequencies of firing in the last 5s of light use. For subjects with less reliable baseline firing, this light protocol was also able to improve the firing consistency of the cells. Overall, the subjects responded to the 10s light protocol with similar neuronal firing changes to those seen from the 5s of light, the increases and improvements were simply maintained for a longer period of time.

Due to the nature of the experiment, the number of, and specific parameters of light protocols utilized per subject was often varied. In the earlier stages of research, there were often more light protocols performed per subject. As we refined our techniques and the optimal light parameters, we had less need to test protocols more than 1-2 times; thus, subjects tested during the NE-LTP protocols received only 3 short light protocols before the 10-minute, NE-LTP-inducing sequence. Since after each light protocol adequate time was allowed (at least two minutes) for cells to return to normal baseline firing patterns before any subsequent testing could be performed, we aimed to ensure that these variations would have no effect upon the specific results per light parameter. As outlined above, in the early stages of research, some subjects were tested with a variety of light protocols, where this was the case, only those which utilized our optimal light parameters were included in analysis. Furthermore, for any subject who received multiple light protocols with the same parameters repeated, only the data from the first attempt was included in analysis. It is also worth noting that of the two subjects who, as previously mentioned, received viral infusions which were 4x more concentrated than the other nineteen, only one was ultimately classified as an LC-ChR2(h134r) channel-activated subject. This subject received both the 5s and 10s protocol and boasted the largest increases in firing rates of up to 50Hz. The average colocalization counts of this subject were also slightly higher than the overall average for the experimental group, boasting 76% of DBH⁺ cells expressing GFP, and 71% of GFP⁺ cells expressing DBH. Future directions of this research may therefore want to revisit the dilution chosen for the viral

infusions, however the economic feasibility of using a higher concentration would also need to be considered.

In addition to our primary objective of activating LC neurons *in vivo*, we sought to investigate whether previous models of LC activation effects could be replicated through optogenetic stimulation. With research dating as far back as 40 years, activation of the LC has been repeatedly accomplished via electrical (Assaf, 1979; Dahl & Winson, 1985) and chemical manipulations (Harley & Milway, 1986; Harley et al., 1989; Walling & Harley, 2004). A study by Harley and Sara (1992) utilized 100nl ejections of a glutamate solution, and recorded LC activity through an oscilloscope, a set-up which was very consistent with the current experiment. The reported responses of LC cells to their glutamate ejections were also very similar to those recorded in the current experiment; they reported the glutamate to produce an “immediate, brief and stereotyped” response, which included a dramatic increase in cellular activity that could be heard through an audio-monitor. A later study by Walling et al. (2004) revealed orexin application to the LC could also initiate a transient, robust response from neurons. Similar research has described the specific response of LC neurons to the infusion of orexin as a tonic activation, mediated through the slower G-protein-coupled receptors (Kiyashchenko, Mileykovskiy, Lai, & Siegel, 2001). To date, aside from this research, there has been minimal *in vivo* optogenetics literature which has been able to successfully replicate the conditions and results of these past manipulations.

While there is much variability in the current methodology for LC optogenetic stimulation, there are several consistencies to be noted between their results and those of

the current experiment. The specificity of response seen in our subjects was consistent with previously mentioned research in optogenetics by Carter et al. (2010), in which stimulation of LC neurons with light initiated immediate sleep-to-wake transitions. Hickey et al. (2014) also reported success driving LC cells with 30mW of continuous illumination. Though their experimental set up was quite different and described as “in-vivo like,” they reported the capacity to re-stimulate LC neurons with multiple light protocols, following what they described as a “period of relative quiescence.” As mentioned, much of the current work for optogenetic stimulation of the LC is being completed in vitro. Our results provide data consistent with the in vitro results published by Wang, Pinol, Byrne, and Mendelowitz (2014) who reported LC neurons in a current-clamp configuration to reliably double their firing frequency during light activation, as well as Carter et al. (2010) who additionally published an in vitro optogenetic preparation, which reported 10ms pulses of light to reliably produce single action potentials. The current research is thus a beneficial next step for much of the current literature in this area; it demonstrates that in addition to functioning in vitro, the expression and activation of ChR2 in anesthetized rats, is sufficient to generate action potential firing in LC neurons in vivo.

4.6 Use of Optogenetic Activation of LC to Induce NE-LTP

For the NE-LTP optogenetic manipulation, we decided to utilize a light sequence of 30ms pulses, 10Hz frequency and 150mA, continued for 10-minutes along with the PP stimulation. While we considered this might be excessive, we decided that a stronger

manipulation would be preferential to a weaker one. It was also chosen in an attempt to remain consistent with the 10-minute pairing period which has been reported to be important for PP+NE pairing and NE-LTP (Reid, 2006).

The strongly diminished response of LC units following the first two minutes of the 10-minute light protocol was an unexpected but interesting result. The subjects showed steady initial pre-baseline firing rates, which then increased robustly but transiently for approximately 1 to 3 minutes with the commencement of light. Typical frequencies reached during this transient increase were variable between subjects, but were consistently 2 to 3x that of the respective pre-baseline firing rates. Following the brief increase, the frequencies returned to below pre-baseline levels, where they were maintained for the remainder of the 10-minute light protocol. One of these subjects also reported a second interesting phenomenon. The firing frequencies upon commencement of the light, displayed the initial increase, but it was only maintained for less than a minute, after which it returned to baseline for approximately thirty seconds, before increasing again for 1 to 2 minutes. This pattern of robust, transient increases in LC firing frequencies, followed by an equally dramatic decrease, is reminiscent of a larger-scale “burst-pause” response, which is characteristic of activated LC neurons. It also illustrates the ability of optogenetic stimulation to drive LC neurons past their initial refractory period, at least momentarily. The sustained inhibition of these LC neurons following the initial increase is consistent with an apparent self-limiting ability of the LC, which is typically explained by an activation of autoreceptors. These are α_2 -adrenoceptors located postsynaptically on LC dendrites and which function to inhibit the activity of LC neurons

(Scheinin et al., 1994). Past research has also suggested the release of LC-NE to be under the tonic inhibitory control of these receptors (Quintin et al., 1986; Simson, 2001). These autoreceptors can be stimulated by the release of NE from either LC collaterals or dendrites (Pudovkina & Westerink, 2005), and have been shown to subsequently invoke a reduction in LC firing rate when activated (Egan, Henderson, North & Williams, 1983; Williams, Henderson, & North, 1985). Similarly, the blockage of these receptors has been shown to increase LC activity (Simson, 2001). The pattern seen in our LC firing frequencies could thus be the result of this self-regulating mechanism of negative feedback (Aghajanian, Cedarbaum, & Wang, 1977) which is moderated through these autoreceptors. To our knowledge, there has been no other research reporting the tonic, optogenetic activation of LC neurons to induce a self-limiting effect. Carter et al. (2010) however, did report 10-minutes of 15Hz light stimulation to reduce, as opposed to increase, NE levels in the prefrontal cortex. In addition, they reported this stimulation to induce activity inhibition in mice, rather than the activity increases as seen with 3Hz stimulation. Therefore, this avenue of research is definitely one which could be pursued in the future.

As mentioned in both the methods and results sections of this research, there was one subject who displayed an inverse response to the 10-minute light protocol; as such this animal was analyzed individually. Following the start of the light protocol, the previously steady pre-baseline firing frequency began to increase very gradually. The increase became more significant following the half-way point of the 10-minute protocol, eventually increasing to approximately 4x the pre-baseline frequency. This subject also

displayed the second phenomenon, presenting a first increase around 8 minutes of light, a quick return to baseline and a second, very brief, but robust increase back up to 4x baseline values. Overall, the response pattern of this additional subject seems to closely mirror that of the LC-ChR2(h134r) channel-activated subjects except for the long delay. Since both the identical experimental methodology and sufficient expression of ChR2 channels was determined for this subject, it leads us to believe that the diversity in the pattern of increases must result from the specific placement of the electrode. This will be discussed further in section 4.12.

4.7 Effect of Optogenetic Activation of LC on Evoked Potential

Before the commencement of any light protocols, all subjects had to maintain a baseline period of at least 30 minutes, during which the evoked potential parameters remained relatively consistent. Through the initial accomplishment of these stable baselines, it allowed us to have more confidence that any change, no matter how minimal, was a result of the light protocol. Often there would be some initial variability in the evoked potential parameters, and in these situations, the pre-light baseline would be extended until at least a 30-minute period of stability was achieved. The light protocol utilized to induce NE-LTP was a 10-minute (6000 pulse) sequence, following which the evoked potential waveform parameters continued to be collected for 3-hours post-light. Activation of the LC in subjects who also received the 10-minute sequence, was initially

confirmed by shorter sequences of light; this was done to establish that the typical response to LC optogenetic stimulation (as seen in Experiment 1) was also seen in these specific subjects. The testing period for the light protocols was thus twenty minutes from start to finish, allowing for sufficient recovery periods between the short light sequences and before the 10-minute light protocol was started. Data were recorded for each subject for increases in both average amplitude (mV), as well as in normalized percentages above their respective baseline values.

The activation of LC neurons by our 10-minute optogenetic protocol induced a gradual but significant increase in evoked potential, as indexed by the population spike amplitude. The average population spike amplitude for the pre-light baseline period was 3.69mV (SD = 2.33mV); all subjects presented with a sufficiently stable population spike amplitude during this 30-minute period. During the twenty minutes of light protocols, the average population spike increased slightly to 3.88mV (SD = 2.47mV) or 103.95% (SD = 4.82%) above baseline. These average values remained steady for the following thirty minutes, after which an increase commenced gradually. After a period of thirty minutes, the elevation above baseline was evident, and between 30 to 50-minutes post-light, the average population spike was 4.15mV (SD = 2.74mV) or 109.08% (SD = 12.53%) above baseline. Within the next thirty minutes it had again increased to an average of 4.29mV (SD = 2.70mV) or 114.90% (SD = 12.53%) above baseline. At this point, between 80 to 110-minutes post-light, the peak levels of elevation were generally seen. This was sustained for the entirety of the three-hour post-light baseline, with the amplitudes staying elevated consistently at or just below these levels. Average values of 4.19mV (SD

= 2.62mV) or 112.51% (SD = 10.44%) were reported within the last 40 minutes of recording. In comparison, the light control subject reported an average baseline population spike amplitude of 10.22mV. During the light protocol and in the 3-hours following, the amplitudes showed no response to the light, with only natural variations in population spike amplitudes between 11.15mV (109.20% of baseline) and 8.92mV (87.33% of baseline).

While the activation of LC neurons by our 10-minute light protocol induced a minimal increase in the EPSP slope parameter, it was not found to be significant. The onset of this increase however, coincides with the onset of the light protocol, and follows a previously very stable baseline period of thirty minutes. For the LC-ChR2(h134r) channel-activated group (n=4), the average EPSP slope for the pre-light baseline period was 5.78mV/ms (SD = 2.51mV/ms). During the 20 minutes allotted for the light sequences, there was a brief but notable increase, with average values of 5.91mV/ms (SD = 2.54mV/ms) or 102.29% (SD = 0.656%) above baseline. While this transient increase was tied closely to the period of light protocols, it also seemed to induce a more gradual elevation in EPSP slope overall. At 80-minutes post-light, the average EPSP slope had risen to 5.99mV/ms (SD = 2.23mV/ms) or 105.47% (SD = 7.00%) above baseline. The elevation above baseline for EPSP slope may have been minimal, however it was a response to the light which was sustained for the entirety of the post-light 3-hours, and which was not present prior to the light protocol. In comparison, the light control subject reported an average EPSP slope of 8.88mV/ms at baseline. This remained consistent

during the light protocol and in the 3-hours following, with values only ranging between 8.89mV/ms (100.02% of baseline) and 8.26mV (93.03% of baseline).

A main objective of this research was to determine whether previous models of LC activation and in vivo NE-LTP could be replicated through the optogenetic manipulation of LC neurons in anesthetized rats. Both of the results observed due to our optogenetic manipulations, the elevation of population spike amplitude and the minimal increase in EPSP slope, have been supported by previous research involving various models of LC activation and in vivo NE-LTP. The failure to see consistent potentiation of EPSP slope is similar to the findings of previous studies using both electrical (Assaf, 1979; Washburn & Moises, 1989) and glutamatergic stimulation of LC (Harley & Milway, 1986). The previously described work by Harley and Sara (1992), which utilized 100nl ejections of glutamate to produce increases in cellular activity of LC, also monitored the consequent changes of this LC activation on DG evoked potentials. Their primary result was an increased population spike amplitude, of up to 158% (SD = 25%) of the control mean. This effect began almost immediately however, occurring within the first minute following the glutamate ejection. They also reported increases in EPSP slope, though they were inconsistent. Walling and Harley (2004) also employed in vivo glutamatergic activation of LC to investigate the subsequent potentiation of DG evoked potential, and they too reported findings consistent to those of this research. In the 3-hour period following LC activation, they similarly reported no significant variation in EPSP slope; however, their results also showed a minimal, transient increase in EPSP slope at the time of the NE-LTP inducing protocol (i.e., glutamate injection). Also consistent with

our results was the overall, long-lasting increase seen in the amplitude of population spikes, with a maximal increase of 130%. This was also shown in the above mentioned orexin research by Walling et al. (2004) which reported a significant potentiation effect of population spike amplitude of up to 155% at 3-hours post-injection. Notably, the trend of modest, transient increases in EPSP slope at the time of the infusion protocol was also reported.

Early work by Harley et al. (1989) employed electrical stimulations of the LC at 10 Hz, the same frequency used for our light sequences, for a period of 1 to 5 minutes. This was also an *in vivo* study, and similarly used rats anesthetized with urethane. To date, there remains little additional research which has utilized this frequency for minutes at a time. One-minute of this 10Hz stimulation was reported to produce a maximum increase in population spike amplitude of 152.8% (n=6), which continued for an average of 8.5 minutes. They saw no effect on EPSP slope. They also noted that a characteristic feature of the potentiation was the continuation of effect seen after the stimulation had ceased, as well as the gradual decay of the potentiation effect, as opposed to a more commonly seen biphasic profile. There are several things which can be gleaned from comparisons between this work by Harley et al. (1989), and the results of this current study. First, there is consistency in that significant results were seen only for the population spike amplitude, with nothing of significance reported for EPSP slope. The pattern of potentiation seen here however, is quite different from that of our optogenetically induced NE-LTP; for instance, their potentiation effect was quite immediate and short-lasting, whereas ours was delayed, but sustained over the 3-hours

post-light. This variation in magnitude and delay of effect, is likely due to the relative ease of driving large portions of LC with chemicals or electricity, as opposed to with light. It is thereby possible that our delayed, but sustained potentiation effect may be due to the activation of a smaller number of LC cells present within the illumination from the light source. Thus, this may be a trade-off for the superior specificity of optogenetic methods of activation.

Unfortunately, the comparisons which could be made for the NE-LTP were limited by the fact that there was only one control animal. The small sample sizes for both groups are certainly a limitation of this research, and future research should aim to expand on these results with a larger number of subjects.

4.8 Optogenetic Manipulation of PP-LC ISIs

As previously mentioned, eight subroutines were tested, delivering either a single 30ms or 50ms pulse directly at the LC and occurring either 20, 30, 40 or 50ms after a .2ms electrical pulse had been delivered to the PP. The decision to include two pulse widths was due to the minimal research into the optogenetic manipulations of LC stimulation latencies and parameters. During the initial stages of this research, both the 30ms and the 50ms pulse widths had been found to effectively and reliably increase the neuronal firing rates of LC neurons when used in light sequences. There was concern that a single 30ms pulse of light may be too short to incite the desired response from LC neurons, thus the 50ms pulse width was also included in testing.

Only the subroutines utilizing the 50ms pulse width produced any significant variations, as indexed by population spike amplitude. The largest increase in amplitude was seen for the longest ISI of 50ms, which boasted an average increase of 116.89% above baseline. Though it is difficult to say conclusively due to our small sample size, the increases in population spike amplitude did appear to coincide with the increasing lengths of ISI. It is worth highlighting however that, in addition to the significant variations seen amongst the interval lengths, a quadratic trend was revealed in these data. The average increase in population spike amplitude above baseline was 102.47%, 93.71%, 111.75% and 116.89% for the 20ms, 30ms, 40ms and 50ms ISI respectively.

As previously mentioned, Harley, Milway and Lacaille (1989) performed electrical stimulation of LC to assess the effects of variation in electrical PP-LC stimulations intervals. They reported an increase in population spike amplitude with the 20ms ISI, however their maximum increase was reported by the 40ms ISI. There was no consistent effect of slope. This research led to speculation that there may be a secondary system, activated from the vicinity of LC and capable of potentiating the evoked response in DG at a 40ms ISI. Their peak potentiation at 40ms ISI was consistent with reports that LC neurons are activated antidromically from the hippocampus with a latency between 30-70ms (Nakamura & Iwama, 1975). However, it was speculated that there must be additional, faster fibers which mediate the weaker potentiation that was reported at 20ms ISI. These results are highly consistent with those seen from our optogenetic manipulations of PP-LC intervals, which reported a quadratic trend. While our peak effect was noted in the 50ms ISI, there was also potentiation seen in the 40ms ISI and

most interestingly, potentiation seen in the 20ms ISI. This lends support to the speculation that there may be two effects of from this pathway a rapid release of a co-transmitter such as glutamate followed by a slower G-protein mediated effect of NE. These effects only occur in a millisecond time frame in earlier studies and disappear at very long ISIs which were not tested here.

4.9 Effect of Optogenetic Activation on Paired Pulses

The paired pulse manipulations assessed the dynamics of neural circuits within DG by varying the length of intervals between pulses and subsequently testing the local circuit properties. The intervals chosen for our paired pulse stimulations (30ms, 70ms & 200ms) were modeled from past research, and were programmed into DataWave to occur sequentially as we manually manipulated the current level following each set. The PPR is defined as the amplitude of the second postsynaptic response over the first; thus ratios greater than 1 are representative of facilitation or excitation, while ratios less than 1 suggest inhibition. Typically, shorter intervals (i.e., 30ms) involved a decrease in population spike amplitude or EPSP slope due to the fast feedback effects of GABA; whereas intermediate intervals (i.e., 70ms) can enhance the response due to the recruitment of NMDA-related excitability changes (DiScenna & Teyler, 1994). However, this was inconsistent with our results. There was very little variation in any of the PPRs reported for EPSP slope, regardless of the interval tested, and with all ratios reported less than 1. For population spike amplitude, a significant effect was found with our 30ms interval however, it did not show inhibition in the baseline PPR. The 70ms interval did

appear to enhance the potentiation response, with PPRs consistently greater than 1, while the longer 200ms interval did reliably produce PPRs less than 1. Interestingly, the sole light-control also displayed irregularities, with a post-light PPR for the 30ms interval that was also greater than 1. Amendments could also be made to the intervals tested, for instance utilizing a shorter interval of 25ms as opposed to 30ms. In past research, a shorter 25ms interval has reliably been used to increase the characteristic feedback inhibition response in vivo (Austin et al., 1989; Tomasulo, Levy, & Steward, 1991), with the enhancement of inhibition specific to 25ms, and not occurring with shorter or longer intervals (Sara & Bergis, 1991). This research would have benefitted from more subjects; thus further research should be done in this area in order to elucidate why these typically characteristic responses might differ with optogenetic LC stimulation.

4.10 Effect of Optogenetic Activation on I-O Curves

An input-output current intensity relationship (I-O curve) was analyzed at both the start and conclusion of recording. For the LC-ChR2(h134r) channel-activated group, 3 hours following optogenetic stimulation, the population spike amplitude was consistently increased at current intensities higher than 300 μ A, while the EPSP slope was also higher at all but the lowest current intensity. The light control subject however, showed subtle decreases in both population spike amplitude and EPSP slope. These results were consistent with previous reports from similar research (Walling & Harley, 2004). The effect of NE-LTP on EPSP slope to population spike (E-S) coupling was also examined by plotting the mean percentage EPSP slope versus population spike amplitude

in both the LC-ChR2(h134r) channel-activated group and the light control. There was a small shift to the right present in EPSP–population spike relationship for the LC-ChR2(h134r) channel-activated group at 3-hours post-light. This suggests that the minimal potentiation seen in the EPSP slope did not account for the population spike potentiation seen at the same time. While a leftward shift is typical following high-frequency stimulation-induced potentiation. Tomasulo, Levy and Steward (1991) also reported an unexpected shift to the right, though no explanation was offered.

4.11 Verification of Placements

In order to be classified as an LC-ChR2(h134r) channel-activated subject, all optrode placements were first verified to be within range of LC neurons. The tract damage resulting from the optrode assembly was first examined via cresyl-violet (Nissl) stained sections, in which the sections with the most ventral damage were identified. The alternating sections to those identified as the “deepest probe placements” underwent immunohistochemical analysis, allowing us to examine the more specific placement of the optrode amongst any DBH labelling. This allowed distinctions to be made of whether each optrode placement had been situated among LC cell bodies or dendrites. Any sections with the identified probe damage that were not shown to contain DBH labelling resulted in the categorization of that subject as a light-control.

Of the optrode placements for LC-ChR2(h134r) channel-activated subjects, 9 out of 10 were located on the medial edge of LC; several of the placements were also slightly dorsal relative to the widest area of the nucleus. However, since the tip of the electrode

projected 50-100 μ m ventral to the 400 μ m wide optrode, which would have caused the most visible damage, it can be inferred that the light emitting from the base of the optrode would have been shining upon the area of LC located just below the damage. Thus, dorsal optrode placements may have in fact been favorable to the recruitment and activation of multiple LC cells.

4.12 Consequences of Placements

As mentioned, the majority of placements for the LC-ChR2(h134r) channel-activated subjects were situated rostral-medial to the majority of the DBH⁺ LC cells. Following examination of optrode placement in relation to the magnitude of the LC activation, it was noted that medial placements seemed to be superior to those placed within the actual confines of LC. These subjects consistently reported higher magnitude increases in LC activation, in addition to a more sustained increase in population spike amplitude. In fact, the subject who reported the largest increase in LC activity during the light protocol, had a placement approximately 300 μ m medial to LC cell bodies, with DBH⁺ dendrites clearly visible just below the optrode damage; that is, the subject aside from the previously mentioned subject with a more concentrated viral infusion. According to anatomical structure of LC, our anterior/rostral, medial placements would situate the optrode assembly within the dendritic processes, which congregate in two specific pericoerulear areas – rostroventro-medial to the LC and extending from the caudal juxtapeduncular, medial boundary of the LC, near the fourth ventricle (Gallyas et

al., 1982). This leads to speculation that placement among the dendritic processes of LC may lead to higher levels of activation than placements within the LC cell bodies. This preferential dendritic placement is consistent with findings by Walling and Harley (2004), who described the placement sites surrounding LC as pericoerulear. The pericoerulear placements were more frequently associated with early potentiation of population spike amplitude than intracellular placements, which often showed a brief increase in EPSP slope without the early potentiation of population spike. This research may therefore lend additional evidence to support the theory that the site of LC activation, specifically within cell bodies versus dendrites, can influence NE release and its consequent effects on evoked potential activity. There has been speculation that the two sites of activation could potentially result in differences in NE release patterns, though further investigation is required before drawing any conclusions.

The additional subject, analyzed separately for the 10-minute light protocol and discussed in section 4.6, was also investigated for any placement irregularities that may explain its inverse pattern of increase in LC firing. While the placement for this subject showed evident damage from the 400 μ m optrode within the boundaries of LC, the placement was ventral in comparison to the other subjects. As previously mentioned, the ventral portion of the LC nucleus is known as the subcoeruleus; it is a more sparsely packed region, known to contain large multipolar cells (Bjorklund & Lindvall, 1979). Thus, it is possible that due to the more ventral placement of the optrode assembly when compared to the rostro-medial placements of the others, the light may have activated a different subpopulation of LC neurons. Specifically, it may have activated this ventral

subpopulation of large, multipolar LC neurons, whose processes extend to include several other NE positive nuclei (Dahlstrom & Fuxe, 1964), and travel ventrally to the forebrain (Maeda & Shimizu, 1972). Ventral regions of LC also give rise to descending projections which target the spinal cord and cerebellum (Loughlin, Foote, & Grzanna, 1986). This could potentially explain why there was still an increase in LC firing frequency in response to the light, though the pattern of increase was notably different.

The specificity of optogenetic manipulation allows for researchers to be confident that the cells responding to the light are only those which can express the viral construct; thus, it may allow for future experimentation to expand upon whether the distinct subpopulations of neurons located within LC, in addition to the pericoerulear areas, show variations in their patterns of response to light.

4.13 Future Directions

This research was a very promising exploration into the effects of optogenetic stimulation of the LC on NE-LTP in anesthetized rats, and offers insight into the world of potential that optogenetics can offer researchers. Future directions for this research should first begin with replicating the results produced here in additional subjects, this would allow for comparisons to be made against light controls. It would also allow conclusions to be drawn for the results which failed to reach statistical significance in this research, but which showed promising trends and would benefit from larger sample sizes. Due to the strong self-regulating LC inhibition seen early in our 10-minute light protocol, it would also be beneficial to examine the response seen with 2-minute and/or 5-minute

light sequences. The next steps for this research will be similar to those taken for previous electrical and chemical LC manipulations; for example, investigations into whether the optogenetic stimulation of LC neurons can be blocked by NE antagonists. Ultimately, we would like to apply this research and our established techniques to recording and manipulating behavior in awake subjects.

CHAPTER 5 – CONCLUSIONS

This research revealed that tonic activation of a small population of LC neurons may produce a less dramatic and gradually developing NE-LTP than reported previously, which may correspond to a natural continuum of phasic and tonic modulation on network plasticity. The profile of NE-LTP seen in this research is consistent with the proposed selective role of LC-NE in intermediate and delayed memory, as opposed to short-term memory. To our knowledge, this research is the first to report successful optogenetic stimulation of LC neurons in anesthetized rats and consequent *in vivo* NE-LTP. In addition to successfully replicating previous models of NE-LTP, this research also reported results in accordance with previous literature on LC-PP ISI testing, paired pulse stimulations and I-O curves. Future research should aim to expand upon our results, and further elucidate the distinct characteristics of the optogenetic stimulation of LC and consequent *in vivo* NE-LTP.

Reference List

1. Abcam. (2016, December 16a). Anti-Dopamine Beta Hydroxylase Antibody. Retrieved from: <http://www.abcam.com/dopamine-beta-hydroxylase-antibody-ab96615.html>
2. Abcam. (2016, December 16b). Anti-Noradrenaline Transporter Antibody. Retrieved from: <http://www.abcam.com/noradrenaline-transporter-antibody-ab41559.html>
3. Aghajanian, G. K., Cedarbaum, J. M., & Wang, R. Y. (1977). Evidence for norepinephrine-mediated collateral inhibition of locus coeruleus neurons. *Brain Res*, 136(3), 570-577.
4. Alexander, R. W., Davis, J. N., & Lefkowitz, R. J. (1975). Direct identification and characterisation of beta-adrenergic receptors in rat brain. *Nature*, 258(5534), 437-440.
5. Amaral, D. G., Scharfman, H. E., & Lavenex, P. (2007). The dentate gyrus: fundamental neuroanatomical organization (dentate gyrus for dummies). *Prog Brain Res*, 163, 3-22. doi:10.1016/S0079-6123(07)63001-5
6. Andersen, P., Blackstad, T. W., & Lomo, T. (1966). Location and identification of excitatory synapses on hippocampal pyramidal cells. *Exp Brain Res*, 1(3), 236-248.
7. Andersen, P., Sundberg, S. H., Sveen, O., Swann, J. W., & Wigstrom, H. (1980). Possible mechanisms for long-lasting potentiation of synaptic transmission in hippocampal slices from guinea-pigs. *J Physiol*, 302, 463-482.
8. Aravanis, A. M., Wang, L. P., Zhang, F., Meltzer, L. A., Mogri, M. Z., Schneider, M. B., & Deisseroth, K. (2007). An optical neural interface: in vivo control of rodent motor cortex with integrated fiberoptic and optogenetic technology. *J Neural Eng*, 4(3), S143-156. doi:10.1088/1741-2560/4/3/S02
9. Assaf, S. Y., Mason, S.T. & Miller, J.J. (1979). Noradrenergic modulation of neuronal transmission between the entorhinal cortex and the dentate gyrus of the rat. *J Physiol*, 292, 52.
10. Aston-Jones, G. (2004). Locus coeruleus, A5 and A7 noradrenergic cell groups. In G. Paxinos (Ed.), *The Rat Nervous System* (3 ed., pp. 259-294). San Diego: Elsevier Academic Press.

11. Aston-Jones, G., & Bloom, F. E. (1981a). Activity of norepinephrine-containing locus coeruleus neurons in behaving rats anticipates fluctuations in the sleep-waking cycle. *J Neurosci*, *1*(8), 876-886.
12. Aston-Jones, G., & Bloom, F. E. (1981b). Norepinephrine-containing locus coeruleus neurons in behaving rats exhibit pronounced responses to non-noxious environmental stimuli. *J Neurosci*, *1*(8), 887-900.
13. Aston-Jones, G., & Cohen, J. D. (2005). Adaptive gain and the role of the locus coeruleus-norepinephrine system in optimal performance. *J Comp Neurol*, *493*(1), 99-110. doi:10.1002/cne.20723
14. Aston-Jones, G., Rajkowski, J., & Kubiak, P. (1997). Conditioned responses of monkey locus coeruleus neurons anticipate acquisition of discriminative behavior in a vigilance task. *Neuroscience*, *80*(3), 697-715.
15. Aston-Jones, G., Rajkowski, J., Kubiak, P., & Alexinsky, T. (1994). Locus coeruleus neurons in monkey are selectively activated by attended cues in a vigilance task. *J Neurosci*, *14*(7), 4467-4480.
16. Austin, K. B., Bronzino, J. D., & Morgane, P. J. (1989). Paired-pulse facilitation and inhibition in the dentate gyrus is dependent on behavioral state. *Exp Brain Res*, *77*(3), 594-604.
17. Berridge, C. W., & Waterhouse, B. D. (2003). The locus coeruleus-noradrenergic system: modulation of behavioral state and state-dependent cognitive processes. *Brain Res Brain Res Rev*, *42*(1), 33-84.
18. Bjorklund, A., & Lindvall, O. (1979). Regeneration of normal terminal innervation patterns by central noradrenergic neurons after 5,7-dihydroxytryptamine-induced axotomy in the adult rat. *Brain Res*, *171*(2), 271-293.
19. Bliss, T. V., & Lomo, T. (1973). Long-lasting potentiation of synaptic transmission in the dentate area of the anaesthetized rabbit following stimulation of the perforant path. *J Physiol*, *232*(2), 331-356.
20. Bouret, S., Duvel, A., Onat, S., & Sara, S. J. (2003). Phasic activation of locus coeruleus neurons by the central nucleus of the amygdala. *J Neurosci*, *23*(8), 3491-3497.

21. Bouret, S., & Sara, S. J. (2004). Reward expectation, orientation of attention and locus coeruleus-medial frontal cortex interplay during learning. *Eur J Neurosci*, *20*(3), 791-802. doi:10.1111/j.1460-9568.2004.03526.x
22. Branco, T., & Staras, K. (2009). The probability of neurotransmitter release: variability and feedback control at single synapses. *Nat Rev Neurosci*, *10*(5), 373-383. doi:10.1038/nrn2634
23. Brown, R. A. (2003). *Trifling Matters: Differential Regulation of Feedforward and Feedback Interneurons of the Dentate Gyrus by Synaptically Released Norepinephrine*. (Doctor of Philosophy, Doctoral Thesis), Memorial University of Newfoundland, Newfoundland and Labrador.
24. Campanac, E., & Debanne, D. (2008). Spike timing-dependent plasticity: a learning rule for dendritic integration in rat CA1 pyramidal neurons. *J Physiol*, *586*(3), 779-793. doi:10.1113/jphysiol.2007.147017
25. Cardin, J. A., Carlén, M., Meletis, K., Knoblich, U., Zhang, F., Deisseroth, K., . . . Moore, C. I. (2010). Targeted optogenetic stimulation and recording of neurons in vivo using cell-type-specific expression of Channelrhodopsin-2. *Nat Protoc*, *5*(2), 247-254. doi:10.1038/nprot.2009.228
26. Carter, M. E., Yizhar, O., Chikahisa, S., Nguyen, H., Adamantidis, A., Nishino, S., . . . de Lecea, L. (2010). Tuning arousal with optogenetic modulation of locus coeruleus neurons. *Nat Neurosci*, *13*(12), 1526-1533. doi:10.1038/nn.2682
27. Carvalho, T. P., & Buonomano, D. V. (2009). Differential effects of excitatory and inhibitory plasticity on synaptically driven neuronal input-output functions. *Neuron*, *61*(5), 774-785. doi:10.1016/j.neuron.2009.01.013
28. Cedarbaum, J. M., & Aghajanian, G. K. (1978). Activation of locus coeruleus neurons by peripheral stimuli: modulation by a collateral inhibitory mechanism. *Life Sci*, *23*(13), 1383-1392.
29. Chen, F. J., & Sara, S. J. (2007). Locus coeruleus activation by foot shock or electrical stimulation inhibits amygdala neurons. *Neuroscience*, *144*(2), 472-481. doi:10.1016/j.neuroscience.2006.09.037
30. Choi, J., & Koh, S. (2008). Role of brain inflammation in epileptogenesis. *Yonsei Med J*, *49*(1), 1-18. doi:10.3349/ymj.2008.49.1.1

31. Cintra, L., Diaz-Cintra, S., Kemper, T., & Morgane, P. J. (1982). Nucleus locus coeruleus: a morphometric Golgi study in rats of three age groups. *Brain Res*, 247(1), 17-28.
32. Clark, F. M., & Proudfit, H. K. (1991). The projection of noradrenergic neurons in the A7 catecholamine cell group to the spinal cord in the rat demonstrated by anterograde tracing combined with immunocytochemistry. *Brain Res*, 547(2), 279-288.
33. Cooke, S. F., & Bliss, T. V. (2006). Plasticity in the human central nervous system. *Brain*, 129(Pt 7), 1659-1673. doi:10.1093/brain/awl082
34. Cooper, G. S., Kamel, F., Sandler, D. P., Davey, F. R., & Bloomfield, C. D. (1996). Risk of adult acute leukemia in relation to prior immune-related conditions. *Cancer Epidemiol Biomarkers Prev*, 5(11), 867-872.
35. Dahl, D., & Sarvey, J. M. (1989). Norepinephrine induces pathway-specific long-lasting potentiation and depression in the hippocampal dentate gyrus. *Proc Natl Acad Sci U S A*, 86(12), 4776-4780.
36. Dahl, D., & Winson, J. (1985). Action of norepinephrine in the dentate gyrus. I. Stimulation of locus coeruleus. *Exp Brain Res*, 59(3), 491-496.
37. Dahlstrom, A., & Fuxe, K. (1964). Localization of monoamines in the lower brain stem. *Experientia*, 20(7), 398-399.
38. Dalley, J. W., McGaughy, J., O'Connell, M. T., Cardinal, R. N., Levita, L., & Robbins, T. W. (2001). Distinct changes in cortical acetylcholine and noradrenaline efflux during contingent and noncontingent performance of a visual attentional task. *J Neurosci*, 21(13), 4908-4914.
39. Daoudal, G., & Debanne, D. (2003). Long-term plasticity of intrinsic excitability: learning rules and mechanisms. *Learn Mem*, 10(6), 456-465. doi:10.1101/lm.64103
40. Davare, M. A., Horne, M. C., & Hell, J. W. (2000). Protein phosphatase 2A is associated with class C L-type calcium channels (Cav1.2) and antagonizes channel phosphorylation by cAMP-dependent protein kinase. *J Biol Chem*, 275(50), 39710-39717. doi:10.1074/jbc.M005462200
41. DiScenna, P. G., & Teyler, T. J. (1994). Development of inhibitory and excitatory synaptic transmission in the rat dentate gyrus. *Hippocampus*, 4(5), 569-576. doi:10.1002/hipo.450040506

42. Egan, T. M., Henderson, G., North, R. A., & Williams, J. T. (1983). Noradrenaline-mediated synaptic inhibition in rat locus coeruleus neurones. *J Physiol*, *345*, 477-488.
43. Emptage, N. J., & Carew, T. J. (1993). Long-term synaptic facilitation in the absence of short-term facilitation in Aplysia neurons. *Science*, *262*(5131), 253-256.
44. Eschenko, O., & Sara, S. J. (2008). Learning-dependent, transient increase of activity in noradrenergic neurons of locus coeruleus during slow wave sleep in the rat: brain stem-cortex interplay for memory consolidation? *Cereb Cortex*, *18*(11), 2596-2603. doi:10.1093/cercor/bhn020
45. Fenno, L., Yizhar, O., & Deisseroth, K. (2011). The development and application of optogenetics. *Annu Rev Neurosci*, *34*, 389-412. doi:10.1146/annurev-neuro-061010-113817
46. Foote, S. L., Aston-Jones, G., & Bloom, F. E. (1980). Impulse activity of locus coeruleus neurons in awake rats and monkeys is a function of sensory stimulation and arousal. *Proc Natl Acad Sci U S A*, *77*(5), 3033-3037.
47. Foote, S. L., Bloom, F. E., & Aston-Jones, G. (1983). Nucleus locus ceruleus: new evidence of anatomical and physiological specificity. *Physiol Rev*, *63*(3), 844-914.
48. Fornai, F., Ruffoli, R., Giorgi, F. S., & Paparelli, A. (2011). The role of locus coeruleus in the antiepileptic activity induced by vagus nerve stimulation. *Eur J Neurosci*, *33*(12), 2169-2178. doi:10.1111/j.1460-9568.2011.07707.x
49. Frick, A., Magee, J., & Johnston, D. (2004). LTP is accompanied by an enhanced local excitability of pyramidal neuron dendrites. *Nat Neurosci*, *7*(2), 126-135. doi:10.1038/nn1178
50. Gallyas, F., Gorcs, T., & Merchenthaler, I. (1982). High-grade intensification of the end-product of the diaminobenzidine reaction for peroxidase histochemistry. *J Histochem Cytochem*, *30*(2), 183-184.
51. Grzanna, R., & Molliver, M. E. (1980). The locus coeruleus in the rat: an immunohistochemical delineation. *Neuroscience*, *5*(1), 21-40.
52. Haas, H. L., & Rose, G. M. (1987). Noradrenaline blocks potassium conductance in rat dentate granule cells in vitro. *Neurosci Lett*, *78*(2), 171-174.

53. Haring, J. H., & Davis, J. N. (1983). Topography of locus ceruleus neurons projecting to the area dentata. *Exp Neurol*, 79(3), 785-800.
54. Harley, C. & Evans, S. (1988). Locus coeruleus-induced enhancement of the perforant path-evoked potential: effects of intradentate beta blockers. In: Woody, C.D., Alkon, D.L. and McGaugh, J.L. (Eds) *Cellular Mechanisms of Conditioning and Behavioral Plasticity*. New York: Plenum Publishing Corporation.
55. Harley, C., Milway, J. S., & Lacaille, J. C. (1989). Locus coeruleus potentiation of dentate gyrus responses: evidence for two systems. *Brain Res Bull*, 22(4), 643-650.
56. Harley, C. W., & Sara, S. J. (1992). Locus coeruleus bursts induced by glutamate trigger delayed perforant path spike amplitude potentiation in the dentate gyrus. *Exp Brain Res*, 89(3), 581-587.
57. Hickey, L., Li, Y., Fyson, S. J., Watson, T. C., Perrins, R., Hewinson, J., . . . Pickering, A. E. (2014). Optoactivation of locus ceruleus neurons evokes bidirectional changes in thermal nociception in rats. *J Neurosci*, 34(12), 4148-4160. doi:10.1523/JNEUROSCI.4835-13.2014
58. Hobson, J. A., McCarley, R. W., & Wyzinski, P. W. (1975). Sleep cycle oscillation: reciprocal discharge by two brainstem neuronal groups. *Science*, 189(4196), 55-58.
59. Izquierdo, M., Ibanez, J., Gonzalez-Badillo, J. J., & Gorostiaga, E. M. (2002). Effects of creatine supplementation on muscle power, endurance, and sprint performance. *Med Sci Sports Exerc*, 34(2), 332-343.
60. Jones, S. L. (1991). Descending noradrenergic influences on pain. *Prog Brain Res*, 88, 381-394.
61. Jones, S. L., & Gebhart, G. F. (1986). Quantitative characterization of ceruleospinal inhibition of nociceptive transmission in the rat. *J Neurophysiol*, 56(5), 1397-1410.
62. Jouvet, M. (1969). Biogenic amines and the states of sleep. *Science*, 163(3862), 32-41.
63. Kiyashchenko, L. I., Mileykovskiy, B. Y., Lai, Y. Y., & Siegel, J. M. (2001). Increased and decreased muscle tone with orexin (hypocretin) microinjections in the locus coeruleus and pontine inhibitory area. *J Neurophysiol*, 85(5), 2008-2016.

64. Korf, J., Bunney, B. S., & Aghajanian, G. K. (1974). Noradrenergic neurons: morphine inhibition of spontaneous activity. *Eur J Pharmacol*, 25(2), 165-169.
65. Lacaille, J. C., & Harley, C. W. (1985). The action of norepinephrine in the dentate gyrus: beta-mediated facilitation of evoked potentials in vitro. *Brain Res*, 358(1-2), 210-220.
66. Lacaille, J.C., & Schwartzkroin, P.A. (1988). Intracellular responses of rat hippocampal granule cells in vitro to discrete applications of norepinephrine. *Neurosci Lett.*, 89(2), 176-181.
67. Lancaster, B., Hu, H., Ramakers, G. M., & Storm, J. F. (2001). Interaction between synaptic excitation and slow afterhyperpolarization current in rat hippocampal pyramidal cells. *J Physiol*, 536(Pt 3), 809-823.
68. Lavenex, P., Banta Lavenex, P., & Amaral, D. G. (2007). Postnatal development of the primate hippocampal formation. *Dev Neurosci*, 29(1-2), 179-192. doi:10.1159/000096222
69. Leonard, A. S., & Hell, J. W. (1997). Cyclic AMP-dependent protein kinase and protein kinase C phosphorylate N-methyl-D-aspartate receptors at different sites. *J Biol Chem*, 272(18), 12107-12115.
70. Li, F., Gangal, M., Jones, J. M., Deich, J., Lovett, K. E., Taylor, S. S., & Johnson, D. A. (2000). Consequences of cAMP and catalytic-subunit binding on the flexibility of the A-kinase regulatory subunit. *Biochemistry*, 39(50), 15626-15632.
71. Lin, J. Y. (2011). A user's guide to channelrhodopsin variants: features, limitations and future developments. *Exp Physiol*, 96(1), 19-25. doi:10.1113/expphysiol.2009.051961
72. Lin, J. Y., Lin, M. Z., Steinbach, P., & Tsien, R. Y. (2009). Characterization of engineered channelrhodopsin variants with improved properties and kinetics. *Biophys J*, 96(5), 1803-1814. doi:10.1016/j.bpj.2008.11.034
73. Loughlin, S. E., Foote, S. L., & Bloom, F. E. (1986). Efferent projections of nucleus locus coeruleus: topographic organization of cells of origin demonstrated by three-dimensional reconstruction. *Neuroscience*, 18(2), 291-306.
74. Loughlin, S. E., Foote, S. L., & Grzanna, R. (1986). Efferent projections of nucleus locus coeruleus: morphologic subpopulations have different efferent targets. *Neuroscience*, 18(2), 307-319.

75. Maeda, T., & Shimizu, N. (1972). [Ascending projections from the locus coeruleus and other aminergic pontine neurons at the level of the rat prosencephalon]. *Brain Res*, 36(1), 19-35.
76. Marder, C. P., & Buonomano, D. V. (2004). Timing and balance of inhibition enhance the effect of long-term potentiation on cell firing. *J Neurosci*, 24(40), 8873-8884. doi:10.1523/JNEUROSCI.2661-04.2004
77. Mason, S. T., & Fibiger, H. C. (1979). Regional topography within noradrenergic locus coeruleus as revealed by retrograde transport of horseradish peroxidase. *J Comp Neurol*, 187(4), 703-724. doi:10.1002/cne.901870405
78. Mazzanti, G., Bolle, P., Martinoli, L., Piccinelli, D., Grgurina, I., Animati, F., & Mugne, Y. (1987). Croton macrostachys, a plant used in traditional medicine: purgative and inflammatory activity. *J Ethnopharmacol*, 19(2), 213-219.
79. Menniti, F. S., & Diliberto, E. J., Jr. (1989). Newly synthesized dopamine as the precursor for norepinephrine synthesis in bovine adrenomedullary chromaffin cells. *J Neurochem*, 53(3), 890-897.
80. Millan, M. J. (2002). Descending control of pain. *Prog Neurobiol*, 66(6), 355-474.
81. Milner, T. A., Shah, P., & Pierce, J. P. (2000). beta-adrenergic receptors primarily are located on the dendrites of granule cells and interneurons but also are found on astrocytes and a few presynaptic profiles in the rat dentate gyrus. *Synapse*, 36(3), 178-193. doi:10.1002/(SICI)1098-2396(20000601)36:3<178::AID-SYN3>3.0.CO;2-6
82. Morris, R. G., Garrud, P., Rawlins, J. N., & O'Keefe, J. (1982). Place navigation impaired in rats with hippocampal lesions. *Nature*, 297(5868), 681-683.
83. Nagel, G., Brauner, M., Liewald, J. F., Adeishvili, N., Bamberg, E., & Gottschalk, A. (2005). Light activation of channelrhodopsin-2 in excitable cells of *Caenorhabditis elegans* triggers rapid behavioral responses. *Curr Biol*, 15(24), 2279-2284. doi:10.1016/j.cub.2005.11.032
84. Nagy, A. (2000). Cre recombinase: the universal reagent for genome tailoring. *Genesis*, 26(2), 99-109.
85. Nakamura, S., & Iwama, K. (1975). Antidromic activation of the rat locus coeruleus neurons from hippocampus, cerebral and cerebellar cortices. *Brain Res*, 99(2), 372-376.

86. Neuman, R. S., & Harley, C. W. (1983). Long-lasting potentiation of the dentate gyrus population spike by norepinephrine. *Brain Res*, 273(1), 162-165.
87. Nowak, L., Bregestovski, P., Ascher, P., Herbet, A., & Prochiantz, A. (1984). Magnesium gates glutamate-activated channels in mouse central neurones. *Nature*, 307(5950), 462-465.
88. Olson, L., & Fuxe, K. (1972). Further mapping out of central noradrenaline neuron systems: projections of the "subcoeruleus" area. *Brain Res*, 43(1), 289-295.
89. Pudovkina, O. L., & Westerink, B. H. (2005). Functional role of alpha1-adrenoceptors in the locus coeruleus: a microdialysis study. *Brain Res*, 1061(1), 50-56. doi:10.1016/j.brainres.2005.08.049
90. Pupe, S., & Wallen-Mackenzie, A. (2015). Cre-driven optogenetics in the heterogeneous genetic panorama of the VTA. *Trends Neurosci*, 38(6), 375-386. doi:10.1016/j.tins.2015.04.005
91. Quintin, L., Buda, M., Hilaire, G., Bardelay, C., Ghignone, M., & Pujol, J. F. (1986). Catecholamine metabolism in the rat locus coeruleus as studied by in vivo differential pulse voltammetry. III. Evidence for the existence of an alpha 2-adrenergic tonic inhibition in behaving rats. *Brain Res*, 375(2), 235-245.
92. Ramon, C. S. I. B., W. (1968). *Ramon y Cajal*. Buenos Aires: Centro Editor de America Latina.
93. Reid, A. (2006). *An associativity requirement for noradrenergic dentate gyrus long-term potentiation in the urethane-anesthetized rat*. (Masters Thesis), Memorial University of Newfoundland, Newfoundland and Labrador.
94. Remondes, M., & Schuman, E. M. (2003). Molecular mechanisms contributing to long-lasting synaptic plasticity at the temporoammonic-CA1 synapse. *Learn Mem*, 10(4), 247-252. doi:10.1101/lm.59103
95. Rogawski, M. A., & Aghajanian, G. K. (1982). Activation of lateral geniculate neurons by locus coeruleus or dorsal noradrenergic bundle stimulation: selective blockade by the alpha 1-adrenoceptor antagonist prazosin. *Brain Res*, 250(1), 31-39.
96. Room, P., Postema, F., & Korf, J. (1981). Divergent axon collaterals of rat locus coeruleus neurons: demonstration by a fluorescent double labeling technique. *Brain Res*, 221(2), 219-230.

97. Rossi, M. A., Go, V., Murphy, T., Fu, Q., Morizio, J., & Yin, H. H. (2015). A wirelessly controlled implantable LED system for deep brain optogenetic stimulation. *Front Integr Neurosci*, 9, 8. doi:10.3389/fnint.2015.00008
98. Samuels, E. R., & Szabadi, E. (2008). Functional neuroanatomy of the noradrenergic locus coeruleus: its roles in the regulation of arousal and autonomic function part II: physiological and pharmacological manipulations and pathological alterations of locus coeruleus activity in humans. *Curr Neuropharmacol*, 6(3), 254-285. doi:10.2174/157015908785777193
99. Sara, S.J. (2009). The locus coeruleus and noradrenergic modulation of cognition. *Nature Reviews Neuroscience*, 10, 211-223.
100. Sara, S. J., & Bergis, O. (1991). Enhancement of excitability and inhibitory processes in hippocampal dentate gyrus by noradrenaline: a pharmacological study in awake, freely moving rats. *Neurosci Lett*, 126(1), 1-5.
101. Sara, S. J., & Bouret, S. (2012). Orienting and reorienting: the locus coeruleus mediates cognition through arousal. *Neuron*, 76(1), 130-141. doi:10.1016/j.neuron.2012.09.011
102. Sara, S. J., & Segal, M. (1991). Plasticity of sensory responses of locus coeruleus neurons in the behaving rat: implications for cognition. *Prog Brain Res*, 88, 571-585.
103. Sara, S. J., Vankov, A., & Herve, A. (1994). Locus coeruleus-evoked responses in behaving rats: a clue to the role of noradrenaline in memory. *Brain Res Bull*, 35(5-6), 457-465.
104. Scheinin, M., Lomasney, J. W., Hayden-Hixson, D. M., Schambra, U. B., Caron, M. G., Lefkowitz, R. J., & Fremeau, R. T., Jr. (1994). Distribution of alpha 2-adrenergic receptor subtype gene expression in rat brain. *Brain Res Mol Brain Res*, 21(1-2), 133-149.
105. Schofield, G. G. (1990). Norepinephrine blocks a calcium current of adult rat sympathetic neurons via an alpha 2-adrenoceptor. *Eur J Pharmacol*, 180(1), 37-47.
106. Schuerger, R. J., & Balaban, C. D. (1993). Immunohistochemical demonstration of regionally selective projections from locus coeruleus to the vestibular nuclei in rats. *Exp Brain Res*, 92(3), 351-359.

107. Segal, M., & Bloom, F. E. (1976). The action of norepinephrine in the rat hippocampus. IV. The effects of locus coeruleus stimulation on evoked hippocampal unit activity. *Brain Res*, 107(3), 513-525.
108. Shimizu, N., & Imamoto, K. (1970). Fine structure of the locus coeruleus in the rat. *Arch Histol Jpn*, 31(3), 229-246.
109. Shipley, M. T., Fu, L., Ennis, M., Liu, W. L., & Aston-Jones, G. (1996). Dendrites of locus coeruleus neurons extend preferentially into two pericoerulear zones. *J Comp Neurol*, 365(1), 56-68. doi:10.1002/(SICI)1096-9861(19960129)365:1<56::AID-CNE5>3.0.CO;2-I
110. Sievers, J., Lolova, I., Jenner, S., Klemm, H. P., & Sievers, H. (1981). Morphological and biochemical studies on the ontogenesis of the nucleus locus coeruleus. *Bibl Anat*(19), 52-130.
111. Simpson, K. L., Altman, D. W., Wang, L., Kirifides, M. L., Lin, R. C., & Waterhouse, B. D. (1997). Lateralization and functional organization of the locus coeruleus projection to the trigeminal somatosensory pathway in rat. *J Comp Neurol*, 385(1), 135-147.
112. Simson, P. E. (2001). Blockade of alpha2-adrenergic receptors markedly potentiates glutamate-evoked activity of locus coeruleus neurons. *Int J Neurosci*, 106(1-2), 95-99.
113. Stanton, P. K., Mody, I., & Heinemann, U. (1989). A role for N-methyl-D-aspartate receptors in norepinephrine-induced long-lasting potentiation in the dentate gyrus. *Exp Brain Res*, 77(3), 517-530.
114. Stanton, P. K., & Sarvey, J. M. (1985a). Blockade of norepinephrine-induced long-lasting potentiation in the hippocampal dentate gyrus by an inhibitor of protein synthesis. *Brain Res*, 361(1-2), 276-283.
115. Stanton, P. K., & Sarvey, J. M. (1985b). The effect of high-frequency electrical stimulation and norepinephrine on cyclic AMP levels in normal versus norepinephrine-depleted rat hippocampal slices. *Brain Res*, 358(1-2), 343-348.
116. Sugiyama, D., Hur, S. W., Pickering, A. E., Kase, D., Kim, S. J., Kawamata, M., . . . Furue, H. (2012). In vivo patch-clamp recording from locus coeruleus neurones in the rat brainstem. *J Physiol*, 590(10), 2225-2231. doi:10.1113/jphysiol.2011.226407

117. Sullivan, E. V., & Sagar, H. J. (1991). Double dissociation of short-term and long-term memory for nonverbal material in Parkinson's disease and global amnesia. A further analysis. *Brain, 114 (Pt 2)*, 893-906.
118. Swanson, L. W. (1976). The locus coeruleus: a cytoarchitectonic, Golgi and immunohistochemical study in the albino rat. *Brain Res, 110(1)*, 39-56.
119. Takigawa, M., & Mogenson, G. J. (1977). A study of inputs to antidromically identified neurons of the locus coeruleus. *Brain Res, 135(2)*, 217-230.
120. Tecuapetla, F., Patel, J. C., Xenias, H., English, D., Tadros, I., Shah, F., . . . Koos, T. (2010). Glutamatergic signaling by mesolimbic dopamine neurons in the nucleus accumbens. *J Neurosci, 30(20)*, 7105-7110.
doi:10.1523/JNEUROSCI.0265-10.2010
121. Tomasulo, R. A., Levy, W. B., & Steward, O. (1991). LTP-associated EPSP/spike dissociation in the dentate gyrus: GABAergic and non-GABAergic components. *Brain Res, 561(1)*, 27-34.
122. Tsai, H. C., Zhang, F., Adamantidis, A., Stuber, G. D., Bonci, A., de Lecea, L., & Deisseroth, K. (2009). Phasic firing in dopaminergic neurons is sufficient for behavioral conditioning. *Science, 324(5930)*, 1080-1084.
doi:10.1126/science.1168878
123. Vankov, A., Hervé-Minvielle, A., & Sara, S. (1995) Response to novelty and its rapid habitaiton in locus coeruleus neurons of the freely exploring rat. *Eur J Neurosci., 7(6)*, 1180-1187.
124. Wallace, C. (2015). *Optogenetic Control of the Locus Coeruleus to Generate Long-Term Potentiation of the Perforant Path-Evoked Potential in the Dentate Gyrus*. (Bachelor of Science (Honours) Undergraduate Thesis, Memorial University, Newfoundland and Labrador.
125. Walling, S. G., & Harley, C. W. (2004). Locus ceruleus activation initiates delayed synaptic potentiation of perforant path input to the dentate gyrus in awake rats: a novel beta-adrenergic- and protein synthesis-dependent mammalian plasticity mechanism. *J Neurosci, 24(3)*, 598-604.
doi:10.1523/JNEUROSCI.4426-03.2004
126. Walling, S. G., Nutt, D. J., Lalies, M. D., & Harley, C. W. (2004). Orexin-A infusion in the locus ceruleus triggers norepinephrine (NE) release and NE-induced long-term potentiation in the dentate gyrus. *J Neurosci, 24(34)*, 7421-7426. doi:10.1523/JNEUROSCI.1587-04.2004

127. Wang, J. H., & Kelly, P. T. (1996). The balance between postsynaptic Ca(2+)-dependent protein kinase and phosphatase activities controlling synaptic strength. *Learn Mem*, 3(2-3), 170-181.
128. Wang, X., Pinol, R. A., Byrne, P., & Mendelowitz, D. (2014). Optogenetic stimulation of locus ceruleus neurons augments inhibitory transmission to parasympathetic cardiac vagal neurons via activation of brainstem alpha1 and beta1 receptors. *J Neurosci*, 34(18), 6182-6189. doi:10.1523/JNEUROSCI.5093-13.2014
129. Washburn, M., & Moises, H. C. (1989). Electrophysiological correlates of presynaptic alpha 2-receptor-mediated inhibition of norepinephrine release at locus coeruleus synapses in dentate gyrus. *J Neurosci*, 9(6), 2131-2140.
130. Waterhouse, B. D., & Woodward, D. J. (1980). Interaction of norepinephrine with cerebrocortical activity evoked by stimulation of somatosensory afferent pathways in the rat. *Exp Neurol*, 67(1), 11-34.
131. Weir, K., Blanquie, O., Kilb, W., Luhmann, H. J., & Sinning, A. (2014). Comparison of spike parameters from optically identified GABAergic and glutamatergic neurons in sparse cortical cultures. *Front Cell Neurosci*, 8, 460. doi:10.3389/fncel.2014.00460
132. Williams, J. T., Henderson, G., & North, R. A. (1985). Characterization of alpha 2-adrenoceptors which increase potassium conductance in rat locus coeruleus neurones. *Neuroscience*, 14(1), 95-101.
133. Witter, M. P., & Amaral, D. G. (1991). Entorhinal cortex of the monkey: V. Projections to the dentate gyrus, hippocampus, and subicular complex. *J Comp Neurol*, 307(3), 437-459. doi:10.1002/cne.903070308
134. Zhang, F., Gradinaru, V., Adamantidis, A. R., Durand, R., Airan, R. D., de Lecea, L., & Deisseroth, K. (2010). Optogenetic interrogation of neural circuits: technology for probing mammalian brain structures. *Nat Protoc*, 5(3), 439-456. doi:10.1038/nprot.2009.226
135. Zhou, J. (2004). Norepinephrine transporter inhibitors and their therapeutic potential. *Drugs Future*, 29(12), 1235-1244.